DISSECTING THE NEURAL CIRCUITS OF EARLY VISUAL PROCESSING IN DROSOPHILA

A DISSERTATION
SUBMITTED TO THE DEPARTMENT OF ELECTRICAL ENGINEERING
AND THE COMMITTEE ON GRADUATE STUDIES
OF STANFORD UNIVERSITY
IN PARTIAL FULFILLMENT OF THE REQUIREMENTS
FOR THE DEGREE OF
DOCTOR OF PHILOSOPHY

Limor Freifeld
July 2013

This dissertation is online at: http://purl.stanford.edu/hx376qd9219

I certify that I have read this dissertation and that, in my opinion, it is fully adequate in scope and quality as a dissertation for the degree of Doctor of Philosophy.

Mark Horowitz, Primary Adviser

I certify that I have read this dissertation and that, in my opinion, it is fully adequate in scope and quality as a dissertation for the degree of Doctor of Philosophy.

Thomas Clandinin, Co-Adviser

I certify that I have read this dissertation and that, in my opinion, it is fully adequate in scope and quality as a dissertation for the degree of Doctor of Philosophy.

Mark Schnitzer

Approved for the Stanford University Committee on Graduate Studies.

Patricia J. Gumport, Vice Provost Graduate Education

This signature page was generated electronically upon submission of this dissertation in electronic format. An original signed hard copy of the signature page is on file in University Archives.

Abstract

Visual inputs are high-dimensional, dynamically varying, and may consist of significant levels of noise and redundancies. Nevertheless, visual processing systems in many animals are capable of efficiently extracting information out of these signals and using this information to successfully guide behavior. Flies, in particular, are uniquely successful at using visual information to guide behavior in challenging conditions such as during rapid flight maneuvers that give rise to similarly rapidly changing intensity patterns across their eyes. In this dissertation we examine how early visual processing cells in the visual system of the Fruit Fly, *Drosophila* achieve this feat. In particular, we focus on cells that provide inputs to motion detecting circuits and assess how these cells balance the goal of facilitating computational specializations with the goal of efficiently capturing all visual information.

In these studies, we used two-photon Ca^{2+} imaging *in vivo* to monitor the responses of specific cells in the fly visual system while the flies observed visual stimuli projected on a screen. Using this system, we found that two first order interneurons providing inputs to pathways specialized for the detection of moving bright and dark edges nevertheless similarly encode information about both brightening and darkening. However, an in depth study of the functional properties of one of these interneurons revealed that it responds differently to bright and dark moving objects of different sizes in a manner that could facilitate the downstream specialization. Furthermore, via genetic and pharmacological manipulations it was found that GABAergic circuits providing lateral and feedback inputs to this cell enhance its responses to dark stimuli and thus enable it to relay critical information for the downstream pathway. These

circuits were found to give rise to a center-surround antagonistic, anisotropic and spatiotemporally coupled RF structure in this cell that underlies its observed functional properties. Additional, cholinergic circuits were also identified as involved in shaping the outputs of this cell, modifying the size of its receptive field and the kinetics of responses.

Interestingly, our studies uncovered deep similarities between the function of early visual processing cells in the fly and the function of early visual processing cells in vertebrate retinas. This suggests that different systems have converged on a similar set of solutions for addressing the challenge of efficiently using the resources available to the nervous system to efficiently process visual signals and thus extract useful information.

Acknowledgments

This dissertation would never have been accomplished without the help, guidance and support of my advisors, collaborators, friends and family whom I would like to acknowledge here.

Throughout my graduate career I highly enjoyed and benefited from the guidance and advice provided by my two advisors, Prof. Mark Horowitz and Prof. Thomas Clandinin, each of whom provided me with a different perspective on the research we have pursued together and facilitated its progress in many different and exciting directions. I particularly appreciated Mark's willingness to provide me with support and help both when my research work required knowledge from fields new to me as well as when it required knowledge from areas that were new to Mark. Throughout these different endeavors Mark was always able to guide me towards the right resources and his detailed advice helped me make progress and improved the quality of my work. Mark's ability to reason through problems in any field of science was highly inspiring for me and will hopefully have a lasting impact on my work. The field of neuroscience has fascinated me for a long time, but I had never conducted research in this field before I met Tom. Tom introduced me to the depths of the neuroscience discipline and my interactions with him and his group have made my appreciation of it even deeper. I particularly appreciate the time Tom spent helping me improve my writing and presentation skills to enable me to communicate effectively with the neuroscience community. Importantly, Tom's advising enabled me to phrase and pursue relevant and interesting research questions in this field. Tom's attention to detail and thoroughness in scientific pursuits will continue to serve as guidelines for my science in the future as well.

During the course of my PhD work I have had the chance to pursue many different projects and work with an amazing group of collaborators. While not all of the work is contained in this dissertation, I would like to thank all my collaborators here: Don Stark, formerly a consulting professor in Prof. Mark Horowitz's group, provided me with a significant amount of help when we designed hardware and software for operating two-photon microscopes. Prof. Mark Schnitzer introduced me to the field of imaging and to the cutting-edge research pursued by his group in this domain. Through my interactions with Mark and his group I became highly excited about the potential of using imaging technology to address pressing questions in neuroscience and gained the knowledge required to do so. In particular, I greatly enjoyed working with collaborators from the Schnitzer group: Eric Tatt-Wei Ho, Eric Cocker, Supriyo Sinha, James Fitzgerald and Brian wilt.

Most of the research projects I pursued during my PhD and the ones described in this dissertation were conducted in the Clandinin lab. Damon Clark was my first collaborator in Tom's group and I have worked closely with Damon for many years. Damon provided me with significant technical guidance as he introduced me to the use of two-photon microscopy for imaging neural activity in *Drosophila* and presentation of visual stimuli to flies. In addition, Damon and I had countless invigorating discussions on science, both broad in scope and narrowly focused on our joint work, which I highly enjoyed. I've highly appreciated Damon's insightful comments and aspiration for accurate and rigorous data analysis. In pursuit of a different project, modeling the walking behavior of flies, I have collaborated with Alexander Katsov. Alex's enthusiasm about this project was strongly motivating and I have learned a lot from his perspectives and views on neuroscience. In addition to this, I am currently collaborating with Daryl Gohl on a project whose goal is to identify insertion positions of transposable elements in large collections of transgenic animals. It was a great pleasure to work with someone as knowledgeable and hard-working as Daryl and together find exciting ways in which knowledge from different domains can be combined in a useful manner. Within a very short period of time Daryl has shared with me a significant amount of knowledge in molecular biology and enabled me to pursue a project in a domain that was completely foreign to me.

In addition to pursuing a few large research projects with Clandinin lab members, I have thoroughly enjoyed many additional interactions with members of the lab. Thus, I have greatly enjoyed sharing knowledge in imaging and programming and learning about fly genetics in my interactions with Marion Sillies. I found Marion's energy, persistence and dedication to her scientific work inspiring and highly appreciated her input about my work. It was a pleasure to collaborate with Marion, Daryl and Yvette Fisher in their exciting pursuit characterizing the contributions of multiple pathways to processing different types of motion by the fly early visual processing system. I would also like to thank all Clandinin lab members for many useful and insightful comments about my work in many group meetings and informal interactions: post-docs Mathias Wernet, Tina Schwabe, Sheetal Bhalerao and Erin Barnhart; and PhD students Jessica Tsai, Jonathan Leong, Jennifer Esch,Yvette Fisher and Helen Yang. I particularly would like to thank Helen who has taken over pursuing results of some of my imaging experiments and developing these to a new and exciting research project. Helen is an incredibly fast learner and it is highly reassuring to know that the research I found exciting will be left in her capable hands. I am looking forward to seeing what her work will reveal.

I would like to also acknowledge the generosity of institutions and individuals that provided me with funding in support of my PhD. To the Fulbright program for providing me with an International Science and Technology award, thus providing me financial support for the first 3 years of my PhD. To the office of the vice-provost for graduate education and Bio-X for providing me with funding for the remaining 3 years of my PhD via a Bio-X - Stanford Interdisciplinary Graduate fellowship, and in particular to Bruce and Elizabeth Dunlevie for their generous contribution.

Last but not least, to all my friends and family whose support and encouragement span the distance from Israel (and New Jersey) to California: I would like to express my deepest gratitude for all you have given me. This dissertation is dedicated to you.

Contents

List of Tables

List of Figures

Chapter 1

Introduction

Dissecting the circuits that link sensory inputs to motor outputs is a core challenge in systems neuroscience. To dissect a circuit implies answering the following questions, corresponding closely to Marr's three levels of analysis [165]:

1. What function or goal does the circuit aim to achieve?

2. What algorithm does the circuit use in order to achieve its goal? This algorithm consists of the set of transformations applied to sensory inputs in order to arrive at appropriate behavioral outputs.

3. How is the algorithm implemented by the circuit? Answering this question implies identifying what functional role each circuit element (neuron and synapse) plays in giving rise to different transformations.

Both conceptual as well as technical challenges must be addressed to enable achieving a complete circuit dissection in any model animal. Conceptual challenges include the development of methodologies for probing circuits and deriving computational models to capture their function. This requires, for example, figuring out how to systematically design informative inputs such that the response to any novel input could be derived from measured responses to this limited subset of inputs. This also requires the ability to correlate defined inputs with high-dimensional outputs such as measured neural activity in a large population of neurons, or behavioral outputs.

Technical challenges to accomplish this task include, for example, developing tools enabling to simultaneously monitor the activity of many neurons or entire circuits, *in vivo*, potentially across different brain areas, and at a high temporal resolution. Furthermore, to identify the contribution of specific circuit elements and their connectivity to global circuit function requires the ability to manipulate their activity. By activating or inactivating different circuit elements, or blocking specific types of links between elements, the contribution of the different elements or connections to the computation may be inferred. Since all circuit elements work together to give rise to behavior, computational roles may be assigned to manipulated circuit elements by describing the behavioral response to stimuli and how it changes following these manipulations. However, when describing behavior even the selection of a representation, i.e., of metrics or models for capturing and quantifying behavior is not a trivial one to address when the goal is to identify the full computational capabilities of a circuit to modulate this output. Prior to performing manipulations it is challenging to predict what aspects of behavior will be modulated by the manipulations and hence are critical to capture.

In this dissertation we focus on the dissection of early visual processing circuits in the fruit fly, *Drosophila* and address some technical as well as conceptual challenges. In particular, we present new tools for deriving the functional characteristics of a cell from outputs measured using Ca^{2+} imaging. In addition, we use these tools to identify roles played by lateral and feedback interactions in early visual processing circuits. Thus, we unravel how the inputs to computationally specialized circuits are shaped. We hope that both the tools as well as the conclusions can be generalized to other model animals and sensory processing circuits; thus representing small steps towards a better understanding of how the brain works.

1.1 Overview of the dissertation

This dissertation describes methods enabling neural circuit dissection and the application of such methods for dissecting a part of a specific circuit of interest - the motion vision circuit of the fruit fly, *Drosophila*. In this introductory chapter, we first motivate our choice to study vision in *Drosophila*. We then provide background on behavioral modulations flies present in response to visual cues, revealing the computations that must be performed by visual processing circuits. Next, we present the available tool-set and methods that can be used to dissect these neural circuits, and in particular tools for monitoring and manipulating neural activity. A particular emphasis is given to imaging methods that enable peering into the dense neuropil of the fly brain and that are used in subsequent chapters of this dissertation. In addition, we review genetic tools that enable one to causally relate neural activity to computation and behavior. With this tool-set in mind we turn to the circuits we are interested in dissecting - the visual processing circuits of the fly. In this section, we review what is known about how the fly visual system is wired and how it functions, providing context for the subsequently presented studies.

In the following chapters we describe our work on dissecting the neural circuits of early visual processing in *Drosophila*. This work was also described in two separate publications [47, 78]. In the first of these chapters, two types of visual processing neurons providing inputs to motion detecting circuits are functionally characterized. We find that, even though the pathways downstream of these neurons are specialized for detecting dark and bright moving edges, both these neurons encode information about both light increments as well as decrements. In the second chapter, we focus on one of these two neurons, the L2 neuron providing inputs to a dark moving edge detecting pathway, and explore its sensitivities to spatiotemporal distributions of light in more depth. We find that this neuron is tuned to facilitate downstream dark edge motion detection by responding differently to bright and dark objects of different sizes, and that its functional characteristics are strikingly similar to bipolar cells, structurally analogous cells in the vertebrate retina. These findings also have potential implications for how motion may be computed downstream of this cell. In

the third chapter we use pharmacological and genetic manipulations to unravel the circuit mechanisms that give rise to the functional specializations of L2 cells described in the previous chapter. In particular, we find that lateral or feedback, GABAergic inputs, rather than direct inputs from photoreceptors, give rise to critical components of the cell response characteristics. In particular, these circuits mediate responses to light decrements, required to enable the downstream circuits to detect moving dark edges.

1.2 Studying visual processing in *Drosophila*

To start answering the question of how neural circuits process sensory inputs and use extracted information to guide behavior, we must first select a neural circuit to focus on. Here we chose the visual processing circuits of the fruit fly *Drosophila*. A few considerations motivated this choice. First, we are interested in understanding how neural circuits compute, and to understand computation it is easier to start from inputs that are well defined and easy to quantify. Visual inputs are naturally represented as patterns of intensity values that vary as a function time and position in space. Other features of visual inputs, such as velocities or contrast dynamics, can be easily derived, facilitating the assessment of which features the animal or a cell are sensitive to. Second, we want to be able to have exact control over the spatial and temporal distribution of inputs arriving at the sensory system of the animal. Visual inputs are easy to generate with a variety of display types, and it is also possible to compute the exact mapping between the display and the animal eye - and thus infer the exact sensory experience of the animal.

Additional considerations motivated our choice to study vision specifically in flies. While it is desired to eventually be able to dissect large and complex circuits as we expect to find in human brains, it is a more tractable task to first dissect smaller and more well-defined circuits or sub-circuits. The underlying assumption here is that the principles underlying the design of all neural circuits in all animals are similar and that basic computation units are combined as building blocks to give rise to the function of larger circuits. Thus, understanding how a few example circuits transform sensory

inputs to behavioral outputs is a critical stepping stone for understanding how the brain computes more broadly. Since fly brains are not only relatively small but also have a more stereotypical wiring pattern that is consistent between animals [185, 222]; they constitute attractive candidates in which we can hope to be able to relate circuit structure and single neuron function to the higher levels of algorithms implemented and goals achieved.

Dissecting a neural circuit further requires the ability to monitor and manipulate the activity of neurons. To gain access to neural populations of interest typically requires invasive operations; such as introducing electrodes into the brain or exposing it (removing a part of a skull or cuticle, depending on the animal model) to gain access to the brain tissue with light. Noninvasive tools for monitoring neural activity, such as EEG, MEG or fMRI [9] do not have comparable spatial and temporal resolutions to electrophysiological measurements or optical sectioning microscopy techniques (see Section 1.3.1). Acquiring data with a high spatial resolution (single neurons and even compartments within neurons, axons and dendrites) and temporal resolution (ideally in the time-scale of neural activity, i.e., milliseconds for monitoring action potential firing) is absolutely required for linking sensory inputs and behavioral outputs to the single neuron and the circuit level. Thus, model animals constitute more appropriate targets for these studies.

The fly is a particularly attractive model animal for studying visual processing (reviewed in [27]), as its lifestyle reflects significant utilization of visual cues for guiding behavior. Since behavioral responses to sensory cues provide opportunities to infer underlying circuit computations, it is highly beneficial that flies present a rich repertoire of visual behaviors, facilitating the dissection of visual processing circuits. In particular, flies are able to rapidly process visual information during complex flight maneuvers. These abilities are applied for chasing conspecifics using vision to track the target, for visual course control during flight, and in deciding whether a looming entity is a surface appropriate for landing or an object that should be avoided by triggering an escape response [246].

In large flies, electrophysiological recordings have enabled researchers to relate sensory inputs to neural activity patterns (reviewed in [26, 66]). However, monitoring

and manipulation of neural circuit components is further facilitated in established genetic model animals, such as the smaller fruit-fly *Drosophila* (see Section 1.3). With genetic tools it is possible to express different effectors in specific types of cells without invasive operations and thus imaging technology can be used to monitor activity in cells expressing indicators which report this activity. Effectors for silencing or enhancing activity can also be expressed in specific cell populations to enable deriving causal relations between activity and function (see Section 1.3). *Drosophila* is a particularly convenient model animal to work with as its short generation time (only 10 days from mating to eclosion) facilitates combining many different transgenes in a single animal, enabling to use sophisticated combinations of tools for specific applications.

With this focus on visual processing in the fruit fly in mind, an important first question to address is what circuits in the visual system of the fly are available for dissection? The rich repertoire of visually guided behaviors, briefly surveyed in the next section, enables to start answering this question.

1.2.1 Visually evoked behaviors in flies

Looking at the different ways in which flies modulate their behavior in response to external visual cues enables one to infer what computations must be performed by visual processing circuits in these animals. Consequently, by monitoring behavior one can try and answer the question of what goals do these circuits aim to achieve and what algorithms are implemented to achieve these goals. Relations between external signals and behavior can be first identified from observation of how animals respond to visual cues in their natural surroundings and what typical behaviors they present. Then, the detailed relations between input parameters and basic elements of behavioral modulations can be examined in more detail in the lab, where responses to more constrained inputs can be measured. With such studies, hypotheses as to how complex behavioral modulation is constructed from specific input-output relations can be directly tested (For reviews see: [23, 192, 222]). Below we provide an overview of a few identified relations between visual inputs and behaviors in flies, serving as a guide

to what computations may be performed by the visual processing circuits examined in more detail in subsequent chapters of this dissertation. We then also describe some of the behavioral assays with which the responses are typically characterized to infer functional relations between sensory inputs and behavioral outputs, allowing one to identify the algorithms implemented by these circuits.

The most simple example for a relation between visual inputs and fly behavior is phototaxis - attraction to light. In addition to preferring light over dark environments, color vision mediates spectral preference, such that the attractiveness of light for the fly depends on its color [20, 44, 84, 111, 265]. Another example for a visually-guided behavior presented by flies is the orientation response to light polarization direction. Natural light is polarized and the e-vector of polarization is used for navigation. Thus, flies can be observed to orient their body axis as a function of the orientation of the e-vector of polarization [257, 261]. While polarization vision may help with navigation at a course-grained level, responses to visual motion are critical for flies to be able to successfully reach their destination as these cues serve flies in course control and stabilization in addition to navigation during flight. Optomotor responses, turns in the direction of observed motion, are thought to be designed to stabilize the fly during flight, e.g., when wind causes a drift that shifts the fly away from its course. This type of response, which minimizes the slip of the image across the fly's retina, would allow the fly to get back to its intended course [94].

When guiding flight behavior, visual processing is often combined with additional sensory inputs. For example, olfactory cues may indicate the direction in which a food source can be found, while mechanical inputs such as wind cues can aid in correcting the course of flight to compensate for drift, together with visual cues supporting the same task. Such multisensory information must be integrated together to appropriately guide behavior (for reviews see [81, 82, 83, 237]). Detection of a different type of motion, loom or expansion, enables flies to recognize approaching danger requiring escape or avoidance, as well as to identify surfaces appropriate for landing when such surfaces are approached during flight. By using context, the details of the observed pattern, and information on the behavioral state of the fly itself, flies are able to appropriately respond to different types of looming cues [40, 56, 161, 200, 246].

Based on these observations, how can the complex, naturally occurring visual input patterns be decomposed to basic components such that the functional relations between visual inputs and behavioral outputs can be inferred? Phototaxis and color preference in flies can be studied with relatively simple accumulation or choice tests (reviewed in [44]). However, many of the other behaviors described above reflect the ability of flies to process complex optic flow patterns across their visual fields and respond in an appropriate manner based on the details of these patterns. While strong deficiencies in performance of these behaviors can also be studied with similarly simple assays, unraveling the detailed algorithms underlying motion vision requires more detailed studies.

The observation that a fly's response depends on the detailed flow patterns, together with clues provided by the structure of motion-sensitive neurons at the output of visual processing stages in the fly (see the description of the lobula complex below), gave rise to the hypothesis that motion detection is initially performed locally [104]. Downstream of such elementary motion detectors, identifying motion between pairs of points in space, neurons can selectively weight these outputs to give rise to specific sensitivities and responses to more complex patterns. Accordingly, many behavioral assays have been designed to enable relating specific visual motion features, such as velocity, size and distribution of moving objects, contrast polarity, spatial frequency and more; to specific behavioral responses - particularly rotational behaviors, or turns. Elementary motion models provide predictions of these relations and thus such experiments enable both estimating model parameters as well as testing model predictions and refining the motion computation models according to identified contradictions.

Many different types of inputs can be presented to induce turns, enabling the readout of the motion computation by the circuit. These stimuli include rotating or expanding sinusoidal or square wave gratings as well as more minimal cues that excite individual pairs of ommatidia, such as pairs of bars and dots sequentially presented in two points in space, consistent with the existence of local motion detection mechanisms [47, 67, 116]. The behavioral assays in which these responses are observed include single fly assays of flies walking on a ball [35, 47, 94, 203] or tethered flying

flies [22, 65, 92, 203, 236, 238] such that the induced or intended turning behavior can be measured. However, probing responses to motion in a variety of assays has shown that responses to motion depend on where in the field of view motion is presented and can modify other features of behavior in addition to rotation [4, 129, 231, 277]. Thus, for example, when motion is presented below a fly the fly moves against, rather than with, the direction of observed motion flow and towards the motion source [46, 123]. This clearly demonstrates that minimizing slip across the retina cannot be the only goal motion detection circuits aim to achieve. Rather, such studies suggest that motion processing is likely to be mediated by multiple, potentially interacting, pathways.

While behavioral assays probing specific types of responses to simple stimuli are useful for characterizing simple relations between specific visual input features and similarly specific behavioral output characteristics, the computations they reflect may differ significantly from computations required in naturally occurring visually guided behaviors. Efforts are made to bridge this gap, to avoid making too simplified assumptions about the computations performed by the neural circuits mediating these responses. For example, many of these assays work in an 'open loop' mode where the fly is stationary and thus its behavioral response does not affect its visual experience. This is corrected via 'closed loop' assays in which behavior is monitored and used to update the visual experience accordingly [161]. Another limitation of these assays is that they are typically performed in single animals, limiting throughput. Thus, assays for monitoring behaviors in large groups of flies are designed to address this concern. Some population assays provide a coarse description of the population response and allow screening for mutations in which motion processing is impaired [46, 93, 277]. However, even more useful population assays address the challenge of maintaining a high-resolution description of the behavior and visual experience of each fly within the assay, for all flies simultaneously [129, 175, 231].

Motion detection as a paradigmatic example for a computation performed by the brain

Due to the central role motion computation plays in fly vision as well as in this dissertation, we review this computation in more depth, and in particular highlight the prominent model for how motion may be computed in the fly visual system. This in depth view of a particular computation also provides an example for what types of computations may be implemented by neural circuits.

Responses to motion are presented not only by flies [94] but also by many other animals (e.g., beetles - [104], fish - [188]) and motion sensitive and direction selective cells are found in both invertebrates and vertebrates. e.g., many retinal ganglion cells are sensitive to different types of motion (for a review, see [24, 25, 49, 91]). Thus, understanding how this specialization arises via earlier visual processing steps, and what computational operations are implemented as intermediate steps, has been a significant challenge for the field of neuroscience for a long time. The minimal requirement for detection of motion is a non-linear interaction between captured intensities in two points in space, yet different models arrive at this computation in different manners (for reviews, see [25, 49]). For example, according to gradient-based models, the local intensity difference is divided by the temporal intensity derivative to obtain a velocity estimate [225]. A different model is based on inhibition and delay [13]. This model gives rise to direction selective (DS) responses, whereby cells strongly respond to motion in one direction, called the preferred direction, and present a suppression of activity (e.g., hyperpolarization or reduction in baseline firing rates) in response to motion in the opposite direction. In this model the asymmetry is arrived at by suppression of responses to motion in the null direction by inhibition applied between neighboring units combined with a delay, in the appropriate direction. Since responses in the opposite direction are not suppressed, direction selectivity arises. The most successful model family in invertebrate motion vision are models based on correlation of two local intensity detector outputs with a time delay. According to these models, variants of the Hassenstein-Reichardt correlator (HRC) model, the contrast change input from one point in space is delayed with respect to the contrast change input from a second point, before the two are multiplied together to generate a signal that

reports motion between these two points. Elementary motion detectors become direction selective by combining two such units in an anti-symmetric manner, such that the output of one unit is subtracted from the output of another, sensitive to motion between the same two points but in the opposite direction. The output of an HRC is thus positive for motion in one direction and negative for motion in the opposite direction [104], reflecting direction selectivity. These models are reviewed in [24].

A different type of model gained popularity in explaining motion vision in other systems. This model, the motion energy model, is based on the initial spatiotemporally coupled filtering of inputs, giving rise to velocity selectivity. These inputs are then squared and summed to give an output that is identical to the output of the HRC, with the appropriate input filtering steps, albeit intermediate operations and thus predicted intermediate signals differ [1]. As this model suggests spatiotemporally coupled filtering of the inputs to motion processing circuits, it is at least in part consistent with the findings presented in Chapter 3, functionally characterizing the cell providing inputs to motion detecting circuits in *Drosophila*.

A significant body of research demonstrates that quantitative predictions based on the HRC model are in fact supported by quantification of behavioral responses in many animals as well as recordings from motion sensitive cells. One such prediction is that a response to the same contrast change occurring in two neighboring points in space sequentially (brightening or darkening in both points, also called "phi" stimulation) is the same, and positive, for both positive and negative contrasts. Thus, direction selective (DS) cells are expected to similarly respond to bright moving objects on dark backgrounds and dark moving objects on bright backgrounds. In contrast, an opposite response is expected when two opposite contrast changes occur in two neighboring points in space sequentially (brightening in one point and darkening in the other point, also called "reverse-phi" stimulation). These predictions, which are also consistent with the motion energy model, are borne out both in animal behavior as well as in physiological responses of DS cells (*Drosophila* behavior - [245]; human psychophysiology - [29]; Primate, neural responses in area MT - [142]; fly, neural responses of lobula plate tangential cells (LPTCs) - [67, 69, 245]). Furthermore, it was recently shown that differential sensitivity to different "phi" and

"reverse-phi" stimulation can give rise to bright or dark moving edge specialization [47]. Additional predicted properties of motion sensitive neurons fed by EMD outputs include the existence of a velocity optimum in the response to moving sinusoidal gratings. In addition, this optimum should linearly depend on the spatial wavelength of the moving grating, reflecting a contrast temporal frequency optimum. Furthermore, responses are expected to quadratically depend on contrast. All these predictions are borne out in recordings from two types of direction selective lobula plate tangential cells (LPTCs), horizontal system (HS) cells and vertical system (VS) cells in *Drosophila* (see Section 1.4.2, except that saturation occurs in responses at high contrasts [115, 212], reviewed in [26].

Having identified circuits of interest by studying behavioral responses to motion, and described at least one computation performed by the fly brain, motion detection, with some detail, it is next desired to pear into the circuits and infer how these computations are implemented by the different types of neurons and synapses within these circuits. In the next section we will review the different types of tools that, together with quantitative behavioral assays, enable neural circuit dissection in *Drosophila*.

1.3 Tools for monitoring and manipulating activity in neural circuits

As described above, quantitative studies of behavioral responses to visual inputs enable answering the two first questions of neural circuit dissection, defining the goal of the circuit and the algorithm implemented to achieve this goal. By manipulating and monitoring activity in each circuit component it is possible to address the final question of neural circuit dissection and infer how computational algorithms are implemented by the circuit. However, the process of dissecting a neural circuit is less sequential and more iterative than implied by this description, since progress made in answering any of the questions can give rise to a revision of the answer to a different question and thus all circuit dissection tools in fact act together to enable

answering all questions. For example, identifying a circuit component that is correlated with sensory input in a manner that is not predicted by the algorithm for any circuit component will give rise to modification of both the implementation details as well as the suggested algorithm. Furthermore, it may be found that the modified algorithm is useful for achieving a distinct goal from the one previously suggested for the circuit, a hypothesis potentially testable with additional behavioral experiments. For this iterative process to converge on the desired outcome, detailed and accurate information about the circuit function must be extracted. This, in turn, is enabled by the continuous development and improvement of neural circuit dissection tools. Below we describe the state of the art of tools available for dissecting neural circuits, focusing on the tools most frequently used for neural circuit dissection in *Drosophila*, the model animal that is the focus of this dissertation.

1.3.1 Tools for neural activity monitoring

Most neurons in mammalian and vertebrate brains communicate via spikes or action potentials events, during which the membrane voltage of the cell changes by several tens of millivolts within a time-course of ~1 ms [125]. Thus, monitoring neural activity implies being able to detect these events. However, in early visual processing systems of both flies and vertebrates, many neurons only present graded voltage changes that are smaller and evolve more slowly, without producing spikes (the advantages of this signaling mechanism are reviewed in [121]). Nevertheless, in both types of neurons, synaptic vesicle release increases with depolarization and decreases with hyperpolarization and thus the depolarization of a graded-potential cell implies an increase in activity or output signaling similarly to an increase in action potential firing rates beyond the baseline level in a spiking cell.

For decades, electrophysiological methods have enabled reading out these electrical signals, either extracellularly or intracellularly, including in the visual systems of flies [26, 66]. However, in the small fruit fly *Drosophila* electrophysiological recordings are rare ([50]) and whole-cell patch clamp (intracellular) recordings were established only relatively recently [176, 263] (reviewed in [41, 107, 169, 192, 202]). Such recordings

provide an accurate readout , including action potential firing event timings as well as sub-threshold voltage changes, at a high temporal resolution. However, these recordings are technically challenging, particularly in a small fly such as *Drosophila*, and are performed one cell at a time, limiting the throughput. In addition, cell identity is not known unless the cell is fluorescently labeled, and signals can only be measured from cell bodies, as the neuropil consists of cell projections that are too fine and dense. Accordingly, alternative methods for neural activity monitoring, and specifically the use of microscopy to monitor neural activity, are becoming more popular, particularly due to continuous improvement of these methods.

1.3.2 Imaging neural activity

By using imaging to monitor neural activity many of the limitations of electrophysiological recordings are addressed, albeit typically at the cost of reduced temporal resolution. With imaging, it is possible to monitor activity in large populations of identifiable cells simultaneously and extract sub-cellular activity information (reviewed in [96, 108, 160]). The ability to optically probe neural activity is typically obtained by introducing fluorescent indicators of neural activity into neurons of interest and measuring fluorescence emission using a fluorescent microscope. A fluorescent molecule is a molecule that can be transiently excited from its ground energy state to an excited state by absorbing a photon and then emits a photon of longer wavelength when it rapidly decays back to its ground state, within nanoseconds. The emitted photons are collected by the microscope enabling to localize the emission source. Fluorescent molecules are characterized by their excitation and emission spectra; defining what light wavelengths are effective for exciting the molecule and what wavelengths are subsequently emitted [154]. In order to enable optical probing of neural activity, fluorescent molecules are combined with other types of molecules in a way that makes the rate of emission dependent upon an environmental variable, such as membrane voltage or intracellular Ca^{2+} concentration [177]. In subsequent sections, we first describe fluorescent indicators linking neural activity to fluorescence emission and then discuss microscopy technology that enables reading out these signals.

Fluorescent indicators of neural activity

Fluorescent indicators can be broadly divided into two types, small molecule synthetic dyes and genetically encoded fluorescent proteins (for a comparison see [136]). Genetically encoded indicators are expressed by the cells themselves, in recombinant animals, alleviating the need to introduce the indicator into the cells, which is required in the case of synthetic indicators. While both types of indicators have been used to monitor activity in larger flies [143], in the dense neuropil of the small fruitfly *Drosophila*, there's a significant advantage for using genetically encoded indicators which can be targeted to specific cell types utilizing appropriate promoters, taking advantage of the rich repertoire of genetic tools available in this genetic model animal (see Section 1.3.3). In contrast, broad expression of synthetic dyes in dense neuropil would make the signals arising from projections of different cells indistinguishable. Thus, the following discussion will be focused on genetically encoded indicators.

Fluorescent indicators of neural activity can further be divided into types according to the activity parameter which affects their emission rate. Voltage indicators are highly desired as they provide a direct measure of activity - reporting membrane voltage changes. The design of these indicators is often based on native membrane proteins, such as ion channels, that change conformation as a function of the membrane voltage applied across their intra-membranal components (for a few examples, see [6, 16, 61, 221]). The performance of genetically encoded voltage indicators (GEVIs) has been limited compared to genetically encoded Ca^{2+} indicators (GECIs), although improved indicators are continuously being developed. The main challenge for developing high-quality voltage indicators is that membrane voltage transients, especially during action potential firing, are very rapid (on the order of a few milliseconds). Thus, many voltage indicators are limited either by a slow rate of activation, which is required to enable ample time for the imaging system to measure the signal but prevents single action potential detection, or by a weak emitted signal and thus low signal to noise ratios (SNR) [107, 156]. As a result, GECIs are often preferred for *in vivo* imaging even though they provide a more indirect measure of activity [135, 193]. Here we will focus on GECIs, such as the one used in subsequent chapters of this dissertation, TN-XXL, due to its high SNR, the ability to target it genetically to

cells of interest and useful ratiometric properties (see detailed explanations on these properties below, and Chapters 2-4).

The use of GECIs to monitor neural activity is justified by the existence of multiple mechanisms that tie the intracellular Ca^{2+} concentration to neural activity. For example, Ca^{2+} concentration is related to membrane voltage via the activity of voltage sensitive Ca^{2+} channels allowing Ca^{2+} entry into the cell during depolarization, leading to an increase in the intracellular Ca^{2+} concentration. Within a pair of active and connected neurons, Ca^{2+} concentrations may increase pre-synaptically as Ca^{2+} is required for mediating synaptic release and post-synaptically via opening of appropriate synaptic receptors, such as glutamate and nicotinic acetylcholine receptors. The large variety of existing Ca^{2+} fluorescent proteins and their properties are described in many recent reviews [85, 88, 97, 135, 156, 202, 233, 241]. A popular family of GECIs are the GCaMPs, which consist of the protein calmodulin (CaM) which binds Ca^{2+} together with a circularly permuted enhanced green fluorescent protein (EGFP) and a CaM-binding peptide M13. A conformational change which occurs in this molecule when it binds Ca^{2+} gives rise to an increase in emitted fluorescence.

A particularly useful class of indicators for *in vivo* imaging are FRET (Fluorescence Resonance Energy Transfer) - based indicators. FRET is the process of non-radiative energy transfer from an excited donor fluorophore to an acceptor fluorophore, which causes donor fluorescence to decrease and acceptor fluorescence to increase. Thus, FRET events are associated with anti-correlated intensity changes in two imaging channels and a simple measure of FRET occurrence is the ratio of donor and acceptor fluorescence. Using this metric in *in-vivo* applications enables one to mitigate the effects of motion artifacts that may occur under these conditions. While motion within an imaged plane can be corrected for by post-hoc image registration, motion along the optical axis, changing slightly the region of the cell that is being imaged, is impossible to correct for as there's no access to the lost information from the part of the cell that shifted out of focus. However, while FRET events give rise to changes in the fluorescence emission ratio, motion causes correlated changes in the signals collected from two imaging channels and thus the ratio signal suppresses

motion artifacts while enhancing the activity-related signal. One example of a commonly used FRET indicator is Yellow Cameleon (YC) 3.6, a member of the cameleon family of GECIs, consisting of an ECFP donor and Venus protein acceptor components linked by CaM. In other FRET-based indicators, such as TN-XXL used in the studies described in Chapters 2-4, CaM is replaced by troponin C variants, which are proteins that bind Ca^{2+} in cardiac and skeletal muscle but are absent in neurons and thus have no endogenous binding partners [163, 164].

The choice of indicator to use depends on the match between indicator properties and the application requirements. For example, indicators vary in their excitation and emission spectra. These are particularly important to note in applications where multiple indicators are used simultaneously or combined with optical manipulation of cell activity (see Section 1.3.3) [2, 274]. In addition, the Ca^{2+} affinity, defined by the dissociation constant of the dye, K_d, the Ca^{2+} concentration at which half of the indicator molecules are bound to Ca^{2+}, defines the dynamic range of Ca^{2+} that induces approximately linear changes in fluorescent emission. Thus, indicators must be matched to the dynamic range of intracellular Ca^{2+} concentration in the imaged cells. Finally, the kinetics with which the indicator binds and releases Ca^{2+} define what activity regimes or event rates can be reliably resolved. GECIs have lagged behind synthetic dyes in Ca^{2+} affinities and thus signaling amplitudes and signal to noise ratios, as well as in kinetics, with synthetic dyes being faster. However, the most recently developed genetically encoded Ca^{2+} indicators may reach comparable performance ([3, 156, 233]).

In addition to the characteristics intrinsic to the indicators themselves, since GECIs are genetically introduced into cells, the manner in which their expression is driven also affects their utility. In particular, the maximal amplitude of fluorescent emission depends on the level of indicator expression. This level can be increased by, for example, increasing the number of copies of the indicator transgene [47], growing flies at a higher temperature or matching the imaging time with the time during development in which the indicator is driven most strongly by the genetic tool used to express it. However, while increasing the level of expression gives rise to larger signals and is thus beneficial, caution is warranted as Ca^{2+} acts as a second messenger in

many cells and its binding to the fluorescent proteins may buffer and thus modulate its operation via native Ca^{2+} binding proteins. Consequently, a high level of indicator expression may interfere with the free Ca^{2+} dynamics inside neurons and thus their function [97, 107].

As it is often difficult to know, prior to conducting the experiment, whether a good match between cell and indicator properties is likely, methods for confirming that the indicator provides a reliable measure of the actual activity are required. One possibility that became available with the recent development of multiple variants of GECIs is to compare activity recorded with multiple types of indicators [3]. As an alternative, the observation of a wide dynamic range of both increases and decreases in emitted fluorescence from a particular cell can provide confidence in the reliability with which the cell activity can be monitored. In Chapters 2-4, we have observed such a range of activities reported via a GECI, TN-XXL. Thus, we have confidence that the presented measurements of fluorescence emission reliably report changes in Ca^{2+} concentration levels. Nevertheless, the indicator kinetics necessarily limit the temporal resolution of the presented data. In spite of this limitation, since a wide range of decay rates is also observed, any signal decay that is slower than the most fast decay measured must represent a response that, physiologically, decays more slowly.

Fluorescence microscopy and optical sectioning methods

Wide field fluorescence microscopy enables imaging the spatial distribution of fluorophores across a sample by fluorescence excitation and emission collection. However, while this works well when imaging a thin sample; light scatter, the deflection of photons from their original trajectories, limits the ability to image thicker samples consisting of refractive index inhomogeneities such as brains of live animals, as it blurs the acquired images. Since live brain tissue is highly scattering, imaging a neural circuit within an intact brain requires to focus the excitation light, or the collected emitted light, to a particular plane within this volume to preserve spatial information. While this can be achieved with optical sectioning methods (described below), even when using such methods, the possible depth of imaging is limited to no more than ~1 mm [106, 183, 184, 233, 264]. Nevertheless, the brain of *Drosophila* is only a few

hundred micrometers deep, and thus can be imaged almost in its entirety with these methods.

Two prominent optical sectioning methods used for *in vivo* imaging are confocal and two-photon microscopy (reviewed in [59, 233]). In a confocal microscope, a laser is focused at a particular point within the scattering brain tissue. While fluorescence excitation occurs in many planes above and below this point, by placing a pinhole in front of the light detector, typically a PMT, fluorescence emission from all planes except one is rejected. Two-photon microscopy is an example of non-linear excitation based microscopy, where excitation is induced with more than one photon and hence depends non-linearly on the exciting light intensity [58]. With two-photon excitation, a single fluorescent molecule is excited by a cooperation of two long-wavelength, low-energy, photons arriving within a very short time-window (~0.5 fs). Since this type of excitation event has a very low probability of occurence, it requires a very high intensity of excitation light, corresponding to a photon flux of approximately 10^{20}-10^{30} photons/(cm^2/s) [58, 184]. To achieve the required excitation light intensity, the laser beam is focused via a high numerical aperture (NA) objective and the back aperture of the objective is filled, increasing the spatial density of light. High temporal light density is achieved using a mode-locked laser, typically a Titanium-sapphire laser, emitting 100 fs light pulses at a 100 MHz repetition rate. In addition, pre-compensation is used to mitigate group-delay dispersion effects of the light pathway, that broaden laser pulses in time.

Two-photon imaging offers several advantages over confocal microscopy, in particular enabling to image at a greater depth and limiting photodamage caused by light excitation. Photodamage, a combined effect of photobleaching and phototoxicity, limits the maximal possible imaging time and is a critical consideration in *in vivo* experiments. A few factors underlie the advantage of two-photon microscopy over confocal microscopy. First, in two-photon imaging, excitation is essentially limited to a diffraction-limited volume, since laser intensity falls quadratically with the distance away from the focal point along the optical axis, while with confocal microscopy a significant amount of tissue is redundantly excited with light, potentially causing

photodamage, without contributing to the resulting signal. In addition, with two-photon microscopy all signal emitted from the focal point can be collected while with confocal microscopy signal emitted from the plane of interest may be subsequently scattered and thus rejected by the pinhole. This increased efficiency in signal use with two-photon microscopy enables to increase the depth of imaging. Finally, the light wavelength used for two-photon imaging, typically IR light, is longer than the visible light often used for single-photon excitation. IR light can penetrate more deeply into tissue and causes less photodamage compared to visible light. The advantages listed above are reviewed in [59, 97, 131, 183, 184, 233, 264]. In the subsequently described studies (Chapters 2-4) we used two-photon microscopy to monitor neural activity. To minimize photodamage effects, the imaging time at each depth was limited to a few minutes and the power measured under the objective was kept below 10 mW.

A second important consideration for neural activity imaging is the frame rate, defining the rate with which neural activity signals are sampled. Both confocal as well as two-photon microscopy are laser-scanning methods. i.e., in order to obtain an image of an entire plane within the scattering brain volume a laser beam must scan across all points in this plane. The typical scanning pattern is raster scanning. This pattern is typically generated using galvanometer mirrors placed at the conjugate plain of the objective, such that their tilt-angle defines the position of the point of focus of the laser beam in the imaged plane. The raster scanning process is slow as the laser beam must reside for a few microseconds within each pixel to provide sufficient excitation to give rise to sufficient fluorescence emission required to obtain a reasonable SNR. The signal is integrated over this dwell time in each pixel and an image is constructed from this data by a computer. As a result, a tradeoff exists between the size of the field of view, which also sets the number of cells imaged, the number of pixels allocated for representing each frame, which sets the SNR obtained during processing where the average signal in all pixels within each region of interest is computed, and the frame rate. Typical two-photon imaging frame rates vary between 1 and 25 Hz [59, 233]. Nevertheless, technology to improve the temporal resolution of optical sectioning imaging methods is continuously being developed. In these systems, an increase in imaging speed is obtained using faster raster scanning speeds,

replacing scanning with random access such that only points of interest within the sample are excited and imaged, using multiple beams for excitation or even exciting the entire plane simultaneously. Fast optical sectioning methods are reviewed in [96, 97, 160, 184, 233, 264]. In the studies described in Chapters 2-4 standard two-photon microscopes were used and the typical frame-rate was approximately 10 Hz.

1.3.3 Manipulation of neural activity using genetics

Monitoring neural activity enables one to identify relations between the function of different circuit components, sensory input dynamics and behavioral outputs. However, only by manipulating the activity in these circuit components can causal relations be derived between their function and the overall computation performed by the circuit. Genetic tools enable both the observation (as described above) as well as the manipulation of neural activity with cell-type specificity by providing the ability to express different types of effectors in different types of cells. Effectors for manipulating neural activity may affect membrane voltage, receptor expression, intracellular ion concentrations or synaptic transmitter release. With some tools, external control over these parameters is mediated by light, temperature or chemical substrates, and with others the effect is constitutive (see examples below). The most useful effectors enable one to modulate activity in an acute and reversible manner. If the modulation is long-lasting, the circuit might adapt to compensate for the manipulation making its effects challenging to interpret. In particular, it is beneficial to defer the manipulation until after the nervous system has fully developed. Tools controlling the expression pattern are often developed separately from the tools modifying cell function, as described below. These tools are reviewed in [19, 23, 185, 222, 248].

Using binary systems to target genetic manipulations to specific cells

Binary systems allow one to separately develop effectors (as well as neural activity indicators) and tools for accessing all different cell types in all different circuits. With these two components, one can generate progeny expressing a particular effector in a particular cell population via a single cross. In *Drosophila*, the most widely used

binary system is the Gal4-UAS system [31]. With this system, the Gal4 sequence, encoding a transcription factor in yeast, is incorporated in the DNA of one parent line, also called the 'driver line'. The position of the Gal4 sequence insertion within the DNA of this fly, downstream of specific promoters, establishes the cell types and time during development in which the Gal4 protein will be expressed. Within the DNA of the second parent line, also called the 'reporter line', a UAS promoter sequence, also from yeast, is incorporated, and downstream of it an effector. In progeny of these two parent lines that have both the Gal4 as well as the UAS elements incorporated into their DNA, the expressed Gal4 protein binds to the UAS element and drives expression of the effector. As a result, the effector is produced in the cells defined by the Gal4 sequence position.

Collections of lines with Gal4 sequence elements inserted in different positions in the genomes have been generated with hope to achieve the ability to access different cell-types [90, 114]. In many of these lines, however, the expression patterns are very broad and include many types of neurons. This is problematic if one wants, for example, to link activity in a specific cell type to a specific behavior. Very dense expression patterns also limit the ability to use these drivers for imaging by expressing fluorescent proteins as the projections of the different expressing cells may overlap. Thus, to obtain more specific expression patterns, additional tools have been developed to enable intersecting the expression patterns of different Gal4 driver lines (reviewed in [23, 89, 107, 157, 185, 222]). Some Gal4 driver lines are, however, specific, such as the drivers used in subsequent chapters.

Increasing the utility of these tools, the development of additional binary systems enables expression of different types of effectors in different types of cells simultaneously in the same animal. Thus, one effector can be driven in one cell population via one driver and the other effector in the other cell population with the other driver. Examples of alternate binary systems include the QF system [196] and the LexA system [32]. Nevertheless, collections of parent lines from these alternative binary systems targeting different cell types are still lagging behind Gal4 driver collections in size. Thus, in the experiments described in subsequent chapters only the Gal4/UAS system was used. Appropriate driver lines for using alternative systems to drive expression

in the manipulated and imaged cells do not yet exist. An additional challenge with using these tools is that expression strengths also vary significantly between drivers. Thus, the effectors often exert only a partial effect on their targets.

Example effectors for modulating neural activity

Here we review a few of the neural activity manipulation tools that can be targeted to specific cell populations with the above described techniques. We focus on widely used tools and ones used in subsequent chapters (such as RNAi knockdown constructs) or in associated studies (such as *Shibire^{ts}* which was used in many of the behavioral experiments that enabled associating early visual processing cells with specific computations). **RNA interference (RNAi) technology** (reviewed in [182]) enables preventing the expression of a specific gene in a specific cell. This is achieved by introducing double-stranded RNA (dsRNA) molecules derived from the gene to be silenced into the cell. As a result, endogenous mRNA molecules transcribed from the same genes are degraded and translation of the gene to protein is prevented. Alternatively, short interfering RNA constructs (siRNA) that are generated from dsRNA as an intermediate step of the above described process can also be directly introduced into cells to silence genes. More broadly, manipulations in which gene expression is blocked between the transcription and the translation steps are referred to as gene 'knockdown'.

Particularly useful in the context of neural activity manipulation is the knockdown of specific type of receptors, thus blocking particular input sources to specific cells. Such a minimal manipulation of a neural circuit can shed light on its detailed operation. One limitation of this manipulation is that it cannot be activated in an acute manner, thus circuits may adapt to it, particularly when it occurs during development. In addition, knockdown effects are often partial, and off-target effects may also occur. In Chapter 4 RNAi constructs are used to knockdown GABA receptors and identify the cellular targets by which the effects of GABAergic circuits on the function of a particular cell are exerted.

While knockdown tools may block one type of input into a cell when applied to knockdown a specific type of receptor, another useful manipulation is blocking the

output of a cell, or silencing it. ***Shibire*** is a dominant-negative mutant[1] for the presynaptic protein (GTPase) dynamin, which is involved in endocytosis. Dynamin is required for synaptic vesicle recycling and thus for synaptic transmission and hence a *Shibire* null mutant constitutively blocks synaptic transmission. ***Shibire^{ts}*** is a temperature-sensitive variant of *Shibire*. Expression of this allele is induced via a shift to a restrictive temperature of more than 29°C, which reversibly eliminates synaptic transmission in the expressing cell population. It is important to note, however, that while this tool prevents neural communication via chemical synapses, electrical connections, such as gap junctions, remain open [133]. *Shibire^{ts}* is often used in behavioral experiments, to acutely silence a particular population of cells while observing behavioral responses to sensory inputs. Nevertheless, in order to completely silence a neuron by affecting both chemical as well as electrical synapses, it is beneficial to more directly control membrane voltage and in particular to hyperpolarize the neuron. A genetic effector that enables achieving this goal is **Kir2.1**, an inwardly rectifying K^+ channel expressed in human cells [12, 118, 191]. Exogenous expression of the channel in *Drosophila* neurons gives rise to membrane hyperpolarization and prevents activation; thereby silencing these neurons. The caveat of using this effector, however, is that its activity is not restricted in time.

To gain full external control on membrane voltage and enable its acute and rapid manipulation **optogenetic tools** have been developed (reviewed in [57, 268]). In particular, delivery of microbial opsin genes, encoding light-sensitive ion channels and pumps, enables one to manipulate membrane potential and induce or eliminate spiking by light with precise temporal control. Continuous development of optogenetic tools differing in their spectral sensitivities and conductances increases the flexibility and applicability of these methods. For example, cells expressing the light-gated cation channel Channelrhodopsin-2 (ChR2) reversibly depolarize upon excitation with blue light (~470 nm). Expression of halorhodopsin, a light-gated chloride pump that moves Cl^- ions from the extracellular into the intracellular space, enables to hyperpolarize neurons upon excitation with yellow light (~580 nm). In order to apply these methods in *Drosophila*, it is required to feed the flies with retinal, a co-factor required

[1] When a dominant-negative mutant protein is expressed the native protein no longer functions.

for opsin function (reviewed in [89, 222]). In addition, when these effectors are used for behavioral experiments, a direct effect of the light on fly behavior must be eliminated, e.g., by using fly mutants with phototransduction deficiencies that are hence blind [55]. Rather than using light to depolarize and thus activate cells, activation can also be obtained by heating, via expression of a warmth-sensitive cation channel, dTRPA1 and a temperature shift to above 25 °C [197].

Having reviewed the tools available for neural circuit dissection in the fly we would like to address the question of how these tools may be applied to dissect the circuits mediating the rich repertoire of visually-guided behaviors described in Section 1.2.1. Even though the details of how the computations enabling flies to link visual inputs to behavior outputs are implemented by specific circuits have not yet been unraveled, a significant body of knowledge exists on the anatomy and function of different types of neurons involved in processing visual information. Thus, in the next section we lay out the known structural and functional properties of the fly visual system enabling to phrase hypotheses regarding the potential implementation of computations which in turn can be tested using these tools.

1.4 Fly vision

To dissect a neural circuit it is first required to understand what inputs are available to the circuit for performing computations and informing behavior. These inputs are defined by the receptors used to measure the characteristics of the external environment. In the case of visual processing in the fly, this implies understanding how the fly's eye samples light intensities in space and time. i.e., what is the temporal and spatial resolution of sampling and with what spectral sensitivities are these samples taken. The eyes of flies are clearly very different from human eyes. Thus, we will start our exploration of fly vision with a description of the fly eye characteristics and a comparison between the visual abilities of flies and humans.

1.4.1 Flies have compound eyes

The eyes of *Drosophila* are compound, comprised of an array of ~800 units, called ommatidia, each capped with a small lens element [174]. Compared to humans, fly vision is characterized by a relatively low spatial resolution, limited by the compound eye structure, and very high temporal resolution. The spatial resolution is limited by both the interommatidial angle defining the spatial sampling frequency as well as the acceptance angle setting the spatial filtering properties of each unit. The acceptance angle of *Drosophila* ommatidia is ~5.7° and the interommatidial angle is comparable, ~5.1°. As a result, the spatial resolution is limited by the sampling frequency [144, 230]. For comparison, the spatial resolution of the human fovea set by both the inter-receptor distance and the eye optics is 1/60°, providing a spatial resolution approximately 100 times higher [144].

Within each ommatidium photoreceptors convert photon inputs to neural activity outputs. A fast G-protein dependent phototransduction cascade, gives rise to fast impulse responses in fly photoreceptors, peaking within 10-50 ms [102, 110]. As a result, the temporal resolution of fly vision, defined by the receptors flicker fusion rate, can be very high. For example, flicker fusion rates of ~200 Hz were measured in large flies, and the temporal resolution in *Drosophila* is slightly lower, with a cutoff frequency of ~150 Hz or less [8, 51, 181, 207, 224]. For comparison, flicker fusion rates in humans do not exceed 55 Hz [125].

In diptera such as *Drosophila* each ommatidium consists of 8 photoreceptors. 6 external photoreceptors, R1-R6, are arranged around the border of the ommatidium. 2 smaller photoreceptors, R7 and R8, are positioned in the center of the ommatidium, with R7 positioned on top of R8 [74, 99, 168, 170]. As a result of this organization, these photoreceptors collect light from different angles in space. However, all 8 photoreceptors from 7 different ommatidia that collect light from the same spatial angle send projections to the same column in the downstream neuropils, giving rise to retinotopy and increased SNR immediately downstream of the retina. This type of organization is called 'neural superposition' [30, 132, 251].

1.4.2 The fly's optic lobe

In addition to characterizing the inputs into the circuit, neural circuit dissection can further be informed by surveying the neural elements available for implementing computations. The brain of *Drosophila* consists of ~100,000 neurons and each of the optic lobes, where visual processing is performed, consists of ~30,000, consistent with vision being a critical faculty for the fly. Anatomical studies of circuit connectivity give rise to hypotheses regarding the function implemented by these circuits. Such studies are particularly useful when combined with physiological and functional characterization of at least some of the circuit elements, allowing one to hypothesize computational roles for other circuit components. In *Drosophila*, a lot is known about the anatomy of the optic lobe. The optic lobe consists of 3 visual ganglia downstream of the retina: the lamina, the medulla, and the lobula complex, composed of the anterior lobula and the posterior lobula plate. Cell bodies typically reside outside these ganglia and their axons and dendrites form these dense neuropils. The retinotopic map formed in the lamina as described above is preserved in subsequent ganglia; although this mapping is inverted twice around the anterior-posterior axis, once between the lamina and the medulla and again between the medulla and the lobula complex [74]. Many different cell types in the optic lobe have been characterized, albeit a connectivity map exists only for the lamina. Functional information is more partial, as studies focused on photoreceptors and first order interneurons in the retina and the lamina, respectively, as well as on downstream cells in the lobula plate, reflecting the outputs of the optic lobe. The density of the intermediate neuropil, the medulla, combined with the small size of most neurons in this region, so far prevented functional characterization. Below we provide a brief overview of the well-known neural components in the *Drosophila* optic lobe, focusing mostly on neural elements that are known to be involved in motion processing, the circuit that will be explored in subsequent chapters.

The retina

The external and internal photoreceptors of the *Drosophila* ommatidium described above, R1-R6 and R7-R8, differ in their spectral sensitivities and send outputs to different processing pathways serving different goals. The first evidence that these photoreceptors serve different pathways comes from anatomy. While R1-R6 provide inputs to laminar monopolar cells (LMCs, see details below) in the lamina, R7 and R8 send projections directly to the medulla, with R7 terminating in M6 and R8 terminating in M3 [74, 235]. Furthermore, behavioral experiments combined with genetic manipulations of neural activity provided additional evidence for a functional separation. In particular, it was shown that the external photoreceptors R1-R6 provide inputs to motion detection circuits while R7 and R8 are thought to be involved in color vision and phototaxis behaviors [105, 266, 277]. Nevertheless, evidence exists for the involvement of both receptor systems in both types of behaviors, suggesting interaction between these pathways [252, 265].

In support of these different functional roles, as mentioned above, the spectral sensitivities of these receptors also differ. External photoreceptors R1-R6 express the opsin Rh1 and are sensitive to blue-green light (the sensitivity of this opsin peaks at ~475) [210, 229]. Each R7 receptor expresses one of two possible rhodopsins, Rh3 and Rh4; both UV-sensitive. Each R8 receptor also expresses one of two possible rhodopsins, Rh5, a blue sensitive opsin with a peak at ~440 nm, or Rh6, a green-yellow sensitive opsin with a peak at ~510 nm [45, 99, 190, 210]. In the dorsal rim of the eye, R7 and R8 both express the UV sensitive rhodopsin Rh3 and are sensitive to polarized light [77].

The response characteristics of photoreceptors, and in particular R1-R6, constitute the first neural signal available for visual processing circuits and encode input intensity information. While vertebrate photoreceptors hyperpolarize to light, the photoreceptors of the fly present sustained depolarizations to light and hyperpolarize to dark. Via a limited dynamic range of voltage outputs, photoreceptors must encode a very wide dynamic range of light intensities, capturing both day light levels as well as functioning in near-complete darkness. Over the course of a day, light intensity amplitudes may increase by a factor of 10^4. Encoding this wide dynamic range

is enabled via light adaptation mechanisms. A logarithmic transformation relates input light intensities to photoreceptor voltage outputs, such that a mean depolarization level encodes the mean intensity and contrast changes cause superimposed fluctuations in photoreceptor voltage. The exact response shape depends on the light intensity: at low light intensities the response is sustained with only a weak decay observed during light presentation, while at high light intensities the response consists of a fast and strong transient followed by a rapid decay to a plateau level. These two response phases reflect two different rates of adaptation [113, 122, 145, 146, 152], reviewed in [149]. Upon depolarization, photoreceptors release the neurotransmitter histamine [98, 100, 235].

The lamina

Downstream of the retina, the lamina is the first visual neuropil, where the processing of light intensity signals represented by photoreceptors initiates. The most important cell types in the lamina from a motion-detection perspective are likely the lamina monopolar cells (LMCs) and in particular L1 and L2 cells (described below). These cells receive direct photoreceptor output and it has been argued that these cells are both necessary and sufficient for mediating optomotor responses [47, 116, 203]. The functional characteristics of these cells are described in depth in Chapters 2 and 3. More recent findings, however, suggest that L3 cells, also receiving direct photoreceptor inputs, provide an additional input to these circuits [cite silies when out]. Furthermore, the dense connectivity between multiple cell types in the lamina [170, 204] may play significant roles in shaping the inputs to motion detecting and other visual processing circuits. In particular, in Chapter 4 we show potential roles for this connectivity in shaping L2 cell responses. Thus, we provide a brief overview of the different neural components of the lamina below.

The lamina is electrically separated from the retina and divided into electrically isolated units called cartridges, encapsulated by epithelial glia. It is hypothesized that these electrical barriers may contribute to signal shaping in LMCs via extracellular effects on the photoreceptor-LMC synapse [219, 256]. Due to the neural superposition principle mentioned earlier, the input arriving at each lamina cartridge represents a

sample from a single angle in space. A characteristic of the *Drosophila* brain connectivity pattern is that synapses often involve multiple post-synaptic elements and thus, for example, the outputs of R1-R6 diverge within tetrade synapses to multiple targets, four in each synapse. Both L1 and L2 cells receive photoreceptor input together in each of these synapses, while the other elements vary [74, 168, 170, 180]. Different LMCs are characterized by different distributions of dendrites in the lamina and positions of axonal terminals in the downstream neuropil, the medulla. L1 cells have two medullar terminals, M1 and M5; while L2 cells project to M2 only [74]. In Chapter 2 we target these terminals to record the outputs of these cells via Ca^{2+} imaging. In addition, L1 cells are suggested to be glutamatergic while L2 cells are suggested to be cholinergic [234]. Other LMCs include L3 cells which project to M3 and two other LMCs, L4 and L5, that receive photoreceptor inputs only indirectly [152, 180]. L4 cells are reciprocally connected to L2 cells and project to both M2 and M4. L5 cells project to M1, M2 and M5, and are reciprocally connected with L1 [74, 170, 235].

We defer the detailed description of the characteristics of LMC responses to light to Chapter 2. Briefly, the photoreceptor-LMC synapse is sign-inverting and LMCs present transient depolarizations to light offsets and hyperpolarizations to light onsets. Thus, if photoreceptors can be described as low-pass filters of light intensities, LMCs high-pass filter these outputs and thus encode contrast changes. The hyperpolarizing response of LMCs to light is mediated via histamine-binding Cl^- channels expressed by the LMCs [98, 100].

While the spread of LMC signals to different medulla layers may represent parallel visual processing pathways [17, 74, 235] and see below, dense connectivity in the lamina gives rise to many potential feedback and lateral interactions within and between these pathways. Thus, for example, reciprocal connections between L2 and L4 cells in dorsal and ventral posterior neighboring cartridges may mediate front-to-back motion computation [234]. In addition, photoreceptors receive feedback from many cell types including L2 and L4 cells, amacrine and wide-field cells, where the latter two cell types collect input from more than a single column [170, 204, 234, 275]. Such feedback circuitry may give rise to non-local intensity information early in the visual processing

stream. Finally, two medullar centrifugal neurons, C2 and C3, project into the lamina and provide feedback inputs to multiple laminar cells. In particular, L1 receives input from C3 and L2 from both centrifugal cells. These cells extend through multiple layers in the medulla and are suggested to be GABAergic [34, 74, 138, 170, 204, 235]. Thus, the activity in early visual processing neurons may be affected by the outputs of more specialized downstream pathways. In chapter 4 we apply pharmacology and genetic tools to start to unravel the functional significance of this dense connectivity and in particular the role played by cholinergic and GABAergic circuits described above.

The medulla

Downstream of the lamina, the medulla is a very dense neuropil, with currently unknown connectivity. The functional properties of most medullar cells are also unknown. Nevertheless, this neuropil is suggested to play a critical computational role in motion detection. In particular, it is hypothesized that local motion detection takes place in the medulla, while downstream cells in the lobula complex are suggested to integrate over these inputs to become motion sensitive and direction selective [115, 212], reviewed in [23, 25, 27].

The medulla is divided into 10 layers and consists of approximately 60 different cell types. Some of these cells, such as the medulla intrinsic (Mi) neurons connect between different medulla layers. Other cell types, such as transmedullar (Tm and TmY) neurons connect the medulla with the lobula complex [74]. These cells are divided between the different parallel processing pathways suggested to arise in early stages of visual processing [17, 74, 235]. Accordingly, L1 is thought to send information through Mi1 and Tm3 to T4 neurons, which connect the proximal medulla with the lobula plate. L2 cells provide inputs to both Tm1 and Tm2 which eventually send information to T5 neurons, connecting the lobula with the lobula plate [17, 74, 235]. Recently, behavioral and electrophysiological investigations combined with genetic manipulations revealed potential functional differences between these pathways (these are reviewed in more detail in Chapter 2). In particular, it was suggested that the L1 pathway mediates responses to bright moving edges while the L2 pathway mediates

responses to dark moving edges [47, 116]. The last elements in the above described pathways, T4 and T5 cells are bushy T-cells. Four different sub-types of these neurons project to the four different lobula plate layers (see below). Recently, activity in these neurons was shown to be required for motion sensitivity in downstream neurons [213].

The lobula complex: lobula and lobula plate

In this neuropil, providing the output of the optic lobe, neural activity represents the outcomes of upstream computations. Thus, many cells in this complex are motion sensitive and reflect significant computational specialization. For example, lobula plate tangential cells (LPTCs), described in more detail below, are sensitive to wide-field motion inputs and are direction selective (reviewed in [26]). More recently, a set of lobula and lobula plate neurons were found to be sensitive to visual expansion associated with looming objects [56].

Structurally, the lobula consists of 6 different layers and the lobula plate consists of 4 [74]. A study using radioactive deoxyglucose labeling to correlate visual inputs with active areas in the *Drosophila* optic lobe found that each layer of the lobula plate is associated with processing of motion with a distinct direction selectivity [36].

Within this complex, LPTCs represent the most thoroughly studied cell types. These neurons are characterized by broad dendritic arbors collecting inputs from many retinotopic columns in preceding neuropils and project to the central brain. Some of these neurons contact descending neurons that mediate behaviors such as head movement and locomotion [74, 212]. Thus, the functional specialization of these neurons likely reflects at least some of the upstream computations that modulate behavior. LPTCs can be divided into two systems based on their morphology and orientation preference. The first system consists of cells sensitive to horizontal motion (HS cells), the second of cells sensitive to vertical motion (VS cells) [74, 115, 212, 216]. The sensitivities of LPTCs to motion patterns across visual space were found to be matched with the optical flow fields expected to arise during typical turning maneuvers performed by flies, such as roll, pitch and yaw turns [74, 140, 141].

Direction selectivity is reflected in HS and VS cell responses to wide-field sinewave grating motion. Both HS and VS cells depolarize, and increase their firing rate, in

response to motion in the preferred direction and hyperpolarize, decreasing their firing rate, in response to motion in the opposite direction. Nevertheless, these cells also respond to flicker [116, 212]. Recently, simultaneous measurement of activity in LPTCs, via electrophysiology or imaging, and behavioral output, revealed that the response properties of LPTCs are sensitive to the behavioral state of the fly [42, 162].

In subsequent chapters, we will try to relate our observations of the functional properties of early visual processing cells to these functional characteristics of the outputs of the optic lobe and the outputs observed by monitoring behavior.

1.5 Specific contributions to dissertation chapters

Chapter 2: The work described in this chapter was done in collaboration with Damon Clark, PhD. My specific contribution to this work included improving the imaging and stimulus presentation system together with Damon, running imaging experiments, writing some of the data processing code, using this code to generate figures and editing the paper [47], with which the text below overlaps. **Chapters 3 and 4**: The stimulus presentation setup modifications described in Chapter 2 were designed by Damon Clark, PhD and implemented by both Damon Clark and Jeniffer Esch. The stimulus code for moving sinusoidal gratings and for presenting circles and annuli of different sizes was written by Damon Clark. My specific contribution to this work included conducting all imaging experiments as well as writing all analysis and stimulus presentation code extensions (with the exceptions mentioned here), as well as writing the paper [78] which overlaps significantly with the contents of these chapters.

Chapter 2

Functional characterization of first order visual interneurons in *Drosophila*

2.1 Introduction

While both L1 and L2 laminar monopolar cells (LMCs) receive inputs from external photoreceptors R1-R6 through shared synapses, these two different cells send output projections to different layers in the medulla, thus providing inputs to two anatomically separate pathways [17, 74]. This anatomical separation gave rise to the hypothesis that the pathways downstream of L1 and L2 must also be functionally distinct, and that L1 and L2 cells themselves are unlikely to be functionally identical. The difference between the pathways was identified recently. In particular, it was found that L1 and L2 provide inputs to bright and dark moving edge detecting pathways, respectively [47, 116] (see details below).

The properties of L1 and L2 cells have been examined over the last 30 years using electrophysiological recordings (reviewed below), in a variety of fly species, but no significant differences between the cells were identified. The development of novel, more sensitive genetically encoded Ca^{2+} indicators, combined with improvements in neural activity imaging technology, opened a new avenue for functional studies of

the lamina. Using such tools, and specifically the genetically encoded Ca^{2+} indicator TN-XXL, a recent study described the responses of L2 terminals to long-duration light flashes. Responses to light offset observed in this study were more prominent than responses to light onset, and it was concluded that L2 is "half-wave rectified", responding primarily to light decrements and not to increments [199]. It was further hypothesized that L1 cells are half-wave rectified in an opposite manner, responding only to increments, and that this early specialization gives rise to the selectivity of the downstream pathways for moving edges of different contrast polarities [116].

In this chapter we present Ca^{2+} imaging data from both L1 and L2 cells, examining responses across a wider range of stimulus conditions. In particular, we test whether rectification is reflected in the outputs of L1 and L2 cells by monitoring responses to dynamically changing contrast inputs. While some asymmetry in the strength of responses to bright and dark inputs is found, with L2 cells responding more strongly to decrements, importantly, both cell types respond to both light increments and decrements. Thus, it seems that if rectification underlies the L1 and L2 pathway selectivity to bright and dark moving objects, it must occur downstream of these cells. Nevertheless, this does not eliminate the possibility that the response properties of these cells facilitate the contrast polarity separation via their detailed response properties and this possibility will be explored in more depth for L2 in Chapter 3.

2.1.1 The functional properties of L1 and L2 cells as revealed by electrophysiological studies

While electrophysiological studies in LMCs did not find differences between the functional properties of L1 and L2 cells, these studies gave rise to a significant body of knowledge characterizing the photoreceptor-LMC synapse. Thus, these studies revealed that under bright illumination, LMCs transiently hyperpolarize to light increments, depolarize to decrements, and have antagonistic center-surround organizations. Consequently, LMCs encode contrast changes around an average illumination level in space and time.

Since photoreceptors present more sustained responses to light [113, 122, 146],

Section 1.4.2, this property must arise at the photoreceptor-LMC synapse. It was suggested that this synapse amplifies contrast signals to efficiently utilize the dynamic range of LMC signaling. In addition, response shapes were found to depend both on the light adaptation state of the cells as well as on the spatial extent of the stimulus. Thus, a decrease in the illumination level gives rise to reduced spatial antagonism and an increase in the spatial extent of the input gives rise to stronger light-off transients [63, 247, 100, 113, 145, 146, 148, 152, 153, 227]. However, in these detailed studies, no significant differences in function were found between different types of LMCs. At most, it was suggested that L2 cells are more strongly affected by lateral antagonism than L1 and L3 [153].

2.1.2 Behavioral studies reveal functional differences between the L1 and L2 pathways

More recently, genetic tools enabling the manipulation of activity in different subsets of LMCs became available. Using these tools it was shown that these cells provide inputs to downstream motion detecting circuits [47, 116, 203]. In particular, synaptic silencing of these two neurons using $shibire^{TS}$ resulted in loss of optomotor behavioral responses to moving gratings [47, 203] and electrophysiologically measured direction selective responses to motion in horizontal system (HS) and vertical system (VS) lobula plate tangential cells (LPTCs) [116]. Thus, L1 and L2 cell function is necessary for mediating responses to motion.

In addition, activity in these neurons was also found to be sufficient to allow motion responses to occur. Specifically, in mutants lacking histamine receptors in all neurons (ort^1 and ort^{US2515} mutants), such that photoreceptor outputs cannot be detected by any downstream target, motion responses were found to be impaired. However, rescue of histamine receptor expression in L1 cells or L2 cells or both cell types, enabling only these cells to respond to photoreceptors outputs, was sufficient to give rise to motion responses indistinguishable from those of negative controls [203]. These results imply that L1 and L2 act redundantly at high contrast conditions in providing inputs to motion detection circuits. Nevertheless, at low contrast conditions

both cell types were found to be required to function together to mediate responses. These studies further identified a few differences in the characteristics of the pathways corresponding to L1 and L2 cell outputs. In particular, the L2 pathway was found to show higher contrast and low-light sensitivity compared to the L1 pathway. Furthermore, at intermediate contrast levels, the two pathways were found to mediate motion responses in different directions: the L2 pathway mediated responses to front to back motion while the L1 pathway mediated responses to back to front motion.

In a subsequent study it was shown that turning and translation behaviors are modulated differently by various motion stimulus parameters [129]. i.e., while both behaviors are modulated by the presentation of a moving dots stimulus, translation is insensitive to the density of the dots but sensitive to their velocity while rotation is sensitive to both. This implies that pathways mediating effects on these two aspects of behavior must be separate. Furthermore, silencing experiments demonstrated that the pathways split immediately downstream of photoreceptors. Of these two pathways, the L2 pathway was found to affect modulation of translation behavior (or forward walking) more strongly than rotation behavior (or turning) under the stimulus conditions presented [129]. More broadly, this study supports the notion that motion processing may occur via multiple parallel pathways and that differential sensitivities to the spatiotemporal properties of inputs may play a role in this segregation.

More recently a clear division of motion processing between the L1 and L2 pathways was identified. In particular, silencing experiments conducted in either L1 or L2 cells only resulted in at least a partial loss of responses to moving bright and dark edges, respectively [47, 116]. This held true for both directional responses to motion recorded electrophysiologically in LPTCs [116] and optomotor responses to motion presented by single flies walking on a ball [47]. These studies imply that each of these cell types provides input to a pathway differentially specialized to detect motion of different types of objects. The L1 pathway is specialized for the detection of moving bright edges and the L2 pathway for the detection of moving dark edges. This raises the questions of where in the circuit and how the specialization arises.

Reiff et al. (2010) proposed that the specialization arises via rectification of L1

and L2 cell outputs. This model is appealing since signal rectification is thought to be a critical component of local motion detection in one possible implementation of the Hassenstein-Reichardt Correlator (HRC) model [104] (see also Section 1.2.1). According to the HRC model, motion between two points in space is computed by introducing a delay between the two input signals and then performing sign-correct multiplication of these inputs. Thus, two negative and two positive inputs give rise to a positive output while a combination of negative and positive inputs gives rise to a negative output. This sign-correct multiplication is difficult to implement within a single synapse, and thus a preceding rectification step, separating negative and positive inputs prior to multiplication, could facilitate the computation.

In order to assess whether such a separation was indeed implemented in the L1 and L2 pathways, the behavioral and electrophysiological responses to minimal motion cues consisting solely of positive inputs (contrast increments), negative inputs (contrast decrements) or combinations of these inputs (a contrast increment followed by a decrement or a decrement followed by an increment) were compared in L1 and L2 silenced flies [47, 117]. Interestingly, both L1 silenced flies and L2 silenced flies responded to motion stimuli combining increments and decrements. In particular, the L2 pathway was shown to specifically mediate responses to increments followed by decrements while the L1 pathway specifically mediated responses to decrements followed by increments. In addition, both pathways were shown to be sufficient to mediate behavioral responses to increment motion cues and to decrement motion cues [47]. These studies provide evidence that increment and decrement information may not be completely segregated between the L1 and L2 pathways, rather these pathways may differentially process different contrast inputs in different ways. Nevertheless, there is controversy in the literature as to what model correctly explains these results, and one suggested model fits these observations together with rectification occurring at the LMC output stage. According to this model, the rectification is partial in the L2 pathway and an additional input component which follows contrast rather than encode contrast changes feeds into the downstream correlators [117].

Putting all evidence together, it remains unclear how and where in the circuit rectification may be implemented and only a thorough examination of L1 and L2

responses to different spatiotemporal distributions of light inputs can decisively show whether rectification occurs at this early stage.

2.2 Methods

The imaging experiments described in this chapter were performed using a Prairie scanning two-photon microscope (Prairie Technologies, Middleton, WI) with a 20X, 0.95 NA objective (Olympus, XLUMPlanFl) and a pre-compensated Chameleon femtosecond laser (Coherent, Inc., Santa Clara, CA). We used an excitation wavelength of 830 nm and maintained a power lower than 20 mW under the objective. The scanning pattern was unidirectional, the average number of rows in each image was 38.2 $\pm$ 8.5 pixels and the average number of columns was 135 $\pm$ 30.4. The average imaging frame rate was 10 $\pm$ 2.7 Hz across all time-series. Imaging experiments lasted approximately 2 hours per fly.

2.2.1 Visual stimulus delivery

Recording the responses of L1 and L2 cells to visual inputs required the design of an imaging system that enables visual stimulus presentation under the two-photon microscope. This system is schematically described in Figure 2.1A. Visual stimuli were coded in C++ using the OpenGL library and projected via a digital light projector (DLP, Infocus DepthQ, Bellevue, WA) onto a 4 $\times$ 4 mm coherent optic fiber bundle (100 fibers/mm, 0.63 NA; from Schott, Elmsford, NY). The fiber span a region covered by ~100 $\times$ 100 pixels and provided a spatial stimulus resolution of ~1°.

The native frame-rate of standard DLPs is 120 Hz, too slow for presenting visual stimuli to a fly [51, 224], and Section 1.4.1. However, within each frame the DLP sequentially presents different color components of the frame - blue, red, green and white. Thus, we have used a modified DLP where the color-wheel was removed and the blue and green frames were used to present 2 different stimulus frames, such that a final rate of 240 Hz was obtained.

An optical fiber bundle in front of the projector delivered the DLP light output

to the front of the fly and served as a screen for presenting the stimulus to the dorsal front portion of one of the fly's eyes. This, in turn, required that the visual inputs be observable by the imaged fly but not detected by the microscope PMTs to avoid contamination of the imaging data. To achieve this, we spectrally separated the presented stimulus from expected fluorescence emission, displaying a wavelength that is distinct from the wavelengths passed by the emission filters in front of the PMTs. In selecting emission filters we first took into account the spectral characteristics of the fluorescent indicator used, TN-XXL. With TN-XXL, an increase in intracellular Ca^{2+} concentration causes an increase in Citrine cp174 fluorescence emission, which is maximal at 525-530 nm [163] and a decrease in CFP fluorescence, which is maximal at 460-470 nm [195]. Another critical consideration for the selection of visual stimulus wavelengths is to efficiently stimulate the photoreceptors R1-R6 providing inputs to L1 and L2. These photoreceptors express the rhodopsin Rh1 that has a broad high spectral sensitivity peak at ~475 nm [210, 229]. Thus, we first selected to present flies with a visual stimulus at a wavelength of ~490 nm using a combination of two bandpass filters, a 475/35 filter and a 497/16 filter in front of the broad spectrum light output of the DLP [1]. For emission collection we then used a 447/60 bandpass filter for CFP collection together with a 536/40 filter for Citrine collection (Semrock, Rochester, NY). CFP and Citrine emitted photons were separated via a 495-LP (low-pass) beam splitter (Semrock, Rochester, NY) (Figure 2.1B, top).

Ideally, with this set of filters no stimulus light should have reached the microscope PMTs. However, light artifacts were observed in the Citrine channel output of the imaging data collected with this filter set. This was due to several reasons. First, we found that the optical fiber bundle that brings the DLP light to the front of the fly auto-fluoresces in response to the 490 nm light input. As a result, light emitted from the fiber under the microscope consisted of spectral components with long enough wavelengths to be passed by the Citrine emission filter. In addition, we found that some auto-fluorescence also occurred when the light reached the fly and the mount. To mitigate these effects we included a second stimulus filter in

[1] All bandpass filters are described by their central wavelength / the width of the pass-band in nanometers

front of the optical fiber bundle between its edge and the fly's eye. In addition, we added neutral density filters between the DLP output and the fiber bundle to reduce the overall light intensity while still effectively stimulating the fly eye (as judged by observed responses). While these modifications reduced the artifacts, these were not completely eliminated. We hypothesize that one remaining source of contamination is that the stimulus light, which is not focused on the sample, reaches the emission filters at a range of different angles. We have measured that for light that does not reach the optical filters perpendicular to the filter plane the pass-band range shifts to higher wavelengths with respect to the range of wavelengths designed to be passed by the filter. Thus, it seems like when using stimulus light with wavelengths lower than emission filter wavelengths, there is in fact no way to completely eliminate this type of artifact. Nevertheless, the effects of the artifact were mitigated by subtracting the background noise from the signal in regions of interest. This strategy works since the artifact is approximately uniform in all regions of the acquired image.

Since the artifact was not completely eliminated, we devised an alternative way to solve this issue. In particular, we selected a different stimulus filter that passes longer wavelengths, a 575/25 filter (Semrock, Rochester, NY). This also allowed us to change the Citrine emission filter to a 525/50 filter, for improved collection (Figure 2.1B, bottom). Even though Rh1 absorption is relatively low in this range of wavelengths, because the DLP output intensity is high, this stimulation was sufficiently strong to reliably drive responses in L1 and L2 cells. Furthermore, comparing responses to a stimulus wavelength of ~490 nm with this longer stimulus wavelength we observed no significant difference in response shapes (Figure 2.3A). The distance between the fiber bundle and the fly eye was 2 mm when the stimulus wavelength was ~490 nm, and an optical filter was positioned between the fiber and the eye. For the longer wavelength stimulus this additional filter was not required and the distance was ~1 mm.

Alignment of cell responses with visual stimulus inputs in time required the simultaneous acquisition of stimulus output information together with the timing of acquired fluorescent images. We obtained this alignment by presenting a brief flash to a photodiode that was positioned above the optical fiber bundle on which the

stimulus was presented, when the stimulus presentation started and every time the stimulus output changed. The output of this photodiode was acquired as a third imaging channel and thus was synchronized with the timing of the other two imaging output channels. This allowed us to align imaging data to the time-points at which different stimuli were presented.

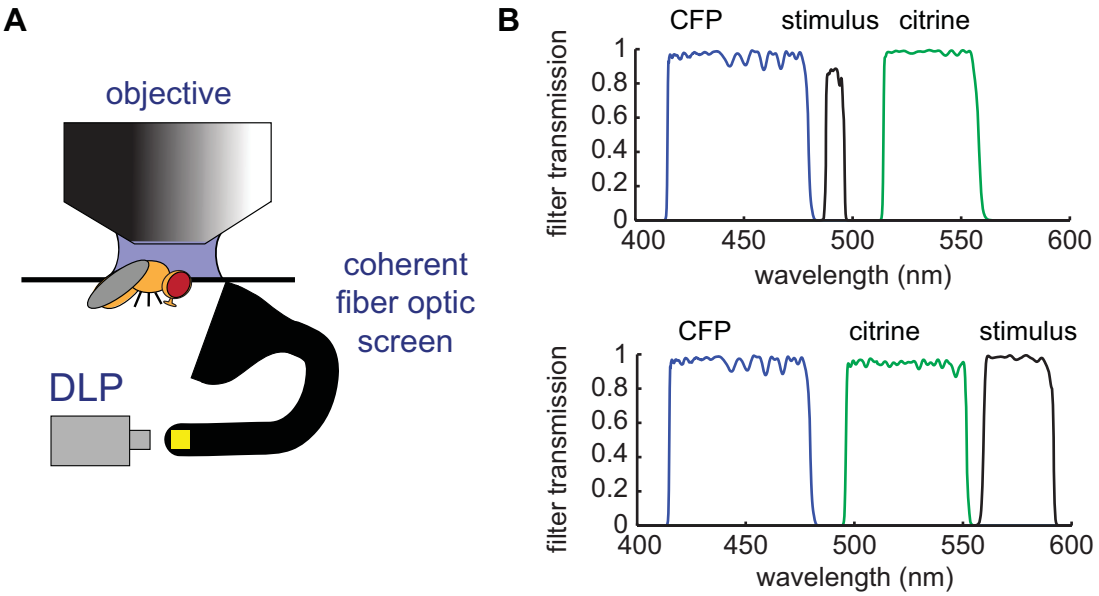

Figure 2.1: Imaging setup and filter sets. **(A)** Schematic illustration of the imaging set-up. DLP = Digital Light Projector. **(B)** The set of emission (CFP, Citrine) and stimulus filters used. Top: Interleaving the stimulus spectrum between the two imaging emission filters, to strongly stimulate the Rh1 rhodopsin expressed by R1-R6 photoreceptors. Bottom: Using a long-wavelength stimulus to completely eliminate contamination of imaging data with the stimulus output.

2.2.2 Fly stocks and handling

Two Gal4 drivers, a split-Gal4 driver ortc1-3VP16ADvglutDBD (from [84]; which has strong expression in L1 but also in a few other cells in the medulla and is hence incompatible with imaging in M5) and L1-Gal4 (c202a from [203]; which has weak expression but is cleaner in the medulla with respect to the alternative driver) were used to express a multi-copy insert of the Ca^{2+} indicator UAS-TN-XXL (from [164];

as in [47]) in L1 cells. For driving expression of the indicator in L2 cells, the Gal4 driver 21D-Gal4 (from [203]) was used. In the list of fly lines provided below, we use standard nomenclature for indicating fly genotypes (see, for example, [95]). In particular, we indicate insertions into chromosomes 1-3 (1 being the sex chromosome), chromosomes are separated by semi-colons, '+' signs indicate non-modified chromosomes and insertions on specific chromosome allels are as listed. While flies have 4 chromosomes, the 4^{th} chromosome is small and flies with insertions in this chromosomes were never used. Thus, the following fly lines were used in imaging experiments:

+ ; + ; 21D-Gal4 / UAS-TN-XXL ("L2")

+ ; L1-Gal4 / + ; UAS-TN-XXL / + ("L1a")

+ ; ortc1-3VP16ADvglutDBD / + ; UAS-TN-XXL / + ("L1b")

Imaging crosses were grown on molasses-based food at 25°C and flipped every 2-3 days. Flies were collected for imaging 1-2 days after eclosion using CO^2 for brief sedation and imaged on the same day or the next. In order to mount flies for imaging, flies were briefly immobilized using cold. The fly mount was made of a stainless steel sheath in which a hole was cut such that it matched the size and shape of the fly thorax and head. The stainless steel sheath was found to be superior to iodized aluminum and thin plastic mount alternatives. The head was tilted forward by ~60° through the hole in the mount such that the back of the head capsule was exposed for dissection and most of the retina (except for 1-2 rows of ommatidia) was below the foil. The fly head was glued to the mount using UV-cured epoxy which was dried by application of UV light for 40-60 s.

When the fly was mounted and glued we covered its back with a cold Ca^{2+}- and sugar- free saline solution [263] and removed the cuticle as well as trachea and fat bodies above the optic lobe. During imaging, this solution was replaced with room-temperature, Ca^{2+} and sugar containing saline which was perfused together with carbogen over the back of the fly.

2.2.3 Imaging protocol

At the beginning of every imaging experiment, the objective was first crudely positioned above the fly eye using bright field illumination. Then, two photon imaging was initialized at low digital zoom. Once the medulla was identified, we zoomed in on superficial, posterior projections in the medulla (receiving inputs from the anterior part of the eye). Small subsets of projections (containing 11.6 $\pm$ 2.9 cell projections on average) were imaged (Figure 2.2). The size and shape of the frame were chosen such that a frame rate of ~10 Hz was achieved with pixel dwell times of a few μs. The zoom factor was chosen such that the projections span a sufficiently large number of pixels to achieve a reasonable SNR for individual cell responses by averaging over the signal in these pixels. On average, projections span 123.3 $\pm$ 42.4 pixels. An example of imaged projections and selected regions of interest (ROIs) is shown in Figure 2.2C.

We first presented a simple flash stimulus to identify active cells. Once such cells were identified, we presented additional stimuli. The responses to each stimulus type were recorded as a separate time-series, selecting an appropriate number of frames for imaging. Due to bleaching and photodamage, imaging at a given depth had to be limited to a few minutes. Thus, time-series were taken from 4-7 different depths per fly, separated by at least 7μm such that different projections from different rows in the medulla were imaged at each depth.

2.2.4 Preprocessing of time-series data

Image stacks were aligned within the plane of imaging using a sub-pixel resolution registration algorithm (Turboreg, [239]) in ImageJ (NIH), then processed in Matlab (Mathworks, Natick, MA). Regions of interest (ROIs) around each terminal were found manually or with an automated script. Intensity values in the pixels within each ROI were averaged for both channels individually and a mean background value was subtracted from each. Then, the Citrine channel value was divided by the CFP channel value to obtain the signal ratio for that terminal. Typical ratios varied between 2 and 3. We note that while image alignment can correct for motion artifacts resulting from motion in the x-y plane of imaging, a change in brightness due to

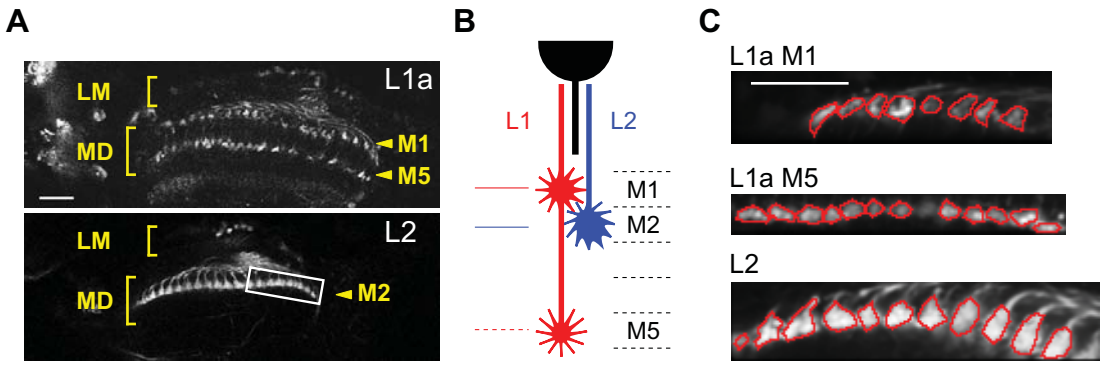

Figure 2.2: Images of L1 and L2 cell projections in the medulla. **(A)** Axonal morphologies of L1 (top panel) and L2 (bottom panel) with two-photon imaging of TN-XXL expression. L1 axons terminate in two medulla layers, M1 and M5, while L2 terminates in the M2 layer. Scale bar = 25 μm. LM, lamina; MD, medulla. The white box delineates an example region focused on for subsequent imaging, covering posterior projections. **(B)** Schematic representation of L1 and L2 projections. **(C)** Sample region-of-interest selections are shown for L1a (layer M1 and M5), and for L2, from time series data. Scale bar = 20 μm.

motion of the sample along the z-axis cannot be corrected in this manner. However, this type of motion causes an increase or a decrease in fluorescence emission at both wavelengths simultaneously while with a ratiometric indicator such as TN-XXL Ca^{2+} concentration changes give rise to anti-correlated changes in intensities in the two channels. Thus, computing the ratio between fluorescence emissions in these two channels, produces a signal that is more sensitive to Ca^{2+} concentration changes than to motion.

One concern with the use of ratiometric indicators is differential rates of bleaching in the two channels. Indeed, we noticed this in some of the time-series data acquired. To correct for this artifact, we first removed baseline drift from ratio signals by fitting a 4^{th} order polynomial to the entire response trace and subtracting it from the trace. Other than a baseline subtraction, we did not observe additional effects on the shape of traces following this procedure, for traces visually inspected before and after performing this procedure.

Since exact frame rates varied between experiments, all responses were first interpolated to the same rate of 100 Hz and aligned with respect to stimulus presentation

time before any further analysis was performed. Mean responses to all stimuli were calculated first by stimulus cycle, then by neuron, then by fly, and the fly means are used to calculate the overall means and standard error of the means presented in this chapter.

Detailed stimulus characteristics and analysis procedures for different experiments described in this chapter are provided below.

2.2.5 Visual stimuli and corresponding analysis procedures

In order to identify responding cells for further investigation as well as characterize the basic response of L1 and L2 neurons to light vs. dark conditions, we presented flies with 2 s light pulses of maximal intensity followed by 2 s of darkness, periodically, for 20 s. For the dark adaptation experiments in Figure 2.4, the stimulus initiated with 3 cycles of 2 s full field flashes separated by 2 s of darkness, followed by 8 s light pulses separated by 15, 30 and 60 s of darkness.

Responding cells were chosen by finding those cells that had significantly different mean responses during light presentation compared with darkness. This represented between 32% and 77% of cells recorded, depending on genotype and layer. Non-responding terminals were often in columns that could not see the screen. The mean of all stimulus repetitions per cell was computed first. Then the response of all cells in each fly was averaged and the reported curves presented show the means and standard errors of the fly means.

2.2.6 Moving edges

We measured the responses of the three axon terminals to moving edges by presenting the fly with a dark screen, across which a light edge moved at a speed of ~80°/s, matching the speed used in the behavioral experiments described in [47]. Once the bright edge passed, the screen was bright for 4 s, after which a dark edge moved across in the same direction. Then the screen was dark again for 4 s. This was repeated in 8 different directions, separated by 45°.

Under these conditions, the trace of the response to this stimulus consisted of

responses to both edge types as sequential events. As no direction-dependent differences were detected in the measured responses (Figure 2.5), all angles were averaged together. Since edges passed the receptive fields of different medulla columns at different times, traces for each direction were aligned by maximizing their cross-correlation with a mean unaligned response. Since traces were often noisy, we set a threshold for inclusion in analysis, asking whether the individual cell trace correlated with the mean of all cells. We included cells in the final average if the correlation coefficient was greater than 0.6, 0.5, and 0.3 for L2, L1 M1, and L1 M5, respectively. These thresholds included between 25% and 75% of cells recorded. In particular, for traces presenting high signal to noise ratios, as a result of strong expression by the cell-type specific driver, such as L2 traces, most traces were included. However, when many of the traces were corrupted by noise, as in the case of L1 M5 traces, a more significant fraction of traces was excluded by this criterion. Cells were first averaged across directions within a fly and traces shown in Figure 2.6 are the mean and standard error computed across fly means.

2.2.7 Gaussian noise

A uniform spatial stimulus varying in intensity with a nearly-Gaussian distribution as a function of time was used to examine the cellular responses to dynamically varying inputs. The intensity distribution had a standard deviation of 35% fractional contrast about a mean luminance of 60% of maximum. Values of greater than 100% or less than 0% luminance were set to 100% and 0% luminance, respectively. The sequence of samples had an exponential correlation function with a time-constant of 200 ms.

Within each axon terminal type, we analyzed the response of cells that were significantly anti-correlated with the input contrast. We computed the cross-covariance of each cell's trace to the input contrast. Cells were selected if their minimum cross-covariance was less than -0.0022, in units of fractional contrast times fractional response. This criterion selected for between 60% and 80% of recorded cells. We found that the cross-correlation between the contrast and measured signal was minimal for

approximately a 100 ms delay (corresponding to a single frame and thus the minimum delay that is measurable under our imaging conditions). Thus, we computed the mean response ratio as a function of the contrast at a time 100 ms earlier, binning the contrast into 50 bins. The mean response 100 ms after each contrast value was computed first for each fly; the mean and standard error shown in Figure 2.8 are computed from the means of the flies. We fit these functions with linear and quadratic polynomials and calculated the variance accounted for by each fit.

This stimulus also enabled us to fit linear-nonlinear (LN) models [11, 43, 209] to L1 and L2 responses where the linear component accounts for the dynamic response properties and the non-linear component allows for a static non-linearity to be subsequently applied. Thus, the linear kernel characterizes the temporal light patterns to which L1 and L2 are sensitive and the non-linearity can account for a difference in responses to light decrements and increments. Accordingly, we assumed that the response in different termini r(t) is defined as a function of the input contrast c(t):

$$r(t) = g(\int c(\tau)k(t-\tau)d\tau) \tag{2.1}$$

where $k(t)$ is the linear kernel and $g(x)$ is a static non-linearity.

For estimating the kernel $k(t)$, the stimulus input (contrast) was first re-sampled to 100 Hz, to match the interpolated rate for the ratio measurements. The ratio was baseline-subtracted and the first 10 s of the response were omitted as during these 10 s the baseline ratio change was most pronounced. 90 s of stimulus and response were used to estimate a kernel for each responding cell. We estimated the kernels $k(t)$ as optimal Wiener filters, correcting for non-white noise input [79]. The filters were computed first in Fourier space as described by the following equation:

$$\widehat{K}(\omega) = \frac{\langle R(\omega)C^*(\omega)\rangle}{\langle C(\omega)C^*(\omega)\rangle} \tag{2.2}$$

where * denotes a complex conjugate and $K(\omega)$, $R(\omega)$ and $C(\omega)$ are the Fourier transforms of the kernel $k(t)$, the response $r(t)$ and the input contrast $c(t)$, respectively. Thus, the numerator in the above equation is an estimate of the cross power spectral

density of the input contrast and response and the denominator is an estimate of the power spectral density of the input contrast.

These power spectral densities were estimated via Welch's averaged periodogram method as follows [258]: The averages denoted by the triangular brackets were taken over overlapping 10 s windows within which spectra were estimated, and consecutive windows were shifted by 5 s. The filters in Fourier space were subsequently transformed back to temporal space using an inverse Fourier transform and these kernels are presented in Figure 2.9A.

To quantify the ability to predict the neural response using the filter, we computed predicted responses by filtering the input traces with the estimated filters. Only filters that successfully predicted the corresponding response traces were included in the computation of average impulse responses. Cells included in this analysis were selected manually based on both the quality of response prediction by the filter and its qualitative smoothness. This selected for between 17% and 56% of recorded cells.

The instantaneous non-linearity component of the LN model, $g(x)$ was estimated by plotting the actual response against the linear prediction. This procedure closely follows [43], where it is shown to derive an optimal estimate of a linear-nonlinear model from the response to a Gaussian noise input. When plotting the actual response versus the linear prediction, means were first taken within the cells in each fly, and the means and standard errors shown in Figure 2.10 were calculated from those fly means.

2.3 Results

2.3.1 L1 and L2 cells respond to both light increments and decrements

In order to characterize the basic responses of L1 and L2 neurons to light vs. dark conditions, we presented the flies with wide-field flashes of restricted-wavelength light. Changes in Ca^{2+} concentrations at L1 and L2 axonal terminals in the medulla in response to these stimuli were recorded. Responses of L1 cells were recorded from termini in both M1 and M5 layers of the medulla while responses of L2 cells were recorded from the M2 layer. The previously reported depolarization responses of L2 cells to light decrements were reproduced by these measurements (Figure 2.3A, [199]), while hyperpolaizing responses to light increments differed slightly in kinetics. Since responses to 490 nm light were similar to responses to 575 nm light, and in the previous study 568 nm LEDs were used for stimulation [115, 199], this difference cannot be attributed to a difference in stimulus wavelength.

Extending these studies to L1 revealed that the terminal of L1 in the M1 layer of the medulla responded similarly to that of L2 to alternating light and dark epochs (Figure 2.3B). In particular, increases in intracellular Ca^{2+} levels were observed during dark periods and decreases were observed during light periods. Similar responses were recorded using two different drivers for expressing TN-XXL in L1. Furthermore, the M5 terminal of L1 responded with the same polarity, but with an attenuated strength with respect to the M1 terminal for responses recorded with the same driver.

We next interleaved long periods of dark presentations between long-duration light flashes to test whether dark adaptation might have an effect on response shapes and to approximate the experimental conditions in [199]. The responses of L2 cells to light flashes following either short or long dark epochs were very similar, indicating that dark adaptation on the scale of up to a minute does not change the strength of L2 responses to light increments and decrements.

Overall, these results show that responses of L1 and L2 cells to flashes do not reflect a strong bias towards responding to either increments or decrements.

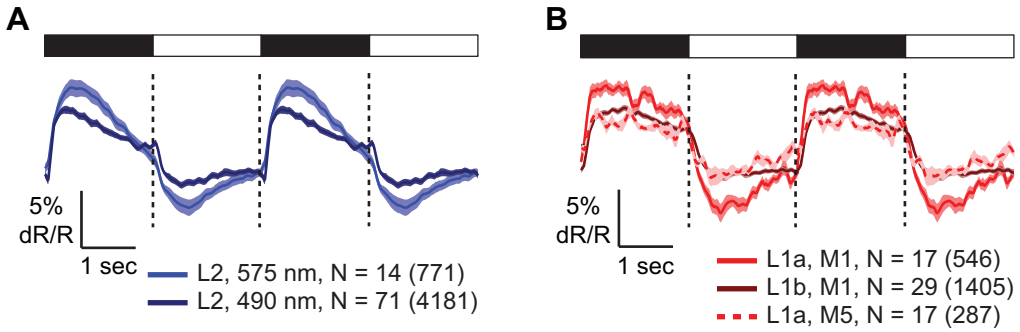

Figure 2.3: L1 and L2 cells respond similarly to light and dark flashes. **(A and B)** Responses to periodic full-field flashes. Two 4 s periods are shown. Light-on epochs are denoted with open sections of the bar and light-off epochs with dark sections. Shading denotes ±1 standard errors of the mean (SEM). Here and in all subsequent figures in this chapter, N for each genotype is given as the number of flies with the number of cells in parentheses. **(A)** Responses of L2 projections into the M2 layer with 490 nm (dark blue) and 575 nm (light blue) light. **(B)** Responses of L1 projections into the M1 layer recorded using two different drivers, L1a (continuous, light red) and L1b (continuous, dark red); and responses of L1 projections into the M5 (dashed, light red) layer, recorded using the L1a driver.

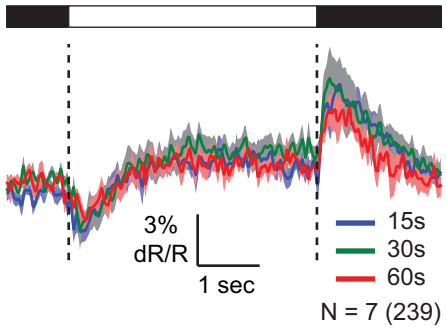

Figure 2.4: Dark adaptation does not change the shape of L2 responses to light increments and decrements. L2 terminals were imaged in response to 8 s light flashes preceded by different durations of darkness. The three curves show responses after 15, 30, and 60 s of darkness. Shading denotes ±1 SEM.

Moving bright and dark edge responses

As the L1 and L2 pathways were associated with selectivities for moving bright and dark edges, respectively, we next wanted to test whether the responses of these cells to non-static light increments and decrements, associated with edge motion, reflected this specialization. Thus, we examined the responses of both L1 and L2 cells to a moving bright edge followed by a moving dark edge presentation.

We first assessed whether responses were orientation or direction dependent, by comparing L2 cell responses to edges moving in different directions and orientations across the screen (similar observations were made with L1 cell responses, data not shown). Since responses to edges moving in all directions were indistinguishable (Figure 2.5), we concluded that these cells are not direction or orientation selective. This result was also consistent with previous observations ([199]). Accordingly, to compare responses in L1 to responses in L2, responses in all directions were averaged together.

The Ca^{2+} concentration in the L1 M1 terminal decreased in response to the bright edge passing and remained low until the dark edge passed, when it increased transiently before returning to baseline. The L1 M5 terminal displayed a broadly similar response, but with a smaller amplitude, consistent with the difference in flash responses (Figure 2.6A). The L2 terminal displayed a transient decrease in calcium in response to the light edge and a transient increase in response to the dark edge (Figure 2.6B). The response was less sustained during the light presentation across the screen with respect to the corresponding response in L1 terminals. This is consistent with lateral inhibitory effects observed in L2 and described in the following chapter.

Quantifying the amplitudes of these responses we found that the Ca^{2+} signals of both L1 and L2 terminals showed responses to both edge types with comparable magnitudes for L1 and a more pronounced response to dark edges for L2 (Figure 2.7). Thus, although the L1 and L2 terminals respond with different long timescale kinetics, responses from both neurons clearly contained information about both edge types. We thus conclude that the L1 and L2 pathway specificity to two different types of moving edges does not arise directly from an absence of response to one of the edge types in either cell; but must depend on additional downstream processing steps.

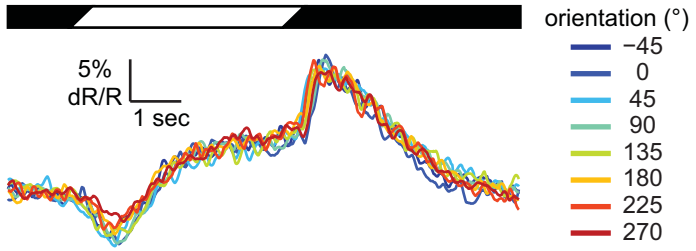

Figure 2.5: Responses of L2 cells to edges moving in all directions are similar. Responses of L2 terminals to a bright edge that moved across the field of view at 80°/s, after which the screen is light for 4 s, before a dark edge passed at 80°/s. Angles denote the different orientations of the moving edge with respect to the horizon. Shading denotes ±1 SEM.

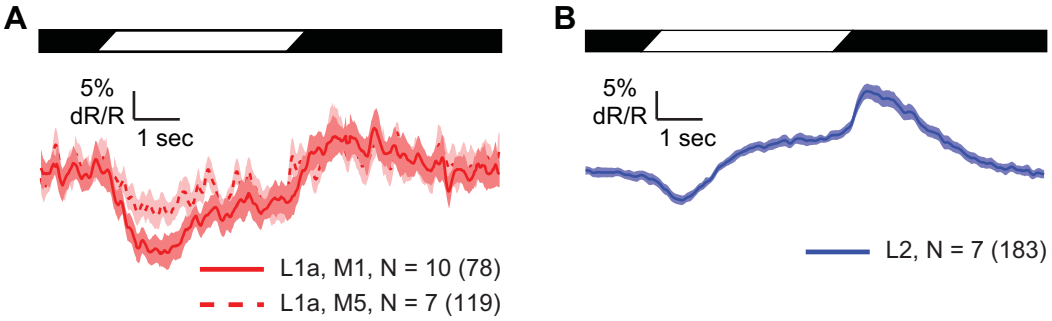

Figure 2.6: Both L1 and L2 cells respond to both bright and dark moving edges. **(A)** Responses in L1 cell terminals in M1 (continuous) and M5 (dashed). **(B)** Responses in L2 cell terminals. Shading denotes ±1 SEM.

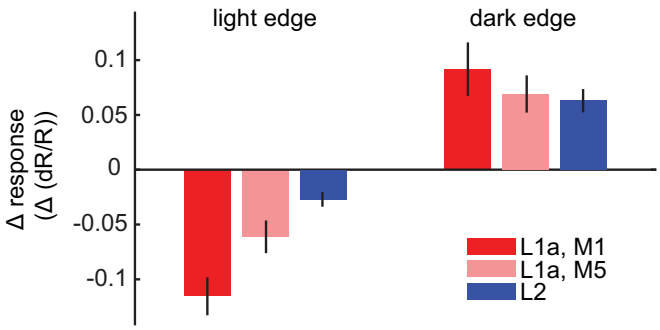

Figure 2.7: The amplitude of responses of L1 and L2 cells to light and dark moving edges are similar. The amplitude of the transient response to each edge type was quantified by subtracting the mean response during the second before the edge passes from the first second after it passes. Mean and SEM are calculated by fly from the traces shown in Figure 2.6. Error bars are ±1 SEM. Left - the amplitude of responses to light edges. Right - the amplitude of responses to dark edges.

2.3.2 L1 and L2 axon terminals respond linearly to changes in contrast

So far we have examined L1 and L2 responses to sustained, long time-scale stimuli consisting of large contrast changes. However, in more naturalistic conditions input intensities vary dynamically and more smoothly around an average luminance level. Thus, we next presented flies with a full-field, random intensity noise stimulus to quantitatively compare the responses of L1 and L2 to a range of positive and negative contrast changes, at timescales relevant to motion detection, and under continuous illumination. The relatively fast intensity changes in this stimulus effectively prevent strong adaptation from taking place on timescales longer than 200 ms.

As expected, intense periods of illumination prompted a reduction in intracellular Ca^{2+} levels in both cell types. Periods of decreased illumination induced an increase in Ca^{2+} levels. To examine whether responses to contrast increases were equal and opposite to contrast decreases, we plotted the mean Ca^{2+}-indicator response ratio against the contrast presented 100 ms earlier, for all three axon terminals (Figure 2.8). The output of all three terminals varied linearly with the delayed input contrast. A purely linear function accounted for 97% and 89% of the mean delayed response variance of the L1 signals in M1 and M5; a quadratic term accounted for less than 1% of additional variance in each case. Similarly, a purely linear function accounted for 99.6% of the variance in L2 responses, while adding a quadratic term accounted for less than 0.1% of additional variance.

As a second approach to measuring response linearity, we fitted a linear-nonlinear (LN) model to the Ca^{2+} response of these cells as a function of contrast history by using methods frequently used to characterize responses in the vertebrate retina [11, 43, 209]. The fitted linear kernels were biphasic, consistent with L1 and L2 cells encoding contrast changes. Specifically, a strong negative lobe reflects the sign inversion between photoreceptors and these cells and a slower, weaker, positive lobe subtracts an average value of contrast at a past time interval from this response, making it transient (Figure 2.9A). Filters similar in shape but different in kinetics were extracted in electrophysiological studies conducted in these cells under bright

illumination conditions [122]. These kernels were strongly predictive of the average responses of L1 and L2 cells to these stimuli (Figure 2.9B). Furthermore, the static non-linearity component of the model fitted to these responses was in fact highly linear (Figure 2.10).

Thus, we found no evidence that edge selectivity could emerge simply through rectification and directed transmission of contrast increases through L1 and contrast decreases through L2.

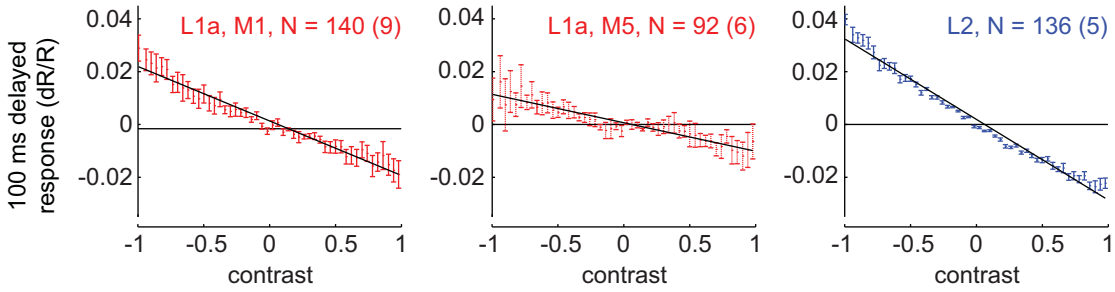

Figure 2.8: Delayed responses of L1 and L2 cell terminals to dynamically varying contrast are linear. The Ca^{2+} response as a function of intensity 100 ms earlier is presented in the M1 layer projections of L1 cells (left), the M5 layer projections of L1 cells (middle) and the M2 layer projections of L2 cells (right). The average response for each preceding intensity was computed for each fly and the means and SEM of the fly means are displayed. The black line is a linear fit to the means.

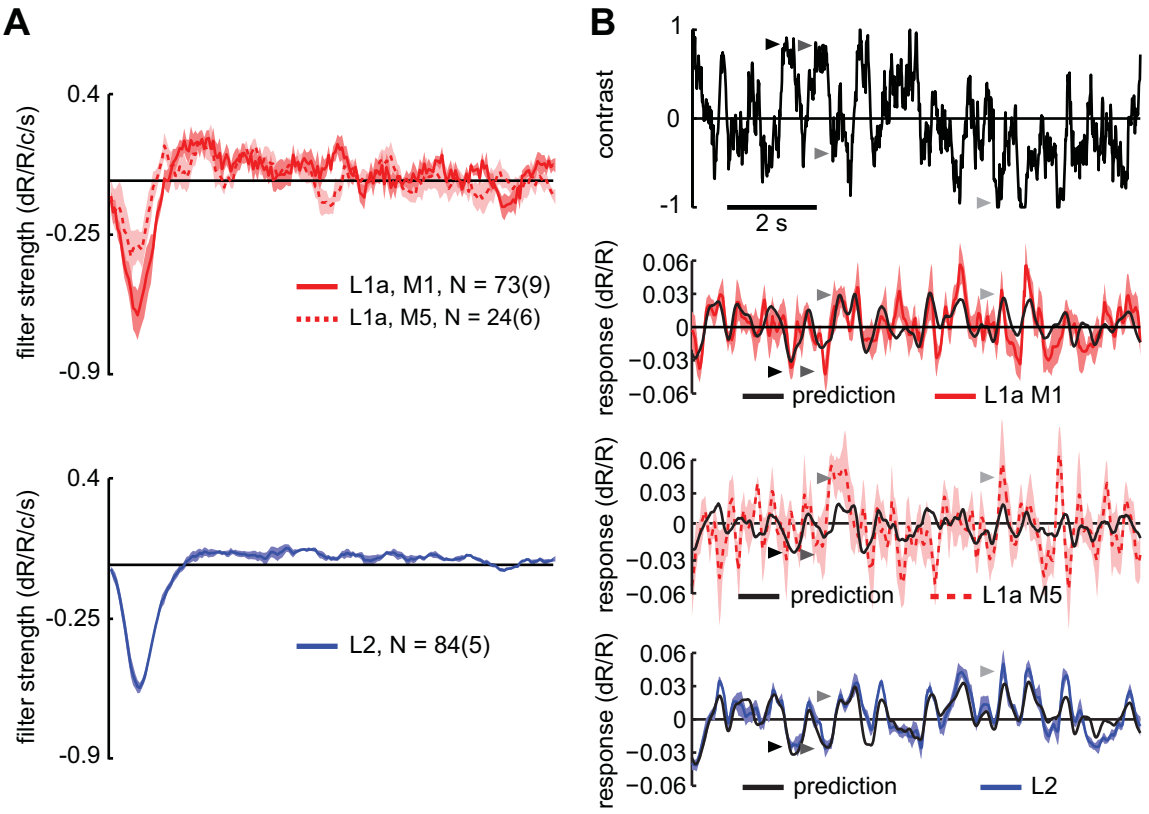

Figure 2.9: Responses of L1 and L2 cell terminals to noise are predicted by linear filters. **(A)** The optimal linear filters fitted to responses of each axonal terminal (see Section 2.2.7). Top: Filters extracted for L1 terminal responses in M1 (continuous) and M5 (dashed) projections. Bottom: Filter extracted from L2 terminal responses. 'c' in the filter units refers to the fractional contrast, measured relative to the mean intensity. **(B)** Top: a 10 s excerpt of the input contrast in the full-field random intensity stimulus. Middle: the corresponding average response observed in projections of L1 neurons into M1 (red) and M5 (red, dashed). Bottom: average response observed in L2 axon terminals (blue). Shading denotes ±1 SEM. Black lines represent the predictions of the linear filters shown in (A). Gray arrowheads in top panel mark peaks and troughs in the input and arrowheads in the middle and bottom panels mark the responses to these peaks (which are inverted by the photoreceptor synapse). For each genotype N is given as the number of cells with the number of flies in parentheses. Shading denotes ±1 SEM.

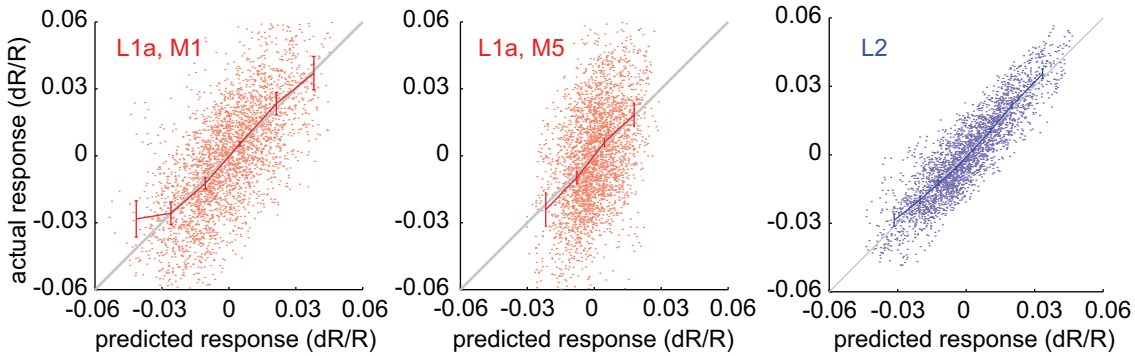

Figure 2.10: No rectification is reflected in the non-linear component of an LN model fit to L1 and L2 cell responses. Mean actual response values are plotted against linearly predicted values for all three terminals, representing the static non-linearity of the LN model. A line with unity slope is shown in each case, representing a completely linear static non-linearity for reference. In L1a M1, L1a M5, and L2, the linear filter alone accounted for 48%, 20%, and 81% of the mean response variance, respectively. These differences in the response variance accounted for by the filter were strongly influenced by the level of noise in the recordings, which was far higher in L1a M5 recordings, for instance, than in L2 recordings. Error bars represent ± 1 SEM.

2.4 Discussion

2.4.1 Integrating imaging and electrophysiological studies of the responses of L1 and L2

Consistent with a sign-inverting, histamine-gated chloride channel mediating L1 and L2 responses to photoreceptor inputs, we observed that increases in contrast caused decreases in intracellular Ca^{2+} in both axonal terminals of L1 and the terminal of L2. These three terminals displayed linear responses to dynamical contrast changes, but different kinetics in response to prolonged stimuli. Such kinetics differences have not been noted in the electrophysiological recordings of LMCs [122, 145], but may be related to differential adaptation in each neuron type. In particular, the L2 terminal adapted to long presentations of a contrast signal, returning to near baseline, while the L1 M1 terminal retained low Ca^{2+} levels throughout a 4 s light presentation and returned to baseline with a small overshoot when the light was removed. The L1 terminal in M5 showed a qualitatively similar, but attenuated, response.

Linear response analysis was previously used in electrophysiological studies to describe LMC filtering properties. Estimated filters had a timescale of 50 ms and responses to flashes decayed at a similarly rapid rate. Furthermore, in dim conditions, LMC membrane voltage responses tended to follow the contrast itself, while under bright conditions, membrane voltage tended to be most sensitive to changes in contrast. We infer that under the bright conditions of our imaging experiments, a step change in contrast elicits a transient change in LMC membrane potential lasting less than 100 ms, as described in previous electrophysiological studies. Following this response, the cell returns to near baseline potential. In contrast, the Ca^{2+} responses we measure in axonal terminals can persist for seconds. This difference is not solely due to the kinetics of the Ca^{2+} reporter, because some of the measured timescales are much longer than the off rate of the indicator [199]. We hypothesize that similar, yet differentially weighted, mechanisms give rise to the different kinetics of L1 cell responses with respect to L2 cell responses. In Chapter 3 we explore the mechanisms mediating the decay rate of long-term responses in L2 cells in more depth.

2.4.2 Rectification emerges downstream of L1 and L2 terminals

A central aspect of implementing arithmetic multiplication in the brain is thought to be "half-wave rectification" of the inputs to each multiplier [104]. That is, because it is difficult to conceive of how a single synapse or circuit could implement sign-correct multiplication of all possible combinations of positive and negative inputs, it seems plausible that multiplied inputs would be rectified prior to multiplications so that each sign pairing could be multiplied independently. Given the apparent need for rectification, a key question becomes where these rectification events get implemented within the motion detection circuitry. Recent work used imaging studies of Ca^{2+} signals in the L2 axon terminal to argue that the output of this cell was half-wave rectified such that it primarily transmitted information about decreases in brightness [199]. In particular, when these cells were exposed to long periods of darkness, followed by light flashes, these axon terminals responded strongly to the onset of darkness, but only relatively weakly to the onset of light.

Our imaging data with the same Ca^{2+} indicator support the existence of some asymmetry under similar conditions. However, our data also demonstrate that under continuous dynamical illumination, the Ca^{2+} signal in this cell varies nearly linearly with contrast. In addition, if the outputs of this cell were rectified, then flies bearing only active L2 cells should be unable to respond normally to any visual stimulus whose content requires information about increases in brightness (because a rectified L2 output cannot transmit this information). However, behavioral studies demonstrate that this is not the case [47]: flies with only active L2 cells respond normally to one of the two "reverse-phi" minimal motion stimuli. This stimulus consists of a light increment in one position in space followed by a light decrement in a neighboring position in space. Thus, a central component of this signal is brightening. Furthermore, the same flies also respond to a normal "phi" minimal stimulus consisting of brightening in two points in space. Finally, a reasonable prediction from a model in which L2 outputs are half-wave rectified would be that the outputs of the L1 cell would also be half-wave rectified in the opposite direction. However, the imaging data

presented here demonstrates that L1 conveys information about both brightening and darkening to the HRC, similarly to L2. Thus, while a model of the HRC may require rectification, this rectification is not implemented within L1 or L2 and therefore must be implemented in the circuitry downstream of these neurons.

2.4.3 Outlook

The studies presented in this chapter showed that L1 and L2 responses to rapid wide-field contrast changes are similar, while long duration responses show some differences in kinetics and contrast polarity sensitivity. Thus, we conclude that rectification does not arise in the outputs of these two cells. Nevertheless, the subtle differences in responses that are observed may facilitate rectification downstream. In addition, by keeping all stimuli broad in space, these studies did not probe the effects of the spatial stimulus characteristics on responses. Accordingly, it remains possible that while the responses of these cells to spatially broad changes in contrast are similar, they could process local stimuli differentially. This, in turn, would give rise to differences in responses to objects that vary in size in addition to contrast. An indication that spatial stimulus characteristics may be significant comes from both previous electrophysiological studies [247] as well as from the observation of variability in response shapes even with the broad stimuli presented here (data not shown, but see subsequent chapter). Thus, the studies presented in the next chapter address the broader question of the spatial as well as the temporal response characteristics of one of these cells, L2, where strong driver expression enables a more thorough investigation of response properties.

Chapter 3

Pathway specific tuning at the inputs to motion detection circuits

In the previous chapter we compared responses of L1 and L2 cells to increments and decrements and assessed to what extent an asymmetry in these responses may give rise to a downstream specialization for the detection of bright and dark moving edges. We concluded that both cells transmit information about both light increments and decrements and hence selectivity for moving bright and dark edges must arise via additional mechanisms downstream of these cells. Here we broaden the scope of our studies, and explore the functional properties of one of these cell types, L2, in more depth, to test whether its detailed spatiotemporal sensitivities may facilitate the downstream detection of dark object motion cues. More broadly, we ask what information is encoded in L2 cell responses. Furthermore, we seek and find explanations to observed variability in the shapes of different L2 cell responses. Specifically, we find how the spatial extent and contrast of inputs into L2 cells shape the kinetics of responses to intensity changes as a function of time. This functional tuning has implications for how downstream motion detection computation may be performed and may become specialized to dark rather than bright moving objects.

We start this chapter by providing some background on the specializations characteristic of early stages of visual processing as represented by L2 cells, and in particular the suggested roles of lateral inhibition which we identify in L2 cell responses.

3.1 Introduction

The complexity of the visual world demands significant neural processing to extract behaviorally relevant information. What processing strategies enable peripheral visual circuits to capture and transform these inputs? Photoreceptors are tuned to maximize the amount of information encoded [151], while downstream neurons are specialized to encode specific features, such as motion, discarding irrelevant information [27, 91, 166, 211, 215]. How these two competing objectives are functionally and mechanistically balanced at intermediate processing steps is poorly understood.

3.1.1 The role of lateral inhibition in early visual processing

Lateral inhibitory interactions among peripheral input channels constitute an essential part of neural processing across many sensory modalities in both vertebrates and invertebrates [33, 53, 137, 262]. In the visual system, lateral inhibition produces a variety of center-surround receptive field (RF) structures in many different types of interneurons, including vertebrate bipolar and retinal ganglion cells, as well as in first order interneurons in flies and other arthropods [53, 63, 73, 80, 103, 247, 113, 127, 153, 178, 214, 260]. Lateral inhibition enhances basic visual features such as edges and suppresses responses to spatially uniform intensity [145, 150, 152, 198]. Several theories derive ideal antagonistic center-surround organizations based on assumptions regarding the goals of early visual processing. Predictive coding, for example, proposes that redundancy is removed from visual inputs by utilizing the spatial and temporal correlation structure of natural stimuli [7, 14, 187, 228]. Information maximization assumes that RFs encode as much information as possible given neural signaling constraints [247]. Finally, matched filtering posits that the spatiotemporal RFs of first order interneurons are tailored to detect behaviorally relevant features such as moving edge velocity distributions [225]. These studies considered the functions of lateral inhibition in the context of filtering constrained by input statistics and broad behavioral requirements. However, it is poorly understood how input channels might satisfy broadly efficient encoding goals while simultaneously enhancing features central to specific downstream computations.

3.2 Methods

The methods used to conduct the experiments described in this chapter are similar to those described in the previous chapter. Accordingly, only differences between procedures performed in this chapter and the previous chapter will be described in this section.

The experiments presented in this chapter were conducted using a similar set-up for two-photon Ca^{2+} imaging and presentation of visual stimulation as described in the previous chapter, but with the following modifications: Two-photon imaging was performed using a Leica TSC SP5 II microscope (Leica, Bensheim, Germany) equipped with a pre-compensated Chameleon femtosecond laser (Coherent, Inc., Santa Clara, CA) and using a Leica HCX APO 20X/1.0 NA water immersion objective (Leica, Bensheim, Germany). All data was acquired at a constant frame rate of 10.6 Hz and a line-scan rate of 700 Hz, using unidirectional scanning mode. The frame size was held constant at 200 $\times$ 50 pixels. Imaging experiments lasted no more than 2 hours per fly.

Synchronization between imaging and stimulus presentation was established using triggering functions provided by the LAS AF Live Data Mode software (Leica). A DAQ (NI USB-6211) connected to the computer used for stimulus generation was used to generate a trigger signal at the beginning of stimulus presentation. This trigger was read by the imaging software and used to initialize imaging at the same time. In addition, a trigger was produced by the imaging software to indicate the beginning of the acquisition of each frame and was acquired via the same DAQ on the stimulus computer such that stimulus presentation details were saved together with imaging frame timings and used in subsequent processing.

The output of the digital light projector was passed through an optical fiber bundle as before, but then projected onto a 8 $\times$ 8 cm^2 back-projection screen positioned in front of one of the fly's eyes. The screen span 55° of the fly visual field horizontally and 58° vertically (Figure 3.1A).

The spectrum of presented stimulation and bandwidths of fluorescence collection

were also modified to increase the amount of photons absorbed by R1-R6 photoreceptors with a minimal reduction to YFP fluorescence collection. Specifically, the visual stimulus was passed through a 40 nm wide band-pass spectral filter centered around 562 nm. CFP photons were collected via a 447/60 emission filter as before and Citrine photons with a 514/30 emission filter (Semrock, Rochester, NY). CFP and Citrine emitted photons were separated via a 495-LP beam splitter (Semrock, Rochester, NY), as before (Figure 3.1B). A reduction of 15% in YFP collection occurred with respect to the previous filter settings. With this modified setup, the stimulus had a luminance of approximately 76.4 cd/m^2.

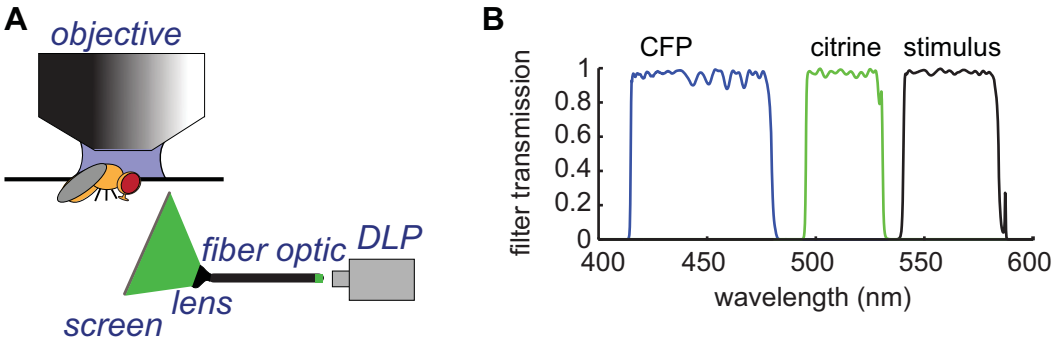

Figure 3.1: Modified imaging setup and filter sets. **(A)** Schematic illustration of the modified imaging set-up. DLP = Digital Light Projector. **(B)** The modified set of emission (CFP, Citrine) and stimulus filters used.

3.2.1 Fly stocks and handling

As in the previous chapter, the Gal4 driver 21D-Gal4 (from [203]) was used to express a multi-copy insert of UAS-TN-XXL (from [164]). Thus, the same line of flies expressing TN-XXL in L2 as in the previous chapter was used:
+ ; + ; 21D-Gal4 / UAS-TN-XXL, Sections 3.3.1-3.3.4,
In addition, a line where the Gal4 driver and the UAS-TN-XXL element were recombined to be on the same chromosome allele (facilitating the addition of additional transgenic elements used in the subsequent chapter), was also used:
+ ; + ; 21D-Gal4,UAS-TN-XXL/+, Section 3.3.5

Flies were grown, collected and dissected as described in the previous chapter. Thus, for the experiments shown in Sections 3.3.1-3.3.3; flies were collected on CO_2 1-3 days after eclosion and imaged on the same or the next day. However, for the experiment shown in Section 3.3.5, which also involved knockdown of receptors by RNAi expression (see Chapter 4), older flies were preferred to increase the knockdown efficiency, thus flies (controls and all experiments) were collected 1 day after eclosion but imaged 4-8 days later.

Solutions used in imaging were made and applied as described in the previous chapter.

3.2.2 Data pre-processing

Initial data pre-processing steps included alignment, region of interest extraction and ratio computation as described in the previous chapter. However, responses and time-traces of presented stimuli were interpolated to 10 Hz rather than to 100 Hz prior to averaging. Since frame-rates were held constant and near 10 Hz using the setup described in this chapter, the use of a higher interpolation rate was unnecessary and was observed to result in the addition of noise. Hence, a lower interpolation rate was chosen.

Baseline fluctuations were removed as described before. In order to also remove motion artifacts, the following procedure was added: if the ratio value in raw traces exceeded the median by 75% or was lower than the median by more than 50%, the

value was replaced by the median value for the trace to prevent such noise instantiations from strongly affecting computed mean responses.

The average response computation procedure was also slightly modified. When computing the mean response to different stimulus epochs, we first computed the mean response across presentation of the same epoch to the same cell as before. However, rather than averaging across all cells in each fly, responses were simply averaged across all cells from all flies put together. The preliminary step of averaging across cells within each fly before averaging across flies was eliminated, since for flies with few imaged cells this step introduced noise into the final averages (the relative weight of these few measurements became large).

Furthermore, in all experiments, responses to moving bars were analyzed first, to localize the centers of the RF of each imaged L2 cell on the screen (as shown in Figure 3.2B). Rather than excluding cells based on their response size, this information was used to decide what cell responses to include in averages. The average images of all time-series of the same fly that were acquired in the same depth were compared to the average image of the moving bar time-series in order to identify the same cells as they respond to the different stimuli. Correspondence between identical projections belonging to the same cells in different time-series was manually established using both the unique shape of the projection and its location in the medulla with respect to the other projections. Thus, for all cells in all experiments, when averaging responses the RF center position on the screen was known, and often used to divide responses according to the geometry of the stimulus with respect to each cell's RF. In particular, responses of cells without identified RF centers on the screen were not included in mean response computations. Mean responses to stimuli represent the mean responses of all cells that had RF centers on the screen, unless otherwise stated (for some stimuli, the population of responding cells is divided by position with respect to the stimulus or limited to a single cell as appropriate).

3.2.3 Visual stimuli and corresponding analysis procedures

Periodic full field flash presentation

Light flashes lasting 2 s were periodically displayed, interleaved with 3 s of darkness. The stimulus was typically presented for approximately one minute or 600 imaging frames, such that each cell observed at least 10 flashes of light.

Moving bright bar on a dark background

A bright bar, ~2.5° wide, moved at ~10° per second with ~2.5° jumps (i.e., four jumps with gaps equal to the width of the bar during 1 s) in one of 4 possible orientations presented in random order: a vertical bar moving left or right across the horizontal extent of the screen or a horizontal bar moving up or down across the vertical extent of the screen. A gap was interleaved between the moving bar presentations to allow responses to fully decay. Thus, the time interval between presentations of moving bars in different orientations was 18 seconds, and the total amount of time it took to present the bar moving in all 4 orientations was 72 seconds. The stimulus was typically presented for 1000 imaging frames or approximately 94 seconds, allowing the cells to respond to the bar passing across the screen at least 5 times.

From raw response traces to this stimulus, RF center positions were identified for each imaged cell having an RF center on the screen, as described in Section 3.3.1 and shown in Figure 3.2B. To compute the mean response to the moving bar passing across these RF centers (shown in Figure 3.2A) response traces of different cells were aligned in time using these identified RF center positions. Each trace was aligned such that the response to the passing of the bar through its RF center occurred at the central time-point of the time trace. Further alignment was obtained by shifting different time-traces by the delay that brought the cross-correlation between the specific trace and the mean trace to a maximal value.

To compare responses to bars moving in different orientations, we averaged over responses of cells with RF centers located at the top medial corner of the screen, from the flies' perspective, occupying 15% of the screen area. We then compared mean responses to bars moving from the bottom edge of the screen to the top edge, and

moving from the lateral edge of the screen to the medial edge. In this manner, the bars had ample time to pass through the surround region of the RF prior to reaching the RF center, so that surround responses could be compared. Furthermore, the frequency of finding RF centers in this region of the screen was high, and angular distortions due to the flatness of the screen were small (Figure 3.25). The surround response strength was computed by subtracting the mean response over a 4 s wide time interval ending 2.5 s before the beginning of the hyperpolarization epoch from the mean response during the 1.5 s wide time-interval ending 0.5 s before the hyperpolarization epoch, during which the bar passed through the near surround region (gray patch in Figure 3.25A)

Partial field flash presentation

On an intermediate illumination background, a dark or bright square covering ~44% of the screen positioned at its bottom lateral portion from the fly's point of view was presented for a variable amount of time (3 s in Figures 3.5A and 3.5B; 0.2 s in Figures 3.5C and 3.5D), and eliminated for 3 s.

The amplitudes and strengths of responses were computed as shown in Figure 3.4 (this amplitude and strength computation method was also used for the analysis of responses to the presentation of a bar at a random position and responses to the presentation of circles and annuli around identified RF centers). To compute a response amplitude, within the initial 1.2 s of the response, a 600 ms window was chosen so as to maximize the absolute difference between the mean response within the window and the mean response during a 600 ms seconds interval preceding the stimulus presentation, and ending 200 ms before the presentation (this procedure is described in Figure 3.4A where the procedure of looking for the peak using this moving average window is referred to as "smooth, find peak"). This window thus defined the timing of the peak response and the peak value. This procedure of finding the peak timing rather than using a window with a constant time interval was designed to address different peak times observed in different types of responses, and seen in depolarizing versus hyperpolarizing responses.

For partial field flashes, the difference between the amplitude of the response to

light presentation and the amplitude of the response to dark presentation was defined as the overall response strength (Figure 3.4B). The sign of the response strength was defined by convention such that cells that decreased their Ca^{2+} concentration to light were associated with negative response strengths and cells that increased their Ca^{2+} concentration to light were associated with positive response strengths. Only cells with response strengths larger than 0.025 or smaller than -0.015 are included in Figure 3.5A and the mean response of cells with absolute response strengths exceeding these values are presented in Figure 3.5B.

The amplitude of the response to a 200 ms flash was defined as the difference between the mean response during the 2 frames of stimulus presentation, and the mean response to the flash elimination in a 1 s time window starting 200 ms (or 2 frames) after the flash was eliminated. The overall response strength was defined as the difference between the amplitude of the response to the bright flash and the amplitude of the response to the dark flash. As above, the sign of the response strength was set such that negative strengths corresponded to cells that decreased their Ca^{2+} concentration to light. Only cells with response strengths larger than 0.02 or smaller than -0.02 are included in Figure 3.5C and the mean response of cells with absolute response strengths exceeding these values are presented in Figure 3.5D.

Circles and annuli presentation around identified RF centers

Circles and annuli of 12 different sizes were presented in a random order. Circles had radii of 2°, 5°, 8°, 10°, 15° and 20° and annuli had internal and external radii combinations of [2°,15°],[4°,15°],[6°,15°],[8°,15°],[10°,20°] and [15°,20°]. These stimuli were presented around RF centers that were obtained using the moving bar stimulus presentation and analysis described above. Each cell was shown a complete set of either dark or bright circles and annuli on an intermediate illumination level background with a different order of presentation. Each shape was presented for 3 s and eliminated for 3 s before the next shape was presented. The stimulus was applied for 2400 frames or ~226 s such that each shape was presented 3 times. Taking the geometry of the screen with respect to the fly eye position into account, stimuli were presented such that they generated circles and annuli from the fly's viewing perspective.

Responses were averaged for each cell over repeated presentation of each stimulus to the same cell, before the average across cells was computed. The amplitude of the response of each cell to each epoch was computed as described in the analysis of partial field flash presentation and in Figure 3.4B. The signs were set such that response strengths of cells that showed decreased Ca^{2+} to light were negative and the response strengths of cells that showed increased Ca^{2+} to light were positive. To compute mean response amplitudes at different time points during a response (Figures 3.10, 3.11 and 3.13) the mean response (dR/R) was computed for the following time intervals after stimulus presentation: 0.2-0.8, 0.7-1.3, 1.2-1.8, 1.7-2.3, and 2.2-2.8 s. The extent of decay was computed as the difference between the peak response amplitude and the mean response during a 600 ms window ending 200 ms before the stimulus presentation ended (Figure 3.12).

3.2.4 Computational model for predicting responses to dark circles and annuli

We suggest that all responses of L2 cells to dark circles and annuli can be approximated as a difference between pairs of exponentially rising and decaying inputs associated with different time-constants. Thus, we fit a circle-surround model to these responses [75, 201, 205]. In this model, input components have the following functional form as a function of time from stimulus presentation time, $t = 0$:

$$in_i(t) = 1 - exp(t/\tau_i) \tag{3.1}$$

Two inputs are used in modeling responses to circles. $in_1(t)$ is the primary component and $in_2(t)$ the antagonistic component. Responses to annuli are also modeled using 2 components, $in_3(t)$ and $in_4(t)$, representing the primary and antagonistic components, respectively. These components are shown in Figure 3.19.

Each input component is associated with a strength distribution in space that establishes its amplitude in response to a stimulus by integration. This distribution

is assumed to be circularly symmetric with Gaussian shape. Thus, it is described by:

$$G_i(r,\theta) = G_i(r) = exp(-r^2/2\sigma_i^2) \quad , \quad i = 1, ..., 4 \tag{3.2}$$

where r is the distance from the RF center. By the circular symmetry, the above equation defines the RF shape over a two-dimensional (2D) space. The amplitude with which any input component is added to shape the response to uniform circles or annuli, is set by integrating over the 2D shape derived from $G_i(r,\theta)$. These components are shown in Figure 3.16A. Thus, responses to circles were predicted using the following equation:

$$circ\_resp(t) = amp_1 \cdot in_1(t) - amp_2 \cdot in_2(t) \tag{3.3}$$

where

$$amp_i = \alpha_i \int_{r=R_i}^{r=R_o} \int_{\theta==0}^{\theta=2\pi} G_i(r,\theta) r dr d\theta = 2\pi\alpha_i\sigma_i^2 \left(exp(-R_i^2/2\sigma_i^2) - exp(-R_o^2/2\sigma_i^2)\right) \tag{3.4}$$

with $R_i = 0$ and $R_o = R$, the radius of the circle, for $i = 1, 2$. Responses to annuli were predicted using a similar equation, replacing components 1 and 2 with components 3 and 4 and setting R_i and R_o to be the internal and external radii of the annuli.

We found corresponding model parameters by solving an optimization problem to minimize the mean squared error between simulated and measured responses to both circles and annuli under the constraints of positive amplitudes and standard deviations larger than 1°. The optimal parameters used to predict responses to circles and annuli are detailed in Table 3.1 and Table 3.2, respectively. For annuli with internal radii $R_i = 2°$ and $R_i = 4°$ model predictions were poorly fit with parameters that fitted other responses well, likely because these stimuli are at the transition region between responses with and without direct excitation and the behavior in this transition region is not captured by the above model. Hence, we did not require minimizing the prediction error for these two responses in setting the model parameters for predicting annuli responses. However, we could predict these responses using $in_1(t)$ and $in_3(t)$ as inputs (i.e., while the center response is mediated by the center component as in circle responses, the surround response is rapid as in responses to annuli) and

appropriate values for amp_1 and amp_3 that enabled predicting the responses to these stimuli well using all other model parameters without change. These amplitudes are given in Table 3.3.

Parameter	**Value**
α_1	0.0165 dR/R/(°)^2
α_2	2.78·10^{-4} dR/R/(°)^2
σ_1	1.193°
σ_2	10.736°
τ_1	0.14 s
τ_2	1.667 s

Table 3.1: Model parameters for predicting responses to circles

Parameter	**Value**
α_3	4.98·10^{-4} dR/R/(°)^2
α_4	2.43·10^{-4} dR/R/(°)^2
σ_3	10.888°
σ_4	20.354°
τ_3	0.55 s
τ_4	1.559 s

Table 3.2: Model parameters for predicting responses to annuli

R_i=2°, R_o=15°	
Parameter	**Value (dR/R)**
amp_1	0.1125
amp_3	0.154
R_i=4°, R_o=15°	
Parameter	**Value (dR/R)**
amp_1	0.0388
amp_3	0.099

Table 3.3: Model parameters for predicting responses to annuli of two specific sizes

Moving sinusoidal gratings

Gratings with sinusoidally varying contrast (100% contrast change within a period) as a function of space were presented and moved within a virtual cylinder projected on the screen either around the yaw axis or around the pitch axis. i.e., stimulus images were projected in a manner that corrected for distortions due to the viewing position of the screen by the fly such that the spatial period of the stimulus presented in different regions of the screen subtended a constant angle on the fly's eye. The stimulus consisted of 8 randomly ordered epochs (the order was changed with each stimulus presentation) in which gratings with different spatial periods (5, 10, 20, 30, 40, 60, 90 ° and a sinusoidally varying contrast uniformly spanning the entire screen equivalent to an infinite spatial period) were presented. Velocities (2.5, 5, 10, 15, 20, 30, 45 °/sec) were adjusted such that the contrast frequency remained constant and equal to 0.5 Hz. Each epoch was presented for 10 seconds, allowing the cells to respond to 5 periods of contrast change, and followed by presentation of the intermediate illumination level over the entire screen for 2 s. The stimulus was applied for 2400 frames or ~226 s such that each of the 8 different epochs was presented at least twice.

The mean response at each spatial period was computed for the entire 10 s of presentation across the two epoch presentations and the Fourier transform of this response was computed. The spectral power density at the 0.5 Hz frequency of the presented contrast change was used as the response strength metric. After computing the response strength at every spatial period for a cell, the strengths were divided by the maximal strength observed for that cell to yield the normalized response curve as a function of spatial period. The average normalized response curve across cells was then computed and presented (Figure 3.24). The mean response over the 2^{nd}, 3^{rd} and 4^{th} response periods within the 10 s of presentation was computed for each cell prior to averaging over cells (Figure 3.23). The mean response at each spatial period was divided by the corresponding maximal response strength observed for the corresponding cell. This was done prior to averaging across cells to extract the mean normalized response traces.

3.3 Results

3.3.1 L2 responses to light are shaped by antagonistic lateral inputs

In these studies we focused on the relation between stimulus geometry and L2 cell responses. Thus, to relate stimulus geometry to L2 responses, we first determined the spatial position of each cell's direct input from photoreceptors. To do this rapidly, we examined L2 responses to the movement of a bright bar sweeping across a dark background. As expected, L2 cells first hyperpolarized when the bar reached each RF center, causing a local light increment (Figure 3.2A). Then, the cells depolarized as the bar moved away, causing a local light decrement. The spatial coordinates of the center of the RF were identified by relating the times at which responses occurred to the position of the bar which moved in opposite directions, both horizontally and vertically across the screen (Figure 3.2B). This procedure was performed for all imaged cells.

We next presented L2 cells with flashes of light covering the entire screen. Interestingly, this uniform stimulus evoked responses from individual L2 cells that varied in polarity, shape, and kinetics (Figure 3.3A). These responses changed progressively across individual axon terminals, following retinotopic shifts in RF position across the screen (Figures 3.3B-D). These observations demonstrated that L2 cells with RF centers directly under the stimulus, hyperpolarized to light, while cells at the periphery of the screen, whose centers were not directly stimulated by light, depolarized. We inferred that cells that depolarized to light responded to lateral antagonistic inputs rather than direct inputs from photoreceptors.

To directly relate these responses to the spatial pattern of light, we generated a "partial field flash" stimulus in which only a portion of the screen was transiently brightened or darkened. Furthermore, to prevent confusion of responses to direct light stimulation with responses to indirect effects; for this and all subsequent stimuli only cells that had RF centers on the screen, based on the moving bar response analysis described above, were considered for analysis.

When analyzing responses to "partial field flashes", to compare cellular responses across conditions, we defined a response strength metric as the mean amplitude of responses to light increments and decrements, and set the sign of this metric, by convention, to be negative for cells that hyperpolarized to light (Figure 3.4, Section 3.2). The relation between response strength and RF center locations showed that cells with RF centers inside the flash region hyperpolarized to brightening and depolarized to darkening, while cells with RF centers outside this region responded with opposite polarity (Figures 3.5A and 3.5B). Thus, individual cells produced responses of opposite polarities to both center and surround stimulation, both to decrements and to increments.

L2 cells provide critical inputs to motion processing circuitry [203]. Behavioral responses to the motion of rotating square wave gratings display a contrast frequency optimum between 5-10 Hz [47, 236]. To assess whether surround responses were sufficiently fast to shape signals relevant to motion vision, we presented brief "partial field flashes" (Figures 3.5C and 3.5D). For flashes lasting 200 ms, we detected responses of opposite polarity to center and surround stimulation. Both response types were biphasic and largely differed in amplitude rather than kinetics (Figure 3.5D). The response shape was consistent with kernels extracted from the responses of L2 cells to dynamically varying noise stimuli (Figure 2.9). Thus, surround inputs influence L2 responses even to rapid stimuli, on timescales that impact motion detection.

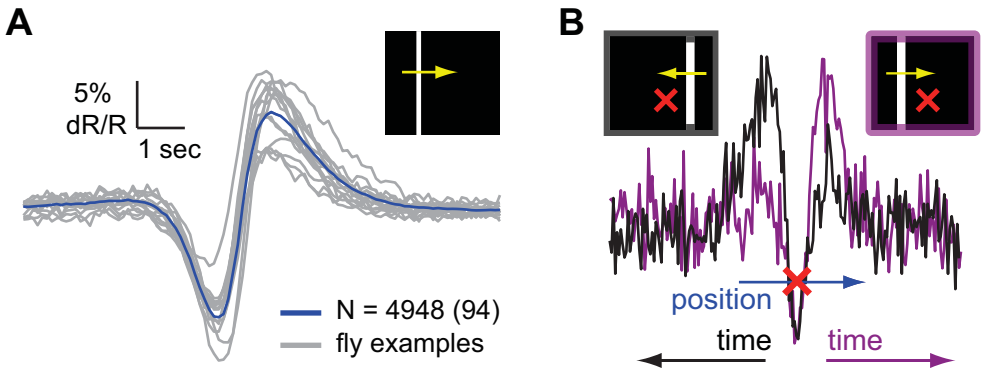

Figure 3.2: L2 cells present a biphasic response to moving bars. **(A)** Mean response of all L2 cells (blue) and average responses from a few example flies (gray) to a bright bar moving on a dark background. In this and all subsequent panels, N denotes the number of cells, with the number of flies denoted parenthetically. Shading denotes ± 1 SEM (standard error of the mean, too small to be observable). **(B)** Identification of the RF center. A single cell's response to a bar moving in two opposite directions, drawn as a function of the bar's position. The time axis for one of the responses (black) is inverted. Red X - the identified RF position.

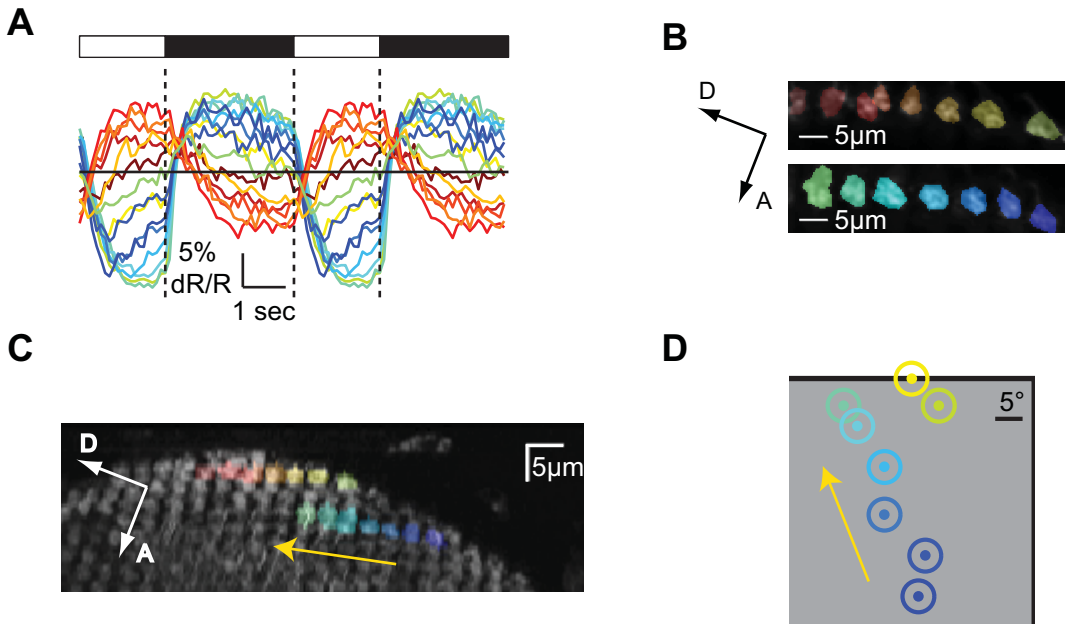

Figure 3.3: L2 cells present variable response shapes to light flashes. **(A-D)** The relation between L2 cell projection locations within the medulla, RF center positions on the screen and response shapes. **(A)** Mean responses of L2 cells to light flashes. Light ON epochs are denoted with open sections of the bar, light OFF epochs with dark sections. Different colors correspond to signals from different regions of interest (ROIs) shown in (B). **(B)** Average images of L2 projections at two distinct depths, overlaid with selected ROIs. Scale bars: 5 μm. **(C)** Maximum intensity projection along the medial-lateral axis of a z-stack of the medulla in which the ROIs shown in (B) reside. Scale bars: 5 μm. **(D)** Location of RF centers on the screen for the ROIs shown in (B) and (C).

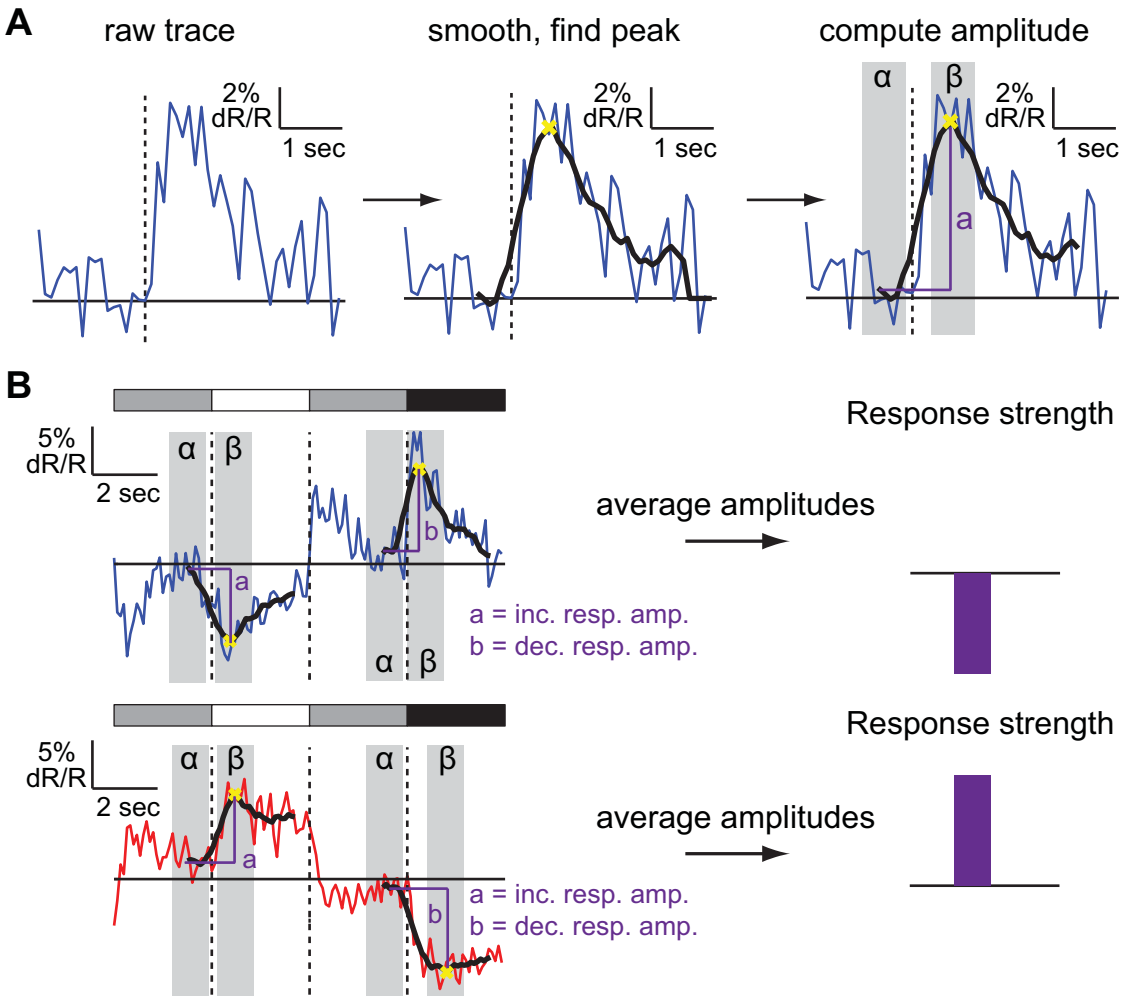

Figure 3.4: Computation of response amplitudes and strengths. **(A)** A schematic description of the procedure for computing response amplitudes. The raw response trace is first smoothed by averaging it using a moving 600 ms window, and the maximum value within the first 1.2 s of stimulus presentation is identified. The response amplitude, denoted as a, is defined as the difference between the maximal average response identified as above (averaged over the gray patch denoted as β in the right most panel) and the average response value in a 600 ms window prior to the stimulus appearance (averaged over the gray patch denoted as α in the right most panel). **(B)** A schematic description of the procedure of averaging the amplitudes of responses to an increment (denoted as a) and a decrement (denoted as b) to compute the overall response strength. The amplitudes of the responses to the increment and the decrement are computed and the response strength is set as the mean absolute amplitude value, with an appropriate sign. Top: negative response strength example - the cell hyperpolarizes to light, bottom: positive response strength example - the cell depolarizes to light.

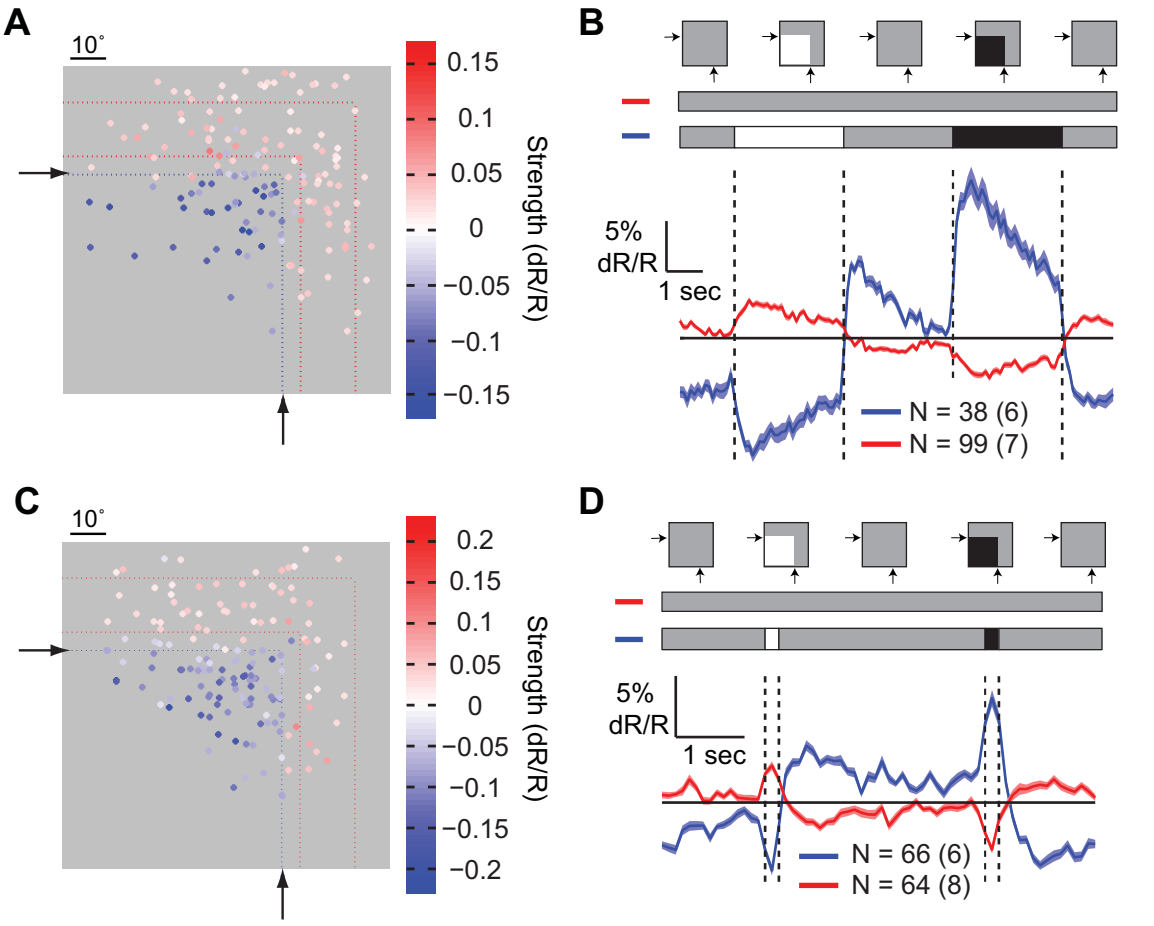

Figure 3.5: The shape of L2 cell responses depends on the relative position between their RF centers and the contrast change area. **(A and B)** The response of L2 cells to a contrast change covering a portion of the screen, on a background of intermediate illumination. **(A)** Heat map of response strengths as a function of the RF center location on the screen, indicated by dots. Colors indicate the strength and sign of the corresponding cell response. Only cells with response strengths >0.025 or <-0.015 are presented. Black arrows and blue dotted lines denote the region of the screen where the flash was presented. Red dotted lines denote the region of the screen where surround responses shown in (B) were observed. **(B)** Mean response of L2 cells to the flash presentation, separated by polarity and position. Blue - cells within the flash presentation region, which hyperpolarized to light; red - cells outside of the flash presentation region, which depolarized to light. Shading denotes ±1 SEM. Top: schematic description of the stimulus, including the contrast inputs into each group of cells (red curves corresponding to cells seeing no contrast changes). **(C and D)** Same as (A) and (B) for cells responding to a 200 ms flash presentation, including only cells with response strengths larger than a 0.02 threshold.

3.3.2 The L2 RF has a narrow center, and an extended surround

We next examined how L2 responses vary as a function of the extent of center and surround stimulation by presenting circles and annuli, of either contrast polarity, around identified RF centers. As expected from a RF with an antagonistic center-surround organization, responses to large circles were weaker than those to small circles (Figure 3.6). In addition, annuli with sufficiently large internal radii so as to reduce center stimulation (4° and above) produced inverse responses (Figure 3.7). We infer that surround effects become stronger than center effects approximately 5° away from the RF center, and extend radially to more than 15°.

To quantify the effects of surround stimulation, we computed response amplitudes as a function of the spatial extent of the stimulus (Figure 3.8). While for both dark and bright circles, increasing the size of the stimulus decreases the amplitude of the repsonse, this analysis showed that the relative effect of surround stimulation differed between increments and decrements. For increments, amplitudes of responses to large circles were ~50% smaller than responses to small circles ($p < 10^{-4}$). For decrements, the fractional decrease in amplitude with stimulus size was smaller, and due to larger noise effects on these measurements this difference did not reach statistical significance.

We finally also tested whether responses of L2 cells to circles and annuli as a function of time could be described as linear combinations of center and surround inputs. To do this, we compared measured responses evoked by combined center and surround stimulation with linear summation of responses to each individual component. For many such combinations, linearly predicted responses significantly differed from measured responses, particularly for contrast decrements (Figure 3.9). Thus, the L2 RF is non-linear in space and any model used to describe these responses must account for this property.

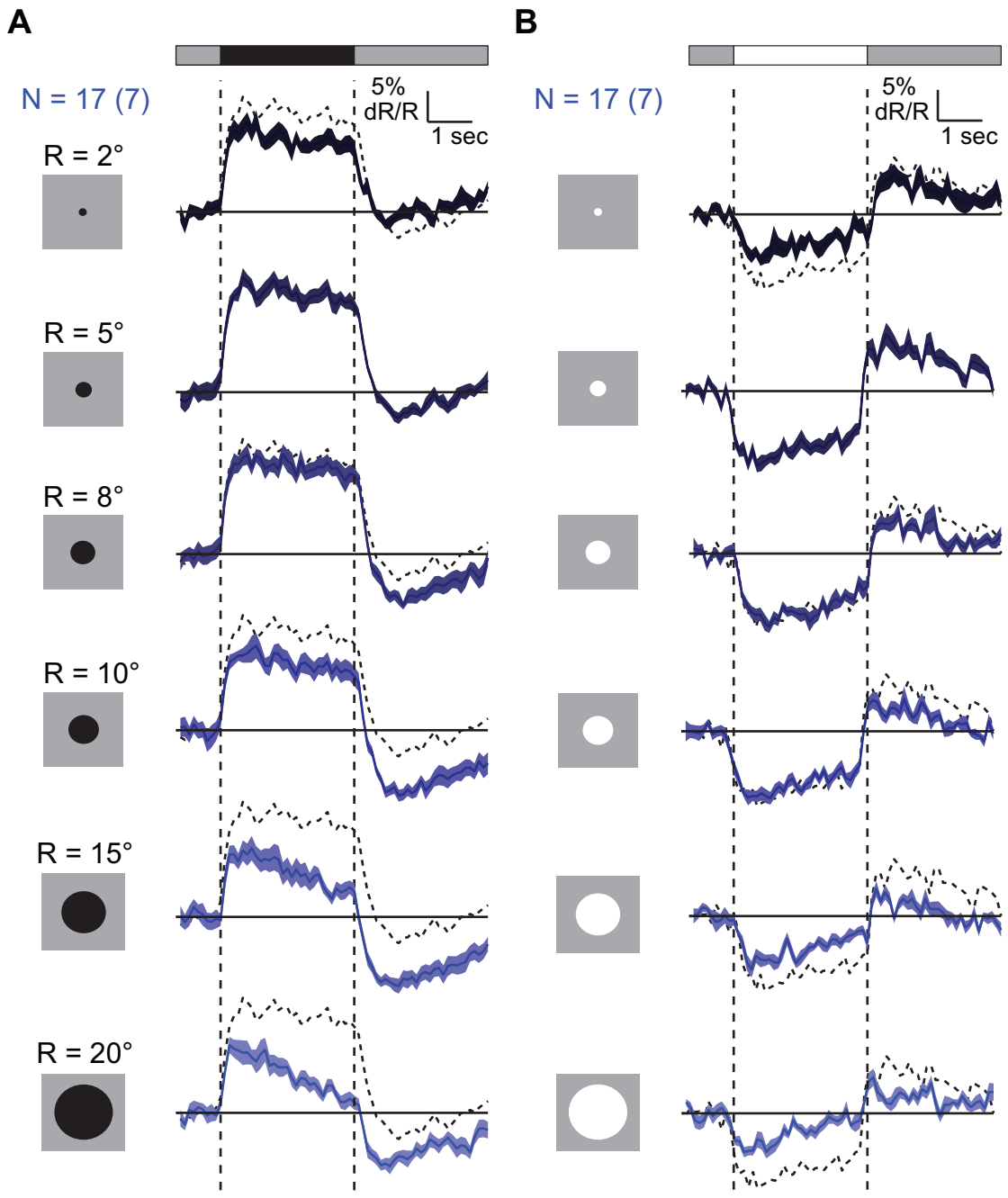

Figure 3.6: Lateral antagonisms makes L2 cell responses to large circles weaker than responses to small circles. **(A and B)** Mean responses to dark (A) and bright (B) circles of different sizes presented for 3 s over an intermediate illumination level background, around identified RF centers, in a random order, together with the presentation of annuli (Figure 3.7). Dashed curves are mean responses to a circle with a radius of 5° drawn for reference. Shading denotes ±1 SEM.

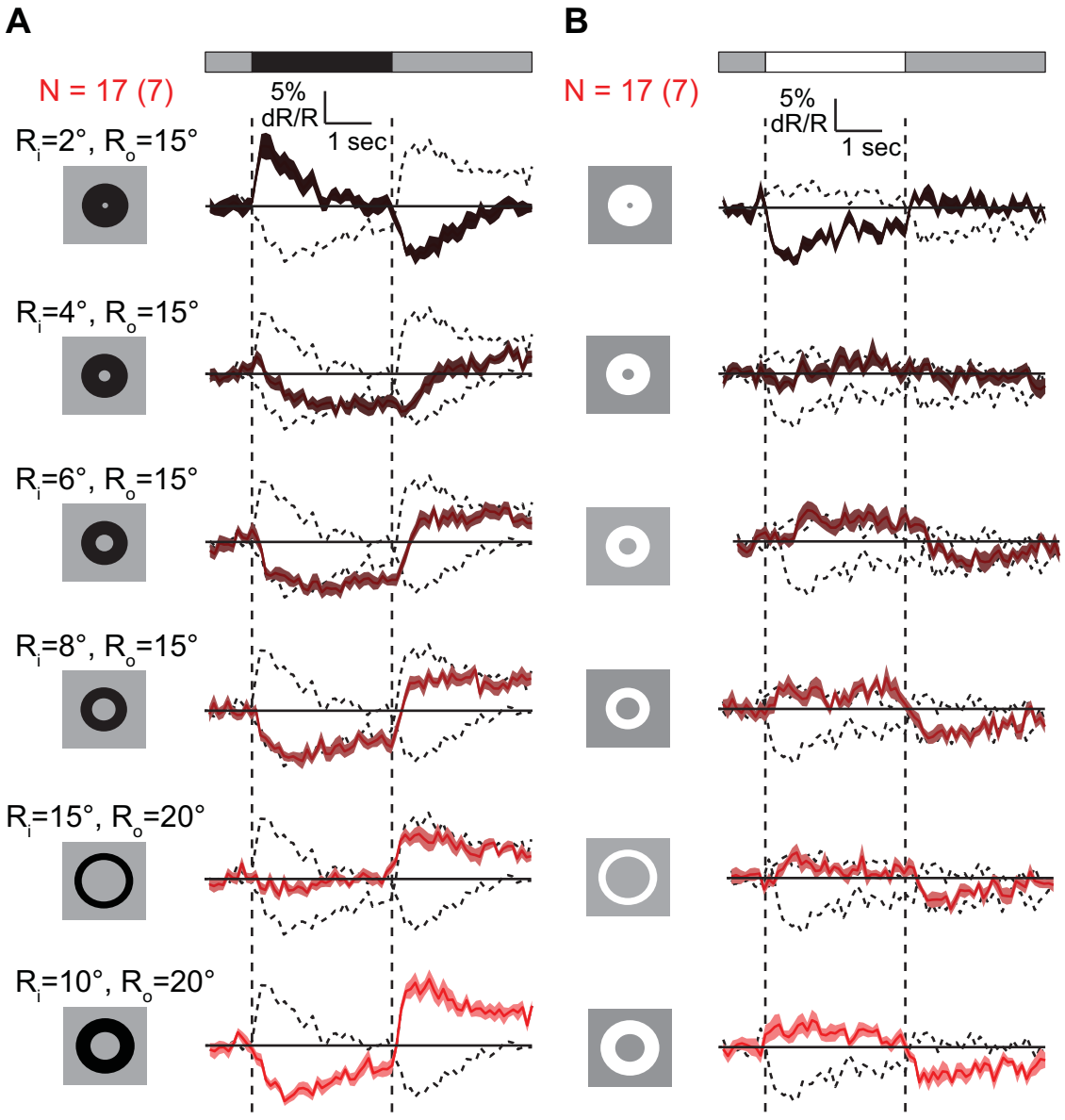

Figure 3.7: Lateral antagonisms makes L2 cell responses to annuli with sufficiently large radii inverted. **(A and B)** Mean responses to dark (A) and bright (B) annuli of different sizes presented for 3 s over an intermediate illumination level background, around identified RF centers, in a random order, together with the presentation of circles (Figure 3.6). Dashed curves are mean responses to annuli with R_i=10° and R_o=20° and with R_i =2° and R_o=15°. Shading denotes ±1 SEM.

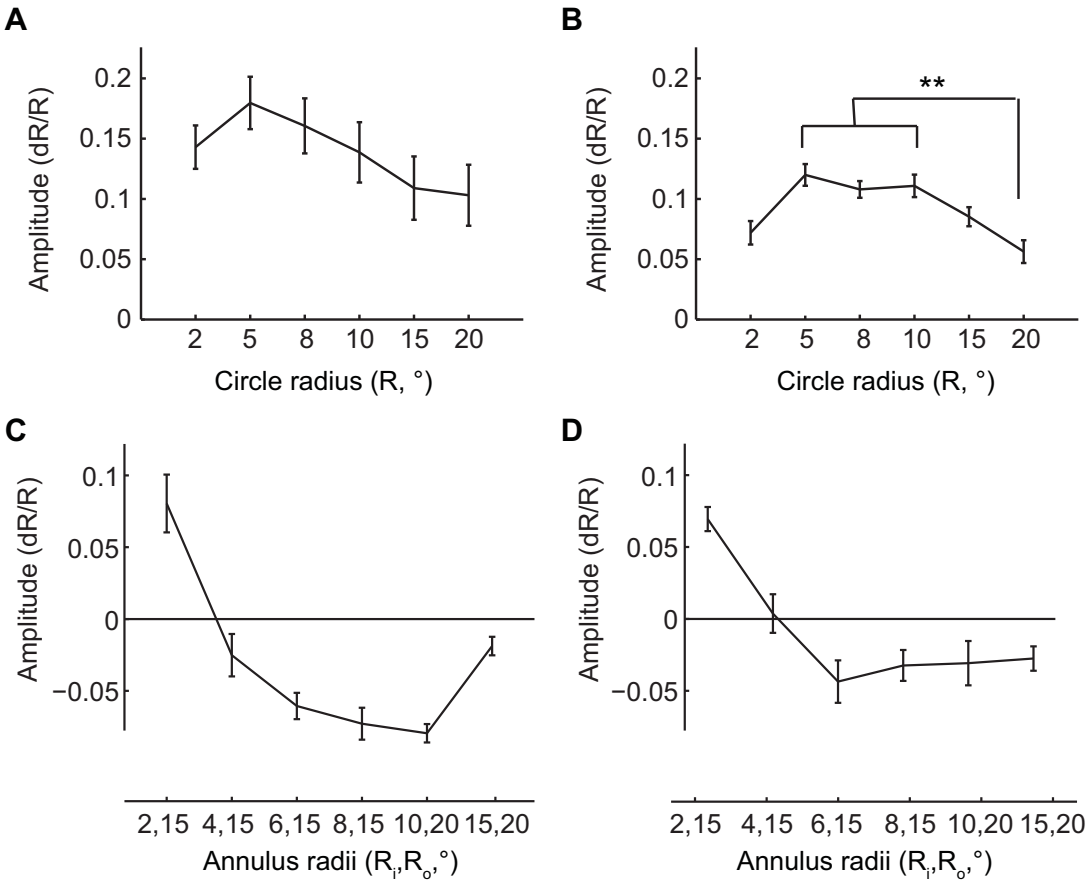

Figure 3.8: Amplitudes of L2 cell responses to circles and annuli. **(A and B)** Mean amplitudes of responses to dark (A) and bright (B) circles, as a function of the radius, R. ** a significant difference between the two means was found using one-way anova, according to Tukey's honestly significant difference criterion (B). **(C and D)** Amplitudes of responses to dark (C) and bright (D) annuli as a function of the internal and external radii, R_i and R_o. Negative amplitudes represent hyperpolarizations to light and positive amplitudes depolarizations to light. Error bars denote ±1 SEM

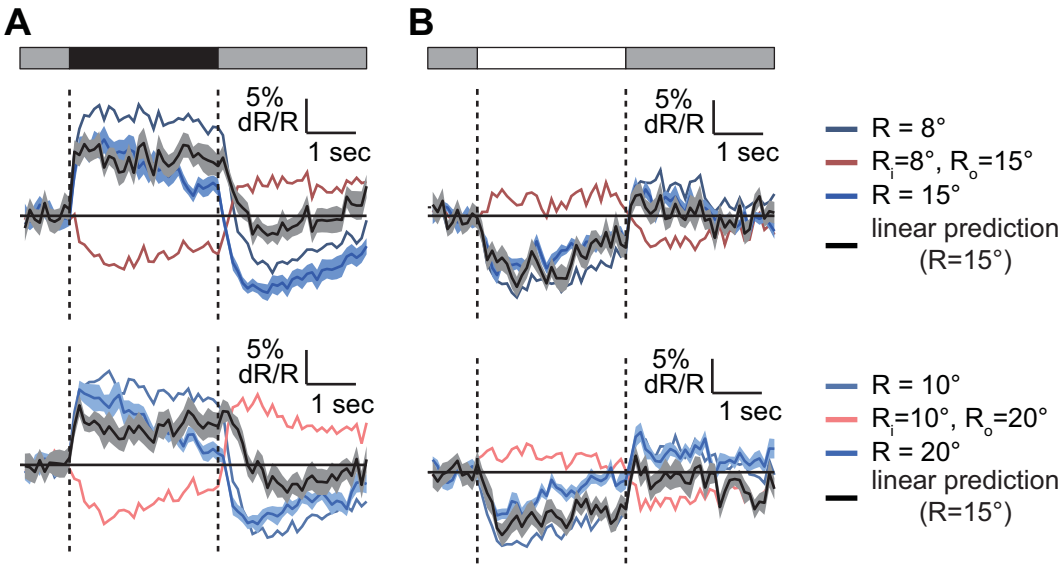

Figure 3.9: L2 cell responses are non-linear in space. **(A and B)** Comparing predicted responses (black continuous traces) to measured responses (blue continuous traces) to the presentation of a 15° circle (top) and a 20° circle (bottom), assuming linearity, as a sum of responses to circles and annuli of appropriate sizes. Dark stimuli responses (A), bright stimuli responses (B). Shading denotes ±1 SEM.

3.3.3 Lateral antagonism links spatial structure to response kinetics

As L2 cells provide inputs to motion detecting circuits, different temporal filtering properties applied to objects of different shapes and contrasts by these cells would change motion sensitive outputs. Responses to circles and annuli revealed that, in addition to affecting response strength, surround inputs influence response kinetics. We quantified these effects by comparing mean response values at different time-points during the presentation of these stimuli. For small circles, response amplitudes changed very little during stimulus presentation, while for large circles, significant decreases in amplitude were observed (Figure 3.10). As more inhibition was provided together with excitation, responses became increasingly transient. As a result, the spatial RF shape effectively became sharpened over time (Figure 3.11).

The effect of inhibition on decay extent was more pronounced for dark circles as compared to bright circles with all hyperpolarizing responses presenting some decay (Figure 3.12). Thus, it is possible that a mechanism that makes hyperpolarizing responses to increments transient does not act similarly on depolarizing responses to decrements. Accordingly, only depolarizing responses require surround inputs for transience. One possibility is that transience in hyperpolarizing responses could be mediated by extracellular potentials within the lamina cartridge [256], with surround stimulation potentially contributing to the decay. We note that an imbalance in the relative strengths of increment versus decrement stimuli may also play a role in determining decay rates.

A separable spatiotemporal RF is described by the multiplication of a temporal filter with a spatial filter [217]. With such an RF, responses to circles of different sizes are predicted to vary in scale but not in kinetics. However, as we observed that decay rates increased with surround stimulation while response amplitudes decreased, the L2 RF must be spatiotemporally coupled (not separable). Interestingly, spatiotemporal coupling can also be observed in responses to annuli, particularly dark ones (Figures 3.13A and 3.13B).

Plotting the mean response values at different time points during the presentation

of annuli of different sizes revealed that, at the edge of the RF center, responses grow stronger over time instead of decaying (Figures 3.13C and 3.13D). Thus, responses to dark annuli with internal radii of 4° or 6° are initially hyperpolarizing (left box, blue curves in Figure 3.13C), and the extent of hyperpolarization increases during the response (left box, red curves in Figure 3.13C). That is, surround responses next to dark edges are sustained, effectively enhancing their contrast. Interestingly, surround responses further away from dark edges, near similarly responding cells, are more transient (right box, Figure 3.13C). This suggests that L2 responses are shaped not only by inputs from neighboring columns directly stimulated by light but also by columns responding only to more lateral inputs. These results argue that models of L2 responses to either center or surround stimulation should include two components: one component that gives rise to a sustained center or surround response, and another component that will transform the sustained response to a transient one.

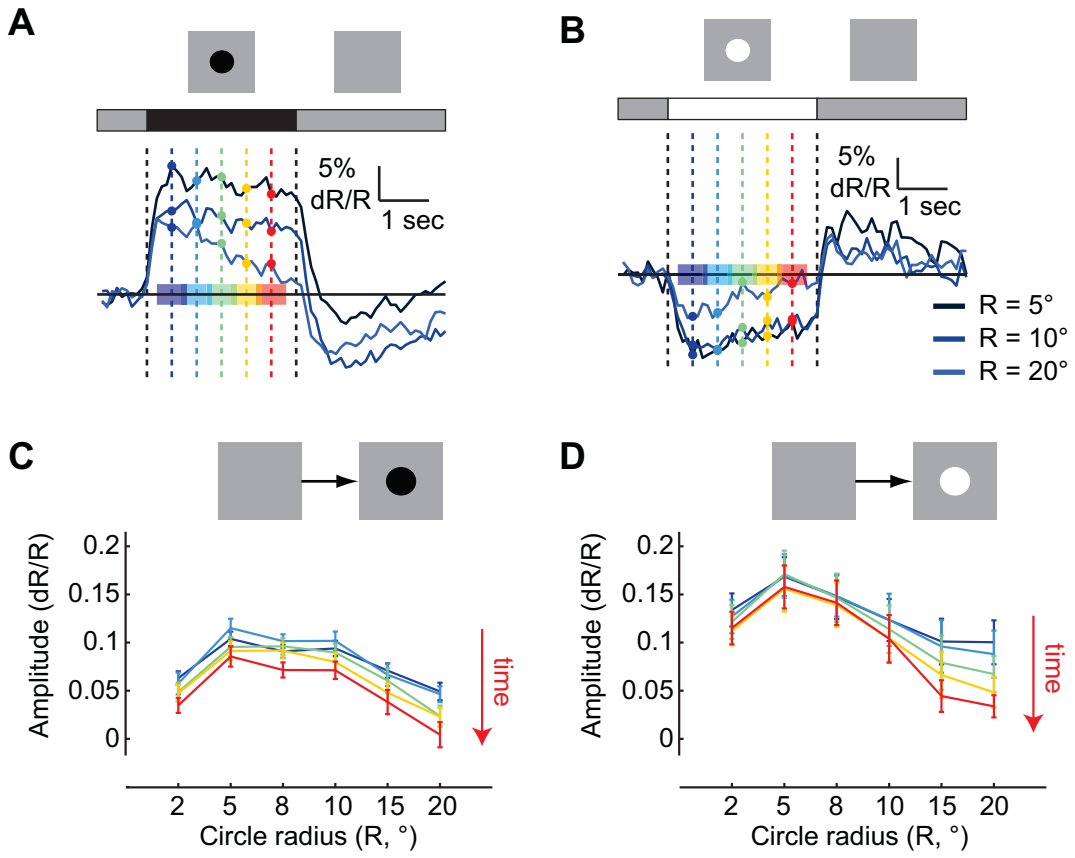

Figure 3.10: Surround stimulation makes L2 responses more transient. **(A and B)** Mean responses to dark (A) and bright (B) circles of different sizes as a function of time. Dark blue curves represent the mean responses to small circles and bright blue curves the mean responses to large circles. Amplitudes were measured for the different responses at different time points, shown as vertical lines and sample points in different colors, to estimate the dynamical changes in the spatial RF shape. Average amplitudes were computed over the intervals indicated by colored patches. Cold colors represent early stages of the response and warm colors late stages. **(C and D)** Amplitudes of responses to dark (C) and bright (D) circles, as a function of the radius R, at different time points during the response, represented by different colors as defined in ((A) and (B)). Error bars denote ±1 SEM.

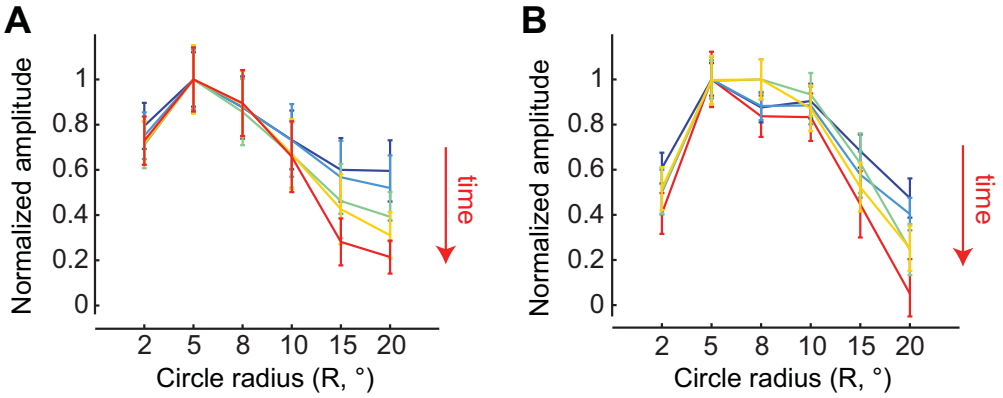

Figure 3.11: Surround inhibition makes the RF narrower over time during the response. **(A and B)** Normalized amplitudes of responses to dark (A) and bright (B) circles of different sizes as a function of their radius R, at different time points during the response. Each curve is normalized to the maximal response strength over all radii. Error bars denote ±1 SEM.

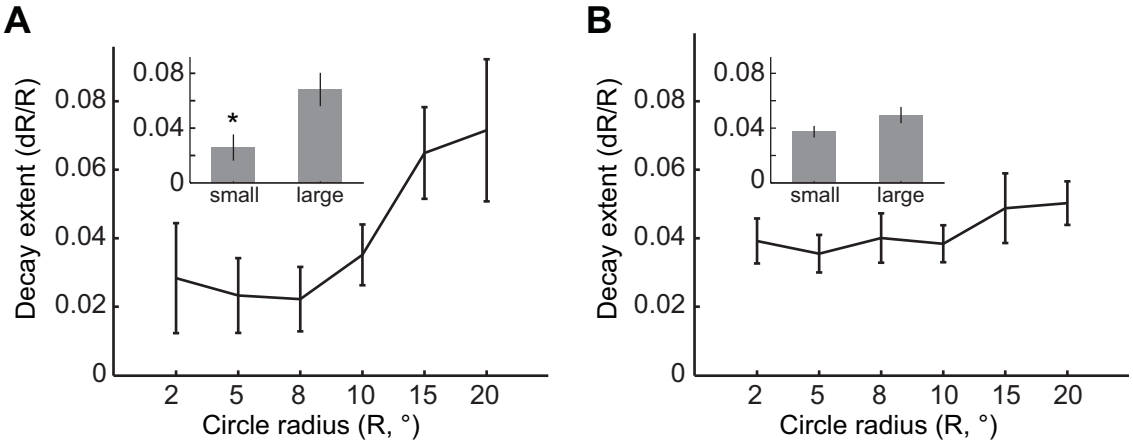

Figure 3.12: Surround inhibition significantly affects decay rates of responses to decrements. **(A and B)** The absolute change in response amplitudes during circle presentation as a function of the radius, R, for dark (A) and bright (B) circles. Inset: Comparison of decay extents for large (R = 15°, 20°) and small (R = 2°, 5°) circles. Error bars denote ±1 SEM. *p $<$ 0.05 in a two-tailed students t-test with unequal variances.

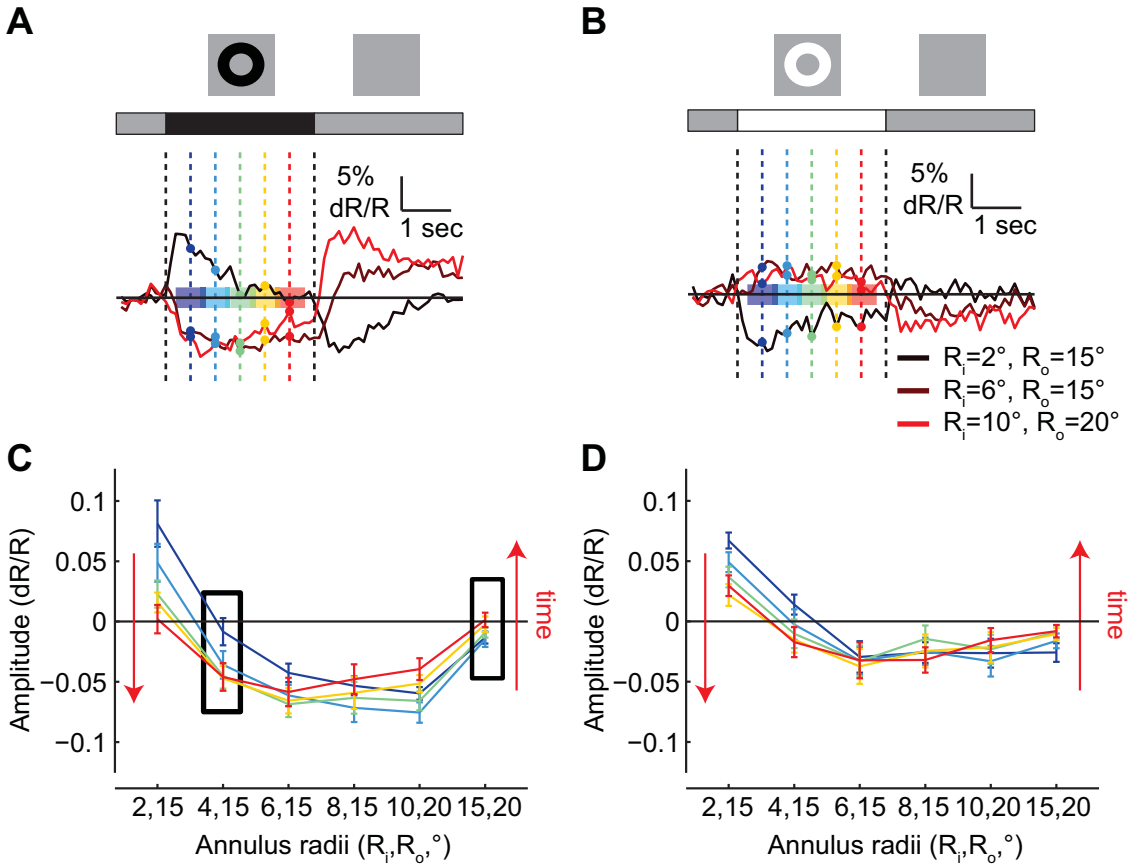

Figure 3.13: Antagonism also affects the decay rates of surround responses. **(A and B)** As in Figures 3.10A and 3.10B, describing responses to dark (A) and bright (B) annuli of different sizes. **(C and D)** As in Figures 3.10C and 3.10D, describing the strength of responses to dark (C) and bright (D) annuli of different sizes.

3.3.4 A simple model captures L2s inseparable spatiotemporal RF

To assess whether the variability in decay rates observed in responses to dark stimuli could arise via simple mechanisms, we constructed a quantitative model of the L2 RF. Previous work demonstrated that a weighted sum of two opposite-signed inputs associated with different time constants can produce responses with different decay rates [75, 76, 201, 205]. Thus, we constructed a model comprising two weighted inputs: a primary input associated with a fast rising exponential and an antagonistic input associated with a slowly decaying exponential (Figure 3.14). With appropriate weights, a fast rising and gradually decaying response, similar to the response to the presentation of a large dark circle, was produced.

We next tested whether the model's weights and time constants could be appropriately tuned to the different responses observed in L2. Indeed, increasing the weight of the antagonistic component decreased the amplitude of the response and increased the rate of its decay (Figure 3.15A) as observed in L2 responses to circles of increasing sizes (Figure 3.6). Interestingly, delaying the development of the antagonistic input by increasing the time constant of the exponential decay produced both increased amplitudes as well as reduced decay rates because the excitatory response can develop further before inhibition suppresses it (Figure 3.15B).

To fit L2 responses with this model using a small parameter set, we assumed that each input is associated with a circularly symmetric Gaussian structure over space (Figure 3.16A). Thus, the weight of each model component was set by appropriately integrating over this structure. As a result, predictions of both responses to circles and annuli were based on a difference of Gaussians spatial model structure (Figure 3.16B).

We first fitted this model to responses of L2 cells to the presentation of dark circles of variable sizes (Figures 3.17 and 3.18A; Section 3.2). The primary input in these responses was associated with the RF center and the antagonistic input with the surround. The fit parameters are described in Table 3.1. Note that while the amplitude of the center component is significantly larger than the amplitude of the

surround component, taking into account the small standard deviation associated with this component, the center and surround strengths shaping these responses are in fact similar in magnitude, as reflected by the spatial RF shape shown in Figure 3.16B. Next, responses to dark annuli with large internal radii (>4°) were fitted with the same model using different parameters (Figure 3.18B), as described in Table 3.2. The primary model component in this case corresponded to a surround while the antagonistic component was a surround antagonist that caused surround responses to decay. The different parameters accounted for the spatial non-linearity of the L2 RF (Figure 3.9), as well as the different kinetics of decaying center responses and surround responses (Figures 3.5B, 3.6, 3.7, 3.9 and 3.19). Thus, the primary surround input giving rise to responses to annuli was stronger, and had a shorter time constant, than the antagonistic input that suppressed responses to center stimulation. However, in spite of amplitude and kinetics differences, both these inputs were fit by the same spatial parameter, which is likely set by the columnar structure of the eye. Finally, the surround antagonist component had a broad spatial extent and a time constant similar to that of the antagonistic input in the circle response model. We hypothesize that this component is mediated by lateral inputs from columns in which surround responses occur.

Overall, the fits to the six circles and four annuli responses explained 98% of the variance in the measured responses (Figure 3.18). Finally, fitting responses to annuli with small internal radii (2° and 4°), that partially stimulate the center but also provide significant surround stimulation required a distinct weighting of inputs (Figure 3.20, Table 3.3 and Section 3.2). In contrast, most responses to bright circles of different sizes could be captured simply as scaled versions of the same response shape (Figure 3.21).

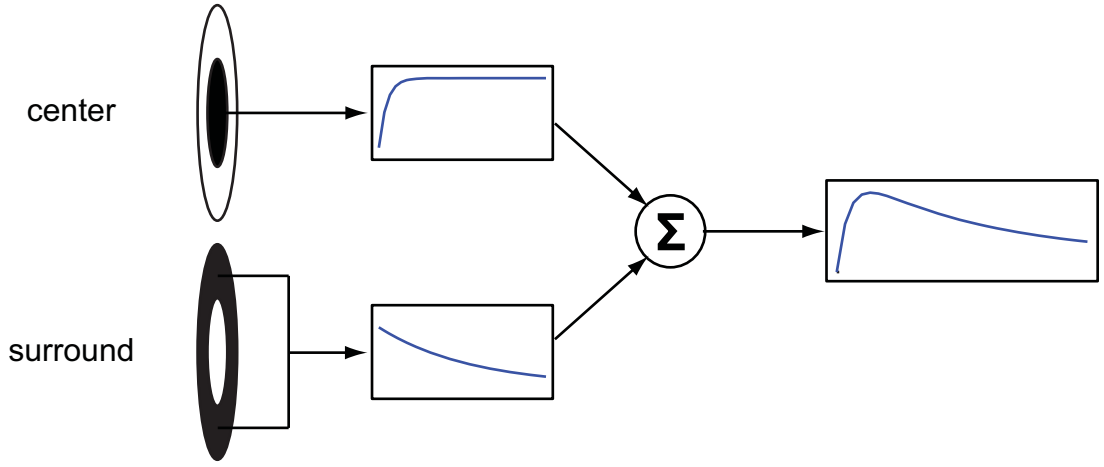

Figure 3.14: A simple model explaining L2's inseparable responses to decrements. A schematic description of the model. The primary component, arising from stimulation of the RF center, is associated with a fast rising exponential (top); the antagonistic component, arising from stimulation of the RF surround, is associated with a slow decaying exponential (bottom). These two inputs are summed to give rise to the response.

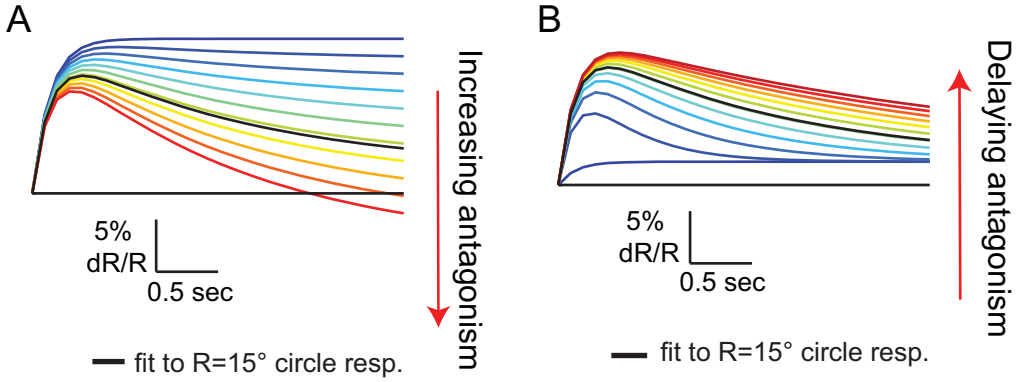

Figure 3.15: Differential weighting and time-constants of model components gives rise to responses with different amplitudes and decay rates. **(A)** The effect of increasing the amplitude of the antagonistic (slow, decaying) exponential on the overall responses. Cold colors - low antagonism (darkest blue - no antagonism); warm colors - high antagonism. **(B)** The effect of delaying antagonism with respect to excitation by making the antagonistic component time-constant longer. Cold colors - short time constants (darkest blue - inhibition and excitation constants are the same), warm colors - long time constants for inhibition.

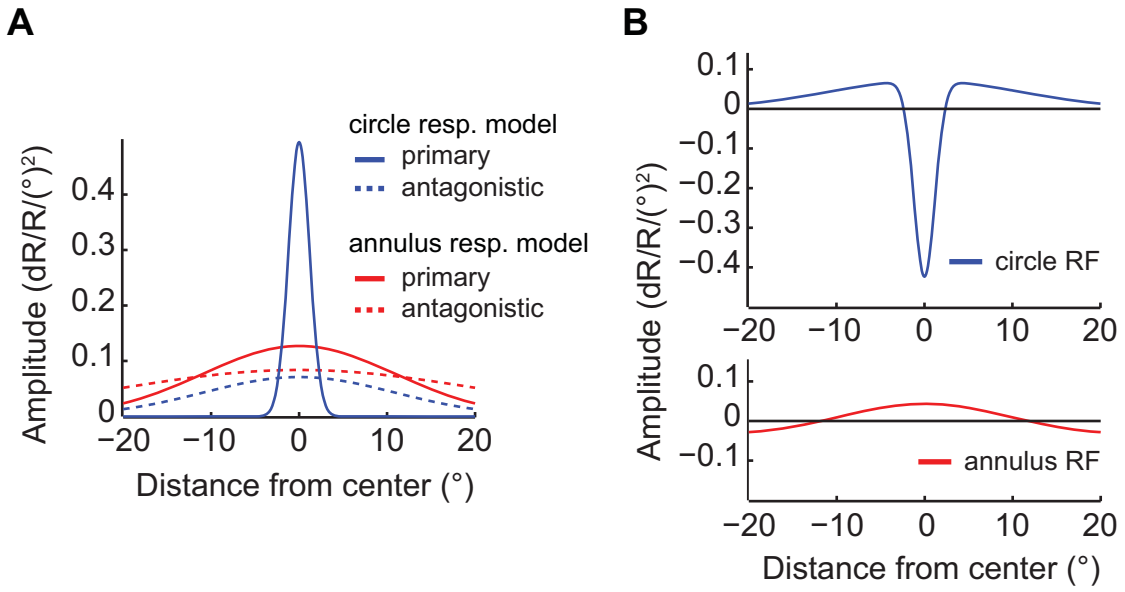

Figure 3.16: Gaussian distributions of model components in space. **(A)** The strength of the primary (continuous traces) and antagonistic (dashed traces) components over space used to set the weights of these components in simulations of circle (blue) and annuli (red) responses. **(B)** The resulting RF shape inferred from the spatial distribution of component strengths used in modeling responses to circles (top) and to annuli with R_i >4° (bottom).

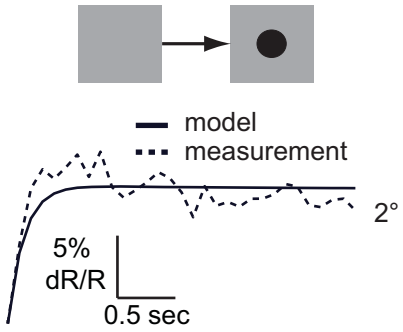

Figure 3.17: The simulated response to a small circle shows no decay. Simulated (continuous) and measured (dashed) response to dark circle with radius R=2°

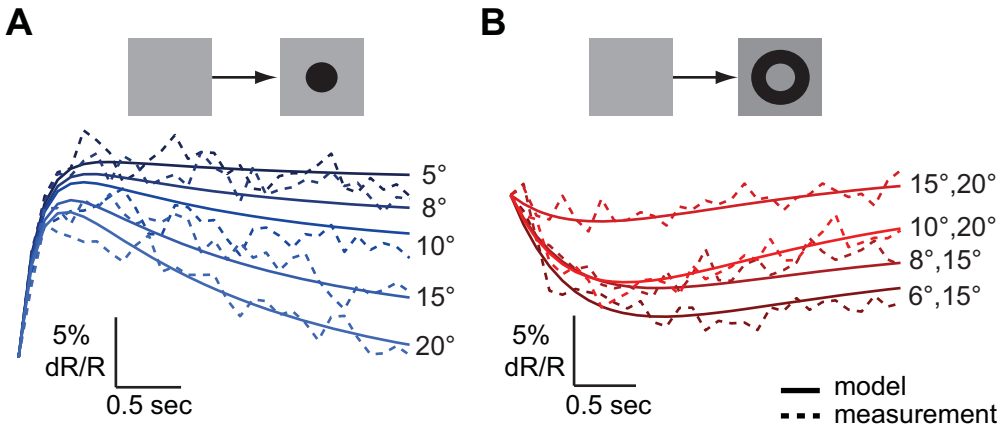

Figure 3.18: Responses to circles and annuli are well predicted by the model. **(A)** Simulated (continuous) and measured (dashed) responses to dark circles of variable sizes. Dark blue curves correspond to small circles, lighter blue to large circles (as in Figure 3.6). Responses were simulated as a difference of an exponential rise and decay associated with a Gaussian distribution of strength over space. **(B)** Simulated (continuous) and measured (dashed) responses to annuli of variable sizes; dark red curves correspond to annuli with small internal radii and bright red curves to annuli with large internal radii (as in Figure 3.7).

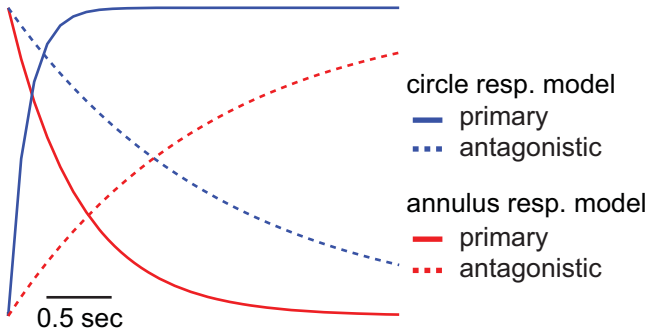

Figure 3.19: The temporal components of the model. Each component is associated with a different time constant and contributes either a rising or decaying exponential response over time to the overall response.

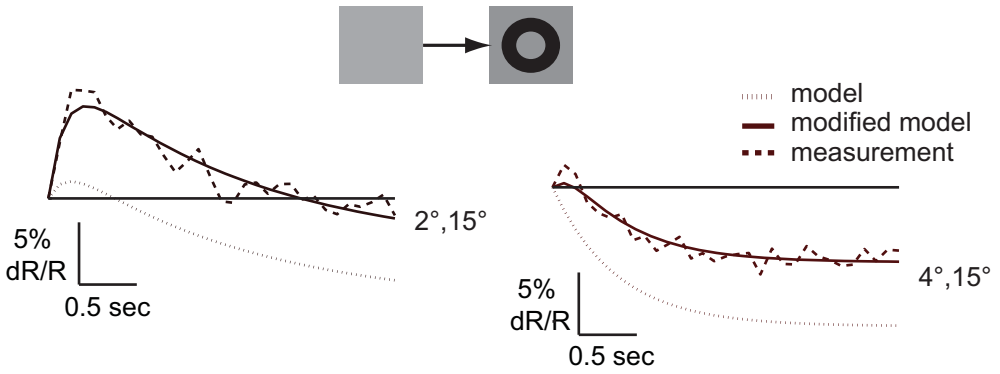

Figure 3.20: Different parameters are required to capture responses to annuli with small internal radii. Simulated and measured responses (dashed) to an annulus with R_i=2° and R_o=15° (left) and an annulus with R_i=4° and R_o=15° (right). The simulated (dotted) responses to annuli with small radii constitute poor fits to the measured responses, as a result of underestimation of the relative contribution of excitation to these responses. Continuous curves show improved model predictions with modified parameters (see Section 3.2 for details).

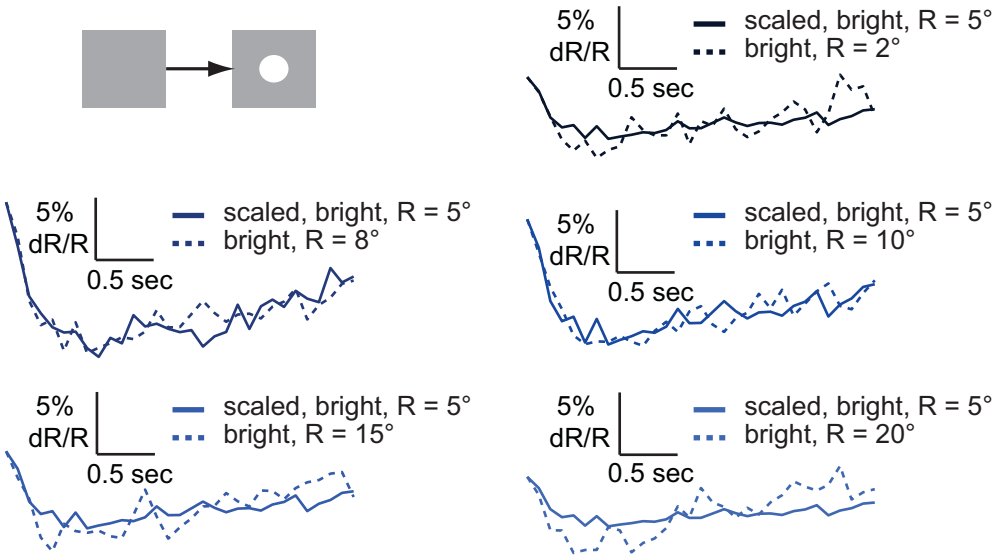

Figure 3.21: Responses to bright circles of different sizes are simply scaled. Responses of L2 cells to bright circles of different sizes approximated by simple scaling. The measured (dashed) and approximated (continuous) responses are overlaid, highlighting the similarity. The approximations are appropriately scaled versions of the response to a 5° large bright circle (scale factor determined by minimizing the mean squared error between the approximation and the measured response).

3.3.5 Lateral antagonism creates anisotropic acuity

A center-surround RF should differentially affect the amplitudes of responses to stimuli with different spatial periods (e.g., [63]). Thus, the relative strengths of responses to sinusoidal inputs with different periods provide a measure of acuity. Furthermore, acuity differences between different axes may represent an early specialization for the detection of motion in a particular orientation ([226]). To examine whether this occurs in L2 cells, we measured responses to sinusoidal gratings with periods ranging from 5° to 90°. The gratings were drawn on a virtual cylinder and projected onto the screen. Each grating was rotated at a different speed so that the temporal contrast frequency was held constant at 0.5 Hz for all gratings, and was oriented to simulate either pitch or yaw rotations of the fly (Figure 3.22).

L2 responses to these stimuli were sinusoidal, as expected for a linear system (Figure 3.23; [47]). Intriguingly, at short spatial periods (10° and 20°), responses to pitch rotations were stronger than responses to yaw rotations ($p<10^{-5}$), Figures 3.23 and 3.24. At a 5° spatial period, responses were weak, as expected from retinal optics and a RF center of approximately 5° ([113, 230]), while spatial periods around 40° drove the strongest responses. Only slight attenuation was observed at larger spatial periods (Figure 3.24). This could be for physiological reasons, arising, for example, from effects of the relative timing of center and surround stimulation on antagonism. However, this could also result from technical limitations of our stimulus presentation, as our display spanned slightly less than 60° of visual space in each direction. Nevertheless, as the observed responses at short spatial periods clearly showed higher sensitivity with pitch rotations, visual acuity must be higher around this axis, making the L2 RF spatially anisotropic.

Analogous results were obtained using a moving bright bar stimulus. When the bright bar reached the RF surround, a depolarization occurred. This early response was weak on average (Figures 3.2A, 3.25) since the bar is bright and narrow, and thus stimulates the surround only weakly, but some individual response instantiations were significant (Figure 3.2B). The strength of this response depended on the orientation of the bar. In particular, if the bar moved upward across the screen this phase of the response was stronger than when the bar moved medially (Figure 3.25).

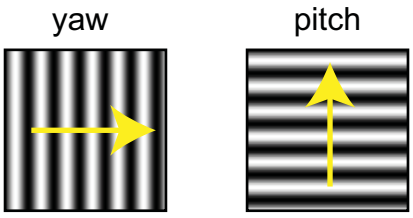

Figure 3.22: Sinusoidal moving gratings: schematic. Schematic description of the stimulus: sinusoidal contrast gratings moving around the yaw (left), and pitch (right) axes.

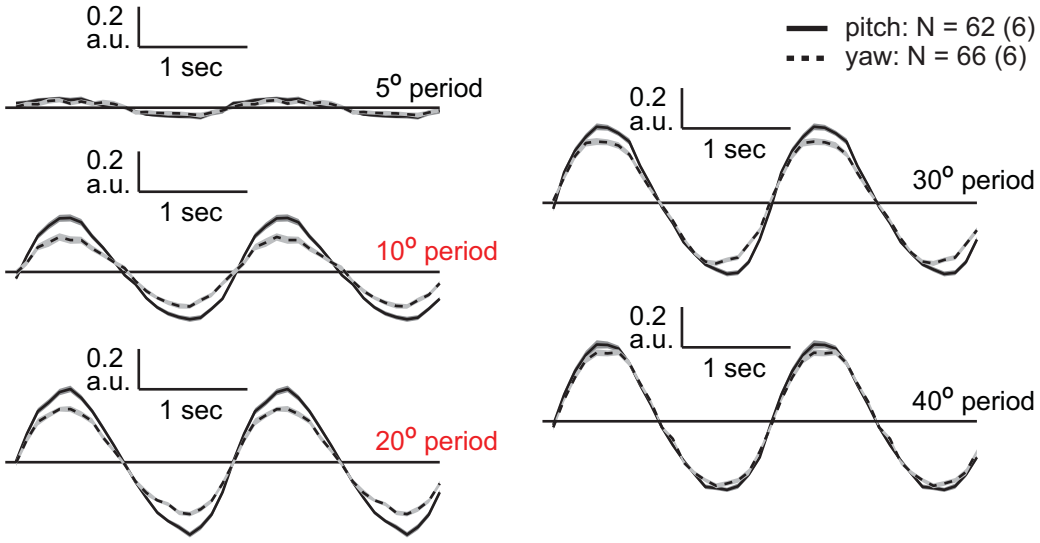

Figure 3.23: Responses to sinusoidal moving gratings are sinusoidal. Normalized mean responses to moving sinusoidal gratings with different spatial periods, moving around the pitch (continuous) and yaw (dashed) axes. Responses were normalized to the maximal response amplitude across all spatial periods. Shading denotes ±1 SEM. Spatial periods where responses to pitch and yaw orientations significantly differed are highlighted in red.

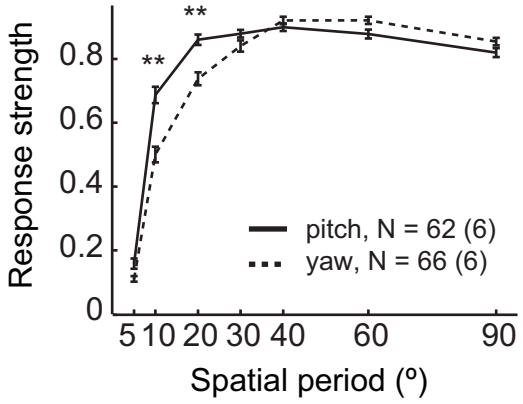

Figure 3.24: The strength of the response to a grating depends on its spatial period. Response strength as a function of the spatial period of the grating moving around the pitch (continuous) and yaw (dashed) axes. Error bars denote ±1 SEM. **p<0.001 in a two-tailed students t-test with unequal variances.

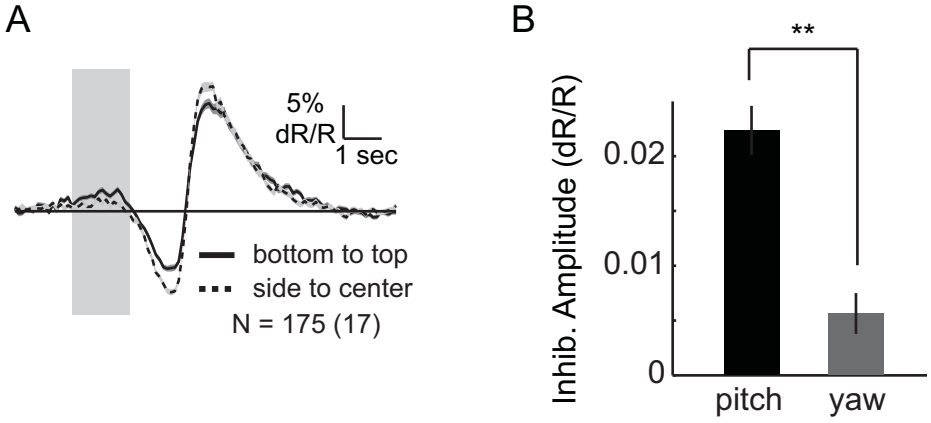

Figure 3.25: Inhibition in a moving bar response is stronger when the bar moves from the screen bottom to the top. **(A)** Mean response to a bright bar moving from the screen bottom to the top (continuous) or from the side of the fly to its front (dashed). **(B)** The extent of inhibition in the response to a moving bar described in (A), quantified by averaging over the dark shaded area and subtracting the mean baseline response.

3.4 Discussion

Using high-throughput methods, we describe a non-linear, spatiotemporally coupled center-surround antagonistic RF structure in L2 cells that causes these cells to respond differently to dark or bright inputs of different sizes. These functional properties have implications for the computations performed by downstream motion processing pathways. In particular, L2 cells provide non-local inputs to elementary motion detectors, and the temporal filtering operations applied to intensity inputs depend on the geometry and contrast of the moving objects.

3.4.1 L2 cells have an antagonistic center-surround receptive field

The L2 RF displays an antagonistic center-surround organization over space (Figures 1 and 2), an observation that is consistent with electrophysiological studies in larger Diptera [63, 153]. The radius of the RF center is between 3° and 5°, while the surround peaks approximately 10° away from the RF center. An additional, diffuse component of the surround persists as far as 15° or more away from the center. Importantly, this spatial RF is non-linear. Center responses dominate surround antagonism such that responses to surround stimulation alone are stronger than predicted from responses to combined center and surround stimulation. Furthermore, the kinetics of surround responses differ from the effect of surround inputs on center responses. As a result, the distance from the RF center at which surround and center effects were balanced varied with stimulus geometry. Nonetheless, across all conditions, surround responses were weaker than center responses, consistent with earlier observations [63, 247, 228].

3.4.2 The L2 RF is spatiotemporally coupled yet can be captured by a simple model

Lateral antagonistic signals shape L2 responses to enhance spatial and temporal contrast by generating a biphasic filter in both space and time, a classical role for inhibition in sensory processing [150, 198]. Furthermore, surround strength decreases with

the distance from the center, consistent with theories assigning efficient encoding goals for early visual processing such as predictive coding and information maximization [247, 228]. However, while such theories often use linearity and spatiotemporal separability to facilitate derivation, L2 responses are inconsistent with these assumptions. In particular, response kinetics depend on the spatial properties of the stimulus and its contrast polarity (Section 3.3.3, [247, 148, 153, 172]). Additional non-linearities, particularly those dependent on light adaptation conditions, have also been observed at this synapse [122, 145, 255].

Nevertheless, the spatiotemporal inseparability of the L2 RF can be captured by a simple computational model that combines two linear and separable inputs [75, 201]. The fitted model consists of two different sustained components, with distinct time-constants, representing a primary input and an antagonistic input (Figure 3.14). For responses to circles, these components correspond to a center and a surround; for responses to annuli, these correspond to a surround, and a surround antagonist. Thus, the spatial non-linearity of L2 is captured by utilizing different amplitudes and time-constants of antagonism, depending on whether the center of the RF is stimulated. Furthermore, for both circles and annuli, the strength of the antagonistic component is set by the spatial structure of the stimulus and determines the decay rate of the response. Thus, L2 responses are affected by interactions with neighboring columns, regardless of whether those columns receive input from stimulated photoreceptors or from lateral pathways. Similar models have been used to describe other visual processing neurons [71, 87, 112, 145, 205].

3.4.3 The spatiotemporally coupled L2 RF efficiently encodes dark object motion cues

Given that L2 responds nearly linearly to rapid contrast changes [47], can L2 be specialized to enhance information relevant to downstream processing? L2 represents a critical input to a neural circuit that specifically detects moving dark edges [47, 116]. Interestingly, the detailed characteristics of L2 responses to decrements are particularly useful for encoding motion related cues (Figure 3.26). When an object

moves in front of an array of photoreceptors, its motion transforms its spatial structure into a temporal pattern of activity in each detector. Thus, small objects give rise to brief cues, observed only by a few detectors at any given time. The challenge posed by such cues is to differentiate these small, local signals from noise. Large objects, on the other hand, give rise to sustained cues, simultaneously observed by many detectors. The challenge posed by these cues is to remove redundancies in space and time. Indeed, inhibitory interactions have long been known to reduce redundancy [14]; but see [194].

L2 response properties present useful strategies for encoding information associated with the motion of both large and small dark objects. Responses to small dark objects are sustained, enhancing evoked signals (Figures 3.6 and 3.27). On the other hand, responses to large dark objects rapidly decay, thus specifically encoding the contrast changes associated with the moving edges of these objects and reducing redundancy (Figures 3.6 and 3.27). Separable RFs cannot implement this response duality because such filters give rise to identical response kinetics to all objects (Figure 3.26). Thus, cells with such RFs can present only transient responses, which are disadvantageous for encoding information about small moving objects, or only sustained responses, which are disadvantageous for encoding information about large moving objects, but not both. In this manner, the functional properties of L2 reflect an intermediate step in a gradual specialization of early visual processing that balances competing objectives: to efficiently represent all available information, and to highlight specific features at the expense of other information. Finally, as a result of delayed surround effects, the spatial shape of L2 RF varies over time, with inhibition becoming gradually stronger (Figure 3.27).

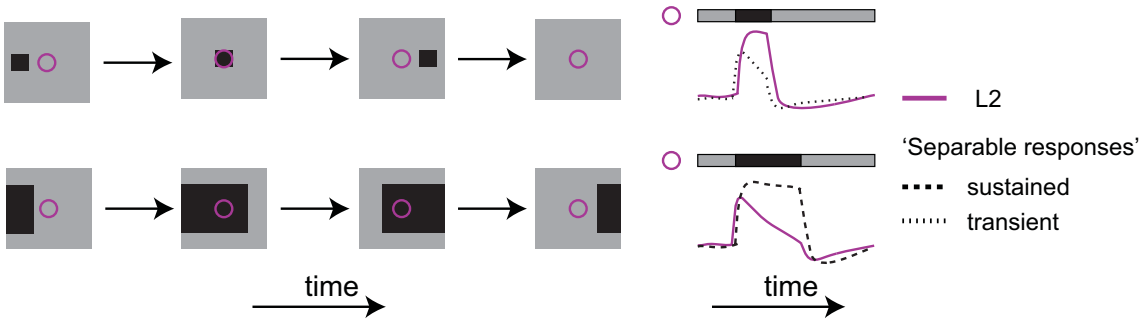

Figure 3.26: The L2 RF efficiently captures cues associated with dark object motion. Schematic representation of the utility of the spatiotemporal coupling of the L2 RF to motion encoding. Left column: example stimuli as a function of time. Right column: schematic responses to stimuli as a function of time. Purple - illustrative L2 responses, spatiotemporally coupled. Black - illustrative responses of hypothetical cells with spatiotemporally separable RFs. Dashed - illustrative responses of a hypothetical cell with sustained responses. Dotted - illustrative responses of a hypothetical cell with transient responses.

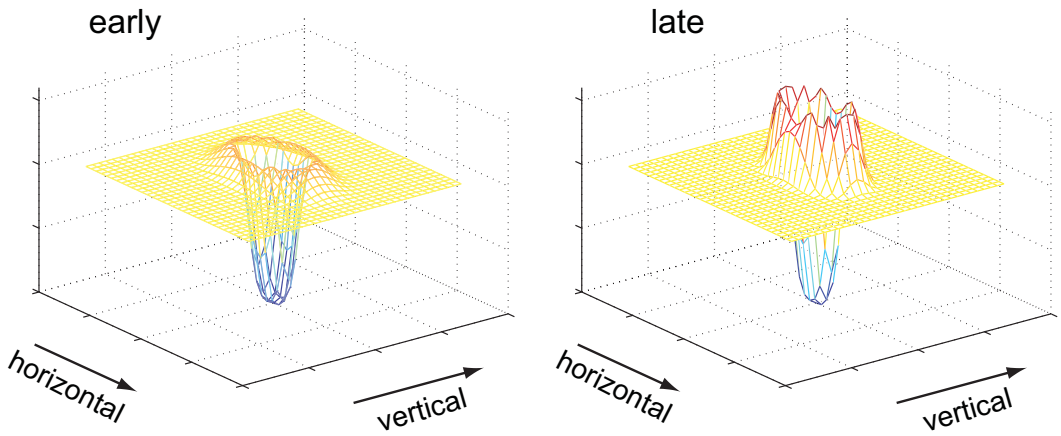

Figure 3.27: The L2 RF surround is enhanced with time. Schematic representation of the 2D L2 RF at an early (left) and late (right) stage of the response to a stimulus, capturing its anisotropy in space with gradually increasing surround lobes.

3.4.4 The L2 RF is anisotropic

Our data demonstrates that surround antagonism has a key role in defining the spatial frequency tuning of L2 outputs and gives rise to differences in tuning properties around specific axes (Figures 3.23 and 3.24). Our measurements reflect higher acuity for stimuli rotating around the pitch axis compared to the yaw axis. Thus, fine spatial features are better captured, producing stronger responses, when they are separated around this axis. Similar anisotropic center-surround RF structures were identified in LMCs of other flies [5, 63, 172, 226] as well as in crayfish [87] and in Limulus [15, 119]. We note, however, that our measurements were largely focused on a particular dorsal and medial region of the retina. Thus, it remains possible that a distribution of spatial orientation sensitivities exists across the eye, analogous to the optic-flow sensitivity fields of motion sensitive lobula plate tangential cells [253]. Regardless of the global pattern of acuity, increased inhibition in a specific orientation accentuates intensity changes and is thus consistent with early specialization for the detection of motion in that orientation [226].

3.4.5 The L2 RF structure has implications for elementary motion detection

A central model of elementary motion detection incorporates two local inputs that each relay contrast information from a single point in space, and identifies motion by correlating these signals with a time delay [104]. These inputs are often assumed to undergo either low-pass or high-pass linear filtering, or both, prior to their multiplication, and the precise characteristics of these filters critically affect elementary motion detector outputs [28]. In addition, a recent study has suggested a DC input to motion computation [69]. Genetic studies have demonstrated that L1 and L2 provide inputs to elementary motion detectors and thus their outputs must represent some of these filtering stages [47, 116, 203]. We show that the temporal filtering characteristics of L2 cells are strongly shaped by the light distribution across a broad region in visual space and thus differ for objects of different shapes and sizes. Consequently, probing elementary motion detectors with minimal motion cues that differ in spatial

extent could produce different results due to input processing properties rather than differences in motion detection per se [47, 67, 69, 104]. Similarly, filtering properties depend on contrast polarity with responses to dark and bright objects having different kinetics and amplitudes. These differences may be used by downstream circuits to become tuned to either dark or bright motion cues.

More generally, spatiotemporal coupling can give rise to speed tuning [227] and the model we fit to L2 responses represents a useful precursor for downstream velocity extraction[75, 76]. Thus, the potential speed tuning properties of the inputs into motion detection, which are differentially regulated for bright and dark objects (Figures 3.10-3.13) would influence both the speed tuning as well as the polarity selectivity of the detectors [24, 120, 227, 269]. Finally, the surround responses of L2 effectively convert a contrast increment at one spatial location into depolarizing L2 responses at neighboring locations, providing another route by which increment information could enter a dark edge detecting pathway, even given downstream half-wave rectification [47].

3.5 Future directions

In this chapter, the functional properties of a first order visual interneuron were studied. The computational specialization presented by this neuron reflects a single processing step with respect to photoreceptor signaling. Thus, a simple relation between the responses of this neuron and light inputs might be expected. However, even at this early stage of processing, simple linear as well as linear-nonlinear models (limited to capturing static or very rapid non-linearities), which are very commonly used in the visual processing literature [171], would fail to capture the computational specialization of L2 cells and to predict the cell responses to the wide range of possible spatiotemporal intensity patterns. Thus, it is likely that this modeling framework will fail to capture the functional properties of most downstream visual processing cells that are expected to be at least as specialized as the earliest processing cells are. Generalizing this conclusion, what this implies is that to experimentally characterize how the brain processes visual, or other sensory, information, a different framework

enabling researchers to measure a finite set of responses to stimuli and generalize these results to all possible inputs is required. Here we make a few suggestions as to how such a framework may be developed.

A model of the response characteristics of a cell is highly valuable for functionally characterizing the cell responses as it is reduces the functional characterization task to the task of estimating the model parameters. One way to limit the set of models that can be applied to describe a cell's function is to use information regarding the physical properties of the sensory system and the anatomy of the neural circuits involved in processing this information. In particular, for characterizing the responses of any given cell it is useful to take into account the set of inputs available to this cell and their own spatiotemporal sampling properties. In this manner, the dimensionality of possible inputs is significantly reduced: rather than defining the response as a function of, taking vision as an example, intensity in every point in space over infinite time, it may only be required to define the response as a function of intensity in several discrete regions and over finite intervals of time. For example, in this chapter we have captured L2 cell responses to dark objects of various sizes using a simple modeling assumption: that the inputs to these cells can be divided into two types - center inputs, defined by the spatial sampling resolution of the photoreceptors providing these inputs, and surround inputs, that in aggregate represent many units from neighboring ommatidia. To derive a more complete model for L2 cell responses, surround inputs need to be further divided into sub-components. Ideally, having control over every input into the cell, or at least knowing its source such that its spatial and temporal sampling properties can be inferred, could significantly facilitate modeling of the cell's function. RNAi constructs (see Section 1.3.3) enabling knockdown of specific types of receptors in a specific cell approach this ideal methodology. However, tools that enable controlling inputs in an acute manner, to prevent adaptation, may be even more effective.

Even in the absence of a complete set of tools to manipulate every input into a cell, progress in characterizing the functional properties of non-linearly and adapting cells, for which simple models may not yet exist, can be made by probing these cells with inputs likely to be relevant according to the known function of the pathway in which

these cells reside. Thus, initial progress in characterizing L2 responses was made by presenting dark versus bright inputs separately. Furthermore, since no direction or orientation selectivity was observed in L2 cell responses, and since these cells receive photoreceptor inputs from a single point in space, we inferred that these cell are not strongly affected by non-linear integration of inputs from more than one point in space. Thus, spatial maps of the RF were extracted by the presentation of single bars. Downstream of L2, where interactions between columns are likely to occur, cells are likely to be more strongly functionally affected by inter-columnar interactions. Thus, the presentation of moving inputs in different orientations may be more informative in these cells than it was in L2. Furthermore, probing such cells by presenting pairs of bars, separated by different gaps and located at various distances with respect to the column in which a cell resides could also be informative. Using elementary motion cues, such as the ones used for behavioral experiments, may facilitate putting together the results of this functional characterization with a large body of knowledge on motion detection in flies (reviewed in [27, 66]).

Additional limitations of modeling a cell function based on Ca^{2+} imaging data arise from the technical limitations of this method. In particular, it is unclear to what extent indicator properties and imaging rate limit our ability to accurately describe the actual Ca^{2+} level transients that occur in any cell. Probing responses under different conditions alleviates some of these concerns, as responses that rise or decay in rates lower than the maximal rates observed, must reflect truly slower processes rather than indicator-based limitations. Thus, for example, surround responses to dark inputs in L2 cells can clearly be shown to be delayed with respect to center responses, because the depolarizing response to light decrements applied to the center is fast, and its decay rate is low without additional surround stimulation, but higher with surround stimulation. However, the ability to measure the rate of decay of hyperpolarizing responses to light increments applied to the center is limited; thus, a model describing responses to bright objects cannot be as accurate as the one that describes responses to dark objects.

Only by using an indicator with a faster off-rate will it be possible to overcome this barrier. Recently developed variants of the GCaMP indicator [3] could be tested for

this purpose. In particular, given the variety of currently available indicators, it would be beneficial to use multiple types of indicators for functionally characterizing cells, such that responses under identical conditions but reported via different indicators could be compared. Neural activity monitoring using imaging is further limited by a low frame rate. Accordingly, using faster optical sectioning methods, or using line scans or smaller frame sizes to increase the frame rate of raster scanning two-photon imaging, could also be beneficial for improving the functional characterization of cells with these tools. In this manner, it may be possible reveal a more accurate and physiological shaping of responses.

Chapter 4

GABAergic circuits tune the early stages of visual processing

The previous chapter presented a detailed characterization of L2 cell responses to different spatiotemporal distributions of light intensities, based on functional imaging studies. Here, by combining imaging with genetic and pharmacological manipulations of neural activity, we unravel some of the circuit mechanisms involved in shaping these responses. These findings link the dense connectivity of the lamina [170, 204] and the function of this first visual neuropil.

4.1 Introduction: The functional role of dense connectivity in the lamina

Many different cell types in the lamina and the medulla of *Drosophila* provide direct and indirect feedback into L2 neurons, some via feedback synapses onto photoreceptors and others via direct synaptic connections with L2 cells themselves. Examination of this dense connectivity pattern gives rise to hypotheses as to what neural mechanisms may mediate the center-surround RF structure characterized in the preceding chapter. For example, in many systems GABAergic circuits play an inhibitory role

(in vision - [68], in olfaction - [186], in audition - [276]). Two centrifugal cells suggested to be GABAergic, C2 and C3 [34, 138], provide direct input to L2 and C3 also provides input to photoreceptors. Amacrine and lamina wide-field cells receive inputs from the centrifugal cells and synapse onto both L2 as well as onto photoreceptors, providing additional pathways for inhibition to reach L2 cells. Furthermore, amacrine and lamina wide-field cells collect inputs from multiple columns, consistent with the requirement of surround effects. Finally, pharmacological studies demonstrated that while histamine release from photoreceptors gives rise to L2 responses similar to those produced by light; other transmitters, particularly GABA, also evoke responses from L2 cells. In particular, application of GABA depolarizes L2 cells [101]. While the dense connectivity in the lamina, giving rise to multiple feedback and lateral circuits, has been thoroughly described [170, 204], what functional role this connectivity plays in shaping the outputs of the lamina has not been determined. We shed light on this question by exploring the effects of GABAergic circuits, using genetic and pharmacological manipulations, on L2 cell responses.

4.2 Methods

The experiments presented in this chapter were conducted using the same two-photon Ca^{2+} imaging set-up described in Chapter 3.

In these experiments, in addition to using the Gal4 driver 21D-Gal4 to express a multi-copy insert of UAS-TN-XXL as in Chapters 2 and 3 the Rh1-Gal4 (Bloomington Drosophila Stock Center, BDSC) was also used. In addition, in the experiments described in this chapter, these drivers were also used to express $GABA_AR$ and $GABA_BR$ RNAi's ($GABA_AR$-RNAi from VDRC (KK104293) and $GABA_BR2$-RNAi from [206]).

Thus, the following fly lines were used in the experiments presented in this chapter:

Flies expressing TN-XXL in L2:

+ ; + ; 21D-Gal4,UAS-TN-XXL/+,

Flies expressing TN-XXL in L2 and photoreceptors R1-R6:

Rh1-Gal4/+ ; + ; 21D-Gal4,UAS-TN-XXL/+,

Flies used in knock-down experiments:
+ ; $GABA_AR$-RNAi/+ ; 21D-Gal4,UAS-TN-XXL/$GABA_BR2$-RNAi, for knockdown of $GABA_A$Rs and $GABA_B$Rs in L2 cells,
Rh1-Gal4/+ ; $GABA_AR$-RNAi/+ ; 21D-Gal4,UAS-TN-XXL/$GABA_BR2$-RNAi, for knockdown of $GABA_A$Rs and $GABA_B$Rs in both L2 cells and photoreceptors R1-R6,
Rh1-Gal4/+ ; $GABA_AR$-RNAi/+ ; 21D-Gal4,UAS-TN-XXL/+, for knockdown of $GABA_A$Rs in both L2 cells and photoreceptors R1-R6,
Rh1-Gal4/+ ; + ; 21D-Gal4,UAS-TN-XXL/$GABA_BR2$-RNAi, for knockdown of $GABA_B$Rs in both L2 cells and photoreceptors R1-R6.

Flies were grown, collected and dissected as described in the previous chapter.

A few experiments presented in this chapter used solution containing pharmacological agents for perfusion. In particular, when GABAR and nAChR antagonists were applied pharmacologically, these antagonists were dissolved into the perfused saline and applied for the entire duration of the experiment. A stock of 250 M CGP54626 (CGP54626 hydrochloride, from Tocris) was first dissolved in DMSO before it was added to the saline used for perfusion, and was used at a final concentration of 50 μM. Picrotoxin (Picrotoxin powder, from Sigma) was dissolved directly in the saline used for perfusion, and was used at a final concentration of 125 μM. Similar concentrations were previously used [186, 206]. Since the perfusate contained DMSO during application of both Picrotoxin and CGP54626, the same amount of DMSO used to dissolve CGP54626 was also added to the perfusate during application of Picrotoxin alone. Mecamylamine (Mecamylamine hydrochloride, from Sigma) and Tubocurarine (Tubocurarine hydrochloride pentahydrate, from Sigma) were both dissolved directly in the saline used for perfusion and were both used at a final concentration of 50 μM. For 2 of the flies imaged after application of nAChR antagonists, 1.25 μM bungarotoxin was also added to this solution. Responses did not differ from responses of flies to which only Mecamylamine and Tubocurarine were applied.

The data presented in this chapter was preprocessed as described in the previous chapter.

4.2.1 Visual stimuli and corresponding analysis procedures

Bar presentation at a random position

A ~10° wide dark horizontal or vertical bar was presented over an intermediate illumination level background around one of 19 different positions on the screen, located 5° apart, at a randomly chosen order. The bar width was chosen such that it filled a significant fraction of RF surrounds and induced strong surround responses, observable with respect to the background noise levels. The bar was displayed for 3 s and removed from the screen for 3 s before re-appearing at a different position. Thus, it took the bar 114 s to be presented at all possible positions. 10 epochs of no bar presentation for 6 s were interleaved with epochs of bar presentation to allow responses to decay. Thus, stimulus presentation lasted 174 s. The stimulus was typically applied for 2000 frames (~189 s) and the first 10 s of the response to the stimulus were excluded from analysis (allowing the response to the presentation of the intermediate illumination level across the screen to decay). Thus, the response at each position was measured once. Responses were aggregated based on distances (in degrees) between the RF centers of corresponding cells and the nearest edge of the bar from the view point of the fly (Figure 4.1).

To enable a characterization of the spatial RF shape with a better spatial resolution than suggested by the bar's width, we took advantage of the fine-grained spatial distribution of center positions of different cells with respect to the bars. Thus, responses were divided into bins separated by 2° and aligned to the edge of the bar, such that each response was associated with the nearest bin center. Based on the position of the RF on the screen, the screen shape and its distance from the fly, as well as the position of the bar on the screen, bars at different positions were viewed as having slightly different widths by different cells. To correct for this distortion, only responses of cells for which the viewed bar extended between 8° and 12° of visual space were kept for further analysis. Response strength was defined as the difference between the response amplitude after the bar elimination from the screen and the response amplitude immediately following the bar presentation, where amplitudes

were computed as described in the previous chapter for partial field flash presentation response analysis (Figure 3.4B). The sign of response strengths of cells was set such that negative strengths corresponded to cells that presented a Ca^{2+} decrease to light. Unless otherwise specified, in all figures presented in Sections 4.3.1 and 4.3.2, responses to vertical and horizontal bars were averaged together. In order to compare the spatial RF shape along the horizontal and vertical screen dimensions, we averaged over responses in the same top-medial corner of the screen, spanning 15% of the screen, which was used to characterize orientation dependence in moving bar responses described in the previous chapter. Responses in this region were separated depending on the bar orientation, horizontal or vertical, and an average spatial RF shape was computed for each dimension separately (Figure 4.3B).

Moving sinusoidal gratings

The moving sinusoidal gratings stimulus presented in the previous chapter was used for manipulation experiments presented here as well (Figures 4.13-4.16). Responses to moving sinusoidal gratings were analyzed as described in the previous chapter. In addition, in order to establish the extent to which responses deviated from linearity, mean responses were compared to sinusoids with identical maximal amplitudes by computing the difference of mean responses at every response value of the reference sinusoid. Mean absolute differences are presented (Figures 4.13-4.15).

4.3 Results

4.3.1 GABAergic inputs to R1-R6 photoreceptors provide surround signals in L2

To explore circuit mechanisms that shape L2 responses, we developed a procedure for rapidly characterizing the spatial RF using sequential presentations of a dark, stationary 10° wide bar, oriented horizontally or vertically at different positions. To efficiently extract an RF shape description with high spatial resolution, we took advantage of the random distribution of distances of the RFs of different cells from

the bar edges. Responses of different cells were aggregated according to the distance between their RF centers and the bar's nearest edge, thereby combining responses of cells that experienced equivalent RF stimulation. Accordingly, the position of RFs on the screen and the side of the RF covered by the bar were disregarded (Figure 4.1).

As expected, cells having RF centers within the bar transiently depolarized when the bar was presented, while cells having RF centers outside the bar responded with inverse polarity (Figure 4.2). To relate these responses to the spatial RF shape, we plotted response strength, measured as the mean response amplitude evoked by the onset and offset of the bar (as in Figure 3.4B), as a function of the distance from the edge. From this analysis, we obtained a proxy of the center-surround RF shape (Figure 4.3A). In Figures 4.2, 4.3A, and all subsequent figures mean responses reflect aggregation over responses to bars with different orientations, as the effect of the anisotropic RF shape on these maps was small (but significant; p=0.0014 in a χ^2 test comparing the response curves; Figure 4.3B).

As the neurotransmitter GABA mediates inhibitory responses in many systems, we next examined whether GABA might mediate surround responses in L2. We took advantage of RNA interference (RNAi) constructs directed against both $GABA_A$ and $GABA_B$ receptors ($GABA_A$Rs and $GABA_B$Rs, respectively), expressed cell-type specifically using the Gal4-UAS system [155, 206]. Knockdown of both GABARs in L2 cells had no effect on the spatial RF shape (Figure 4.4). However, when these RNAi constructs were simultaneously expressed in both R1-R6 photoreceptors and L2 cells, we observed an increase in the effective size of the center region and a decrease in the strength of surround responses (Figures 4.5A, 4.6). Thus, GABAergic input onto L2's pre-synaptic partner, the photoreceptors, shapes the surround region of the L2 RF. Interestingly, neither knockdown of $GABA_A$Rs or $GABA_B$Rs alone had any effect on the RF shape (Figure 4.5B). Thus, both receptors are redundantly required to mediate surround responses.

Since these genetic manipulations did not completely eliminate surround responses, we next examined whether GABARs on more distant cells might have additional effects. We therefore applied the $GABA_A$R and $GABA_B$R antagonists, picrotoxin (125 μM) and CGP54626 (50 μM), simultaneously [186, 206]. Under these conditions,

the normalized strength of surround responses with respect to center responses significantly decreased (Figure 4.7A). While this effect was similar to that observed by knocking down these receptors using RNAi in photoreceptors and L2, the effects of genetic knockdown were weaker and displayed some subtle differences. To define the distinct contribution of the ionotropic $GABA_AR$s and the metabotropic $GABA_BR$s to L2 cell responses, we next applied the antagonists against these receptors separately. Interestingly, application of the $GABA_AR$ antagonist alone was sufficient to suppress the RF surround as strongly as the two antagonists combined (Figure 4.7B), while application of the $GABA_BR$ antagonist alone had no effect on the spatial RF shape. Other antagonists, targeting other types of $GABA_AR$s in mammalian systems [109, 232, 272], Gabazine (50 μM) and Bicuculline (50 μM), had no effect (data not shown).

Taken together, these genetic and pharmacological manipulations demonstrate that GABAergic circuits play a critical role in establishing the spatial RF shape of L2, through pre-synaptic antagonism of photoreceptors. As the pharmacological block of $GABA_AR$s strongly suppressed surround responses, while the knock-down of $GABA_AR$s alone had no effect, we infer that these manipulations act on overlapping but distinct circuit targets. We further note that surround responses were not completely eliminated even by the broad pharmacological manipulations. One possibility is that the antagonists had only partial access to the brain. Alternatively, this could indicate that additional, non-synaptic mechanisms, may also contribute. Thus, multiple circuit components are likely involved in constructing L2's extensive surround.

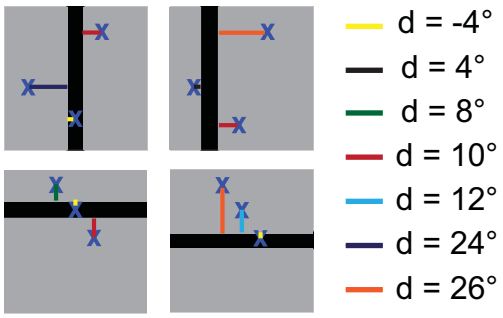

Figure 4.1: Rapid RF mapping stimulus: presentation of a bar at random positions on the screen. Schematic illustration: a dark bar is presented at a random position on a background of intermediate illumination, while responses are aggregated by the distance of RF centers from the bar's edge. Negative distances correspond to RF centers within the bar.

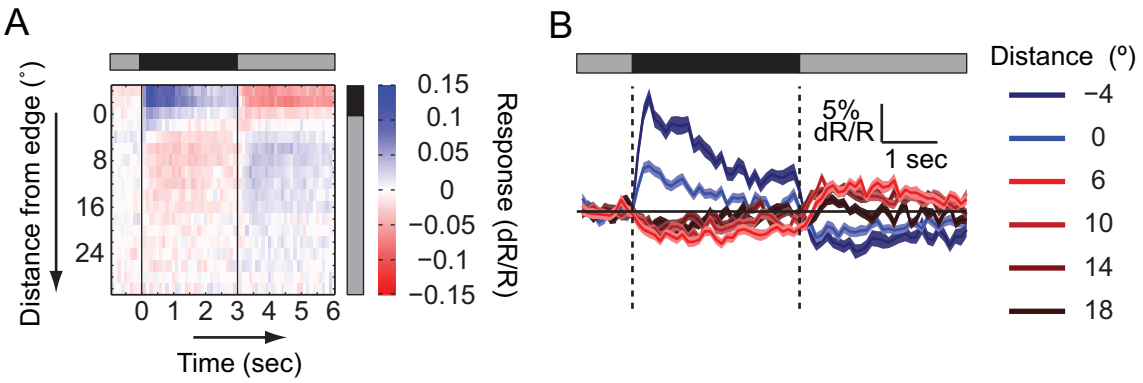

Figure 4.2: The response of cells varies as a function of the distance between their RF centers and the bar's edge. **(A and B)** Responses to a dark bar presented on an intermediate illumination level background. **(A)** The mean response of L2 cells as a function of the distance of the RF center from the bar's edge and the bar presentation time. Response (dR/R) values encoded as described by the color scale. **(B)** The mean response to the presentation of the bar at different distances between the RF centers and the bar's edge, as a function of time. Blue - mean responses of cells with RF centers within the bar presentation region, red - mean responses of cells with RF centers outside the bar presentation region. Shading denotes ±1 SEM.

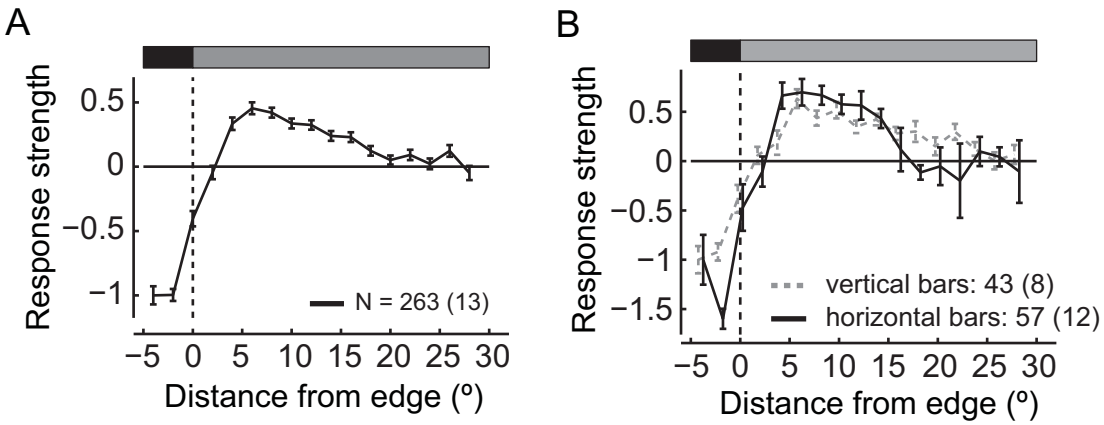

Figure 4.3: A proxy of the spatial RF shape. **(A)** Mean response strength as a function of the distance from the bar's edge, normalized to the strength at a distance of 4°, within the bar. Negative strength values correspond to depolarization during the bar presentation, positive values to hyperpolarization. Error bars denote ±1 SEM. **(B)** The mean response strength is computed for horizontal (solid) and vertical (dashed) bars, spanning the vertical and horizontal dimensions of the screen, respectively.

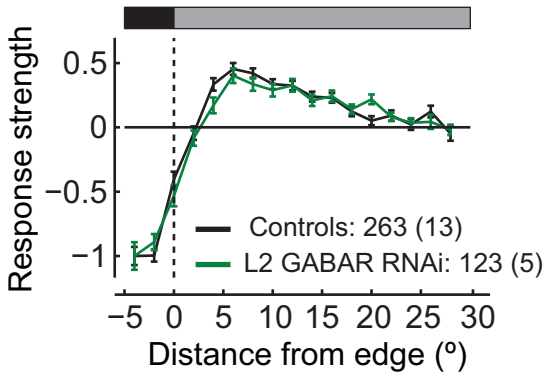

Figure 4.4: Knockdown of GABARs in L2 cells has no effect on the spatial RF shape. As in Figure 4.3, showing the normalized mean strength of the response as a function of the distance from the bar's edge, following knockdown of GABARs in L2 cells only. Error bars denote ±1 SEM. Black - controls.

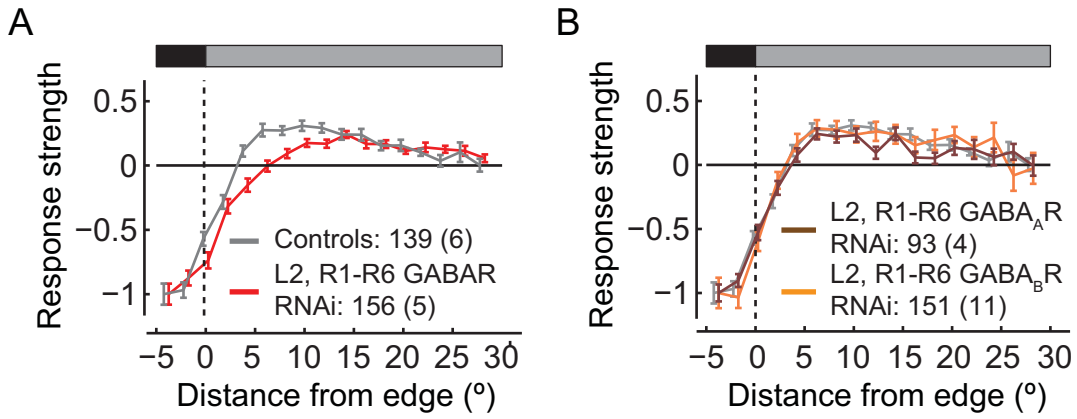

Figure 4.5: Knockdown of GABARs in L2 cells and R1-R6 photoreceptors decreases surround effects in L2. As in Figure 4.3, showing the normalized mean strength of the response as a function of the distance from the bar's edge. Error bars denote ±1 SEM. **(A)** Red - Following knockdown of both GABARs in L2 cells and R1-R6 photoreceptors; gray - controls, TN-XXL expressed in both L2 cells and R1-R6 photoreceptors. **(B)** Brown - knockdown of $GABA_A$Rs in L2 cells and R1-R6 photoreceptors; orange - knockdown of $GABA_B$Rs in L2 cells and R1-R6 photoreceptors.

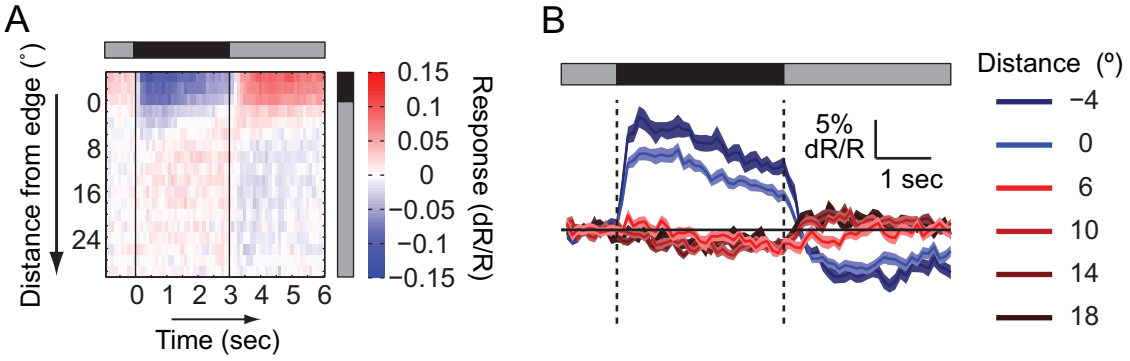

Figure 4.6: L2 cell responses following knockdown of GABARs in L2 cells and R1-R6 photoreceptors, plotted as in Figure 4.2. Shading denotes ±1 SEM.

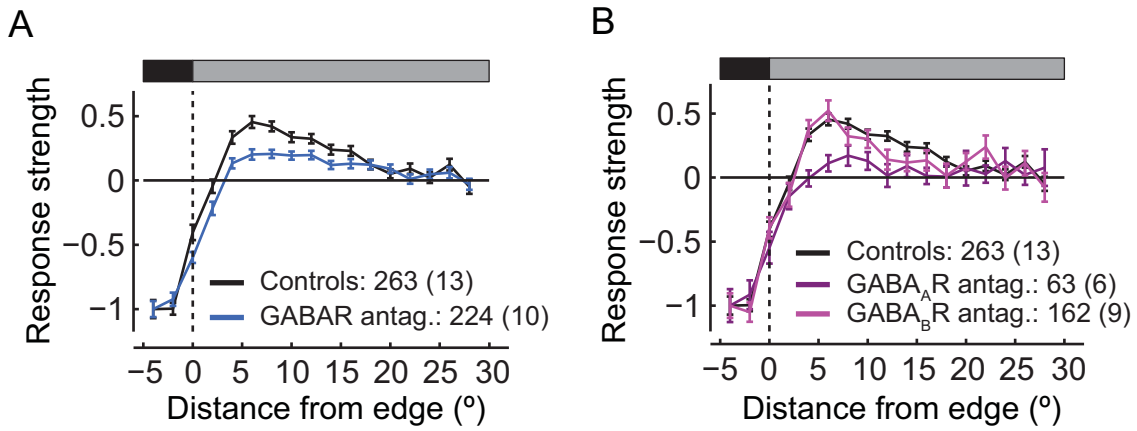

Figure 4.7: Application of GABAR antagonists decreases surround effects in L2 cells. As in Figure 4.3, showing the normalized mean strength of the response as a function of the distance from the bar's edge. Error bars denote ±1 SEM. **(A)** Blue - Following application of both GABAR antagonists; black - controls, TN-XXL expressed in L2 cells. **(B)** Purple - application of the $GABA_AR$ antagonist picrotoxin only; magenta - application of the $GABA_BR$ antagonist CGP54626 only.

4.3.2 GABAergic inputs are required for L2 to respond to contrast decrements

This dissection of the contributions of GABAergic circuits to the L2 spatial RF also revealed that GABAR antagonists induced changes in response amplitudes and kinetics for both the center and the remaining surround responses (Figures 4.8-4.10). We thus examined these effects in greater detail across additional stimulus conditions.

During responses to moving bright bars on dark backgrounds, L2 transiently hyperpolarized as the bar reached the RF center, causing a local light increment, and depolarized as it moved away, causing a local light decrement (Figures 3.2A and 4.11, top). Similarly, during responses to static dark bars, L2 cells with RF centers in the bar transiently depolarized when the bar was presented and hyperpolarized to a sustained level when it was eliminated (Figures 4.2A and 4.11, bottom). Application of GABAR antagonists enhanced the hyperpolarizing responses to increments, and suppressed the depolarizing responses to decrements in both stimuli (Figure 4.11A). In addition, in the presence of antagonists, the depolarizing response to the static bar presentation decayed slowly, and the hyperpolarizing response was no longer sustained. The first of these effects, the reduced rate of decay of the depolarizing response, was anticipated by our previous observations that decay rates of decrement responses depend on stimulation of the RF surround, mediated via GABARs (Figures 3.6 and 3.10). However, the decrease in the amplitude of the response to the light decrement and increase in the response to the increment cannot be explained by reduced surround effects. Thus, GABAergic circuits must play an additional role in shaping L2 cell responses to light inputs, specifically mediating responses to light decrements while inhibiting increment responses.

To identify which type of GABAergic receptor mediated each of the two effects of GABAergic circuits, on the strength of surround responses and on the amplitude and kinetics of center responses, we next applied the $GABA_AR$ and $GABA_BR$ antagonists independently. Both the $GABA_AR$ antagonist alone, and the $GABA_BR$ antagonist alone suppressed depolarizing responses to decrements (Figures 4.11B and 4.11C), contributing to the combined effect, but neither enhanced hyperpolarizing responses.

In addition, both $GABA_AR$ and $GABA_BR$ antagonists made the hyperpolarizing response to the elimination of the static bar more transient, but only the $GABA_AR$ antagonist made the depolarizing response to the bar presentation more sustained. This effect is consistent with the role of these receptors in mediating surround effects.

Interestingly, knockdown of both GABARs in L2 cells and R1-R6 photoreceptors did not have a significant effect on the shapes of responses to either static or moving bar stimuli (Figure 4.12A). Knockdown of $GABA_ARs$ in these cells enhanced the depolarizing responses to light decrements (Figure 4.12B). In contrast, knockdown of $GABA_BRs$ in these cells suppressed depolarizing responses to decrements, and made the hyperpolarizing responses less sustained (Figure 4.12C). These effects were indistinguishable from those caused by pharmacological block of the same receptors (Figure 4.11C). Thus, the effect of $GABA_BRs$ on the shape of L2 cell responses to light decrements and increments is mediated via receptors on either L2, or photoreceptors, or both. The difference between the combined effect of $GABA_AR$ and $GABA_BR$ antagonists, and the genetic knockdown of both of these receptors may be explained by the cancellation of opposite effects of the individual receptor knockdowns on decrement responses. This is also consistent with the notion that the effect of pharmacological block of $GABA_ARs$ is due to receptors distinct from those in L2 cells and photoreceptors. Overall these results demonstrate that GABAergic circuits play a significant role in regulating the amplitude and kinetics of L2 cell responses to both light increments and decrements applied to the RF center, in addition to mediating surround responses.

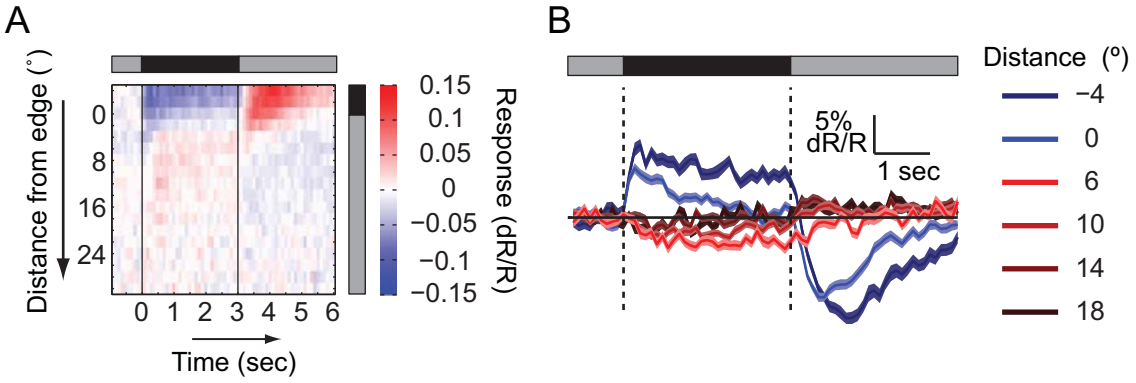

Figure 4.8: L2 cell responses following application of both GABAR antagonists, plotted as in Figure 4.2. Shading denotes ±1 SEM.

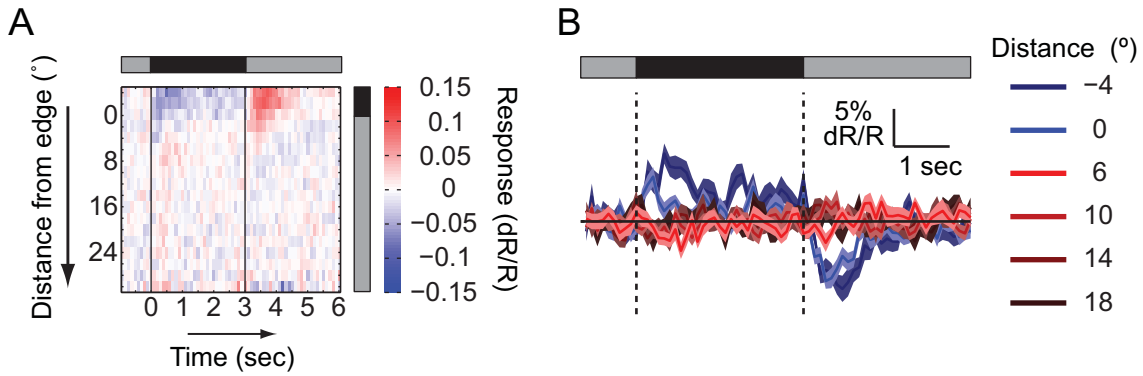

Figure 4.9: L2 cell responses following application of the $GABA_AR$ antagonist picrotoxin, plotted as in Figure 4.2. Shading denotes ±1 SEM.

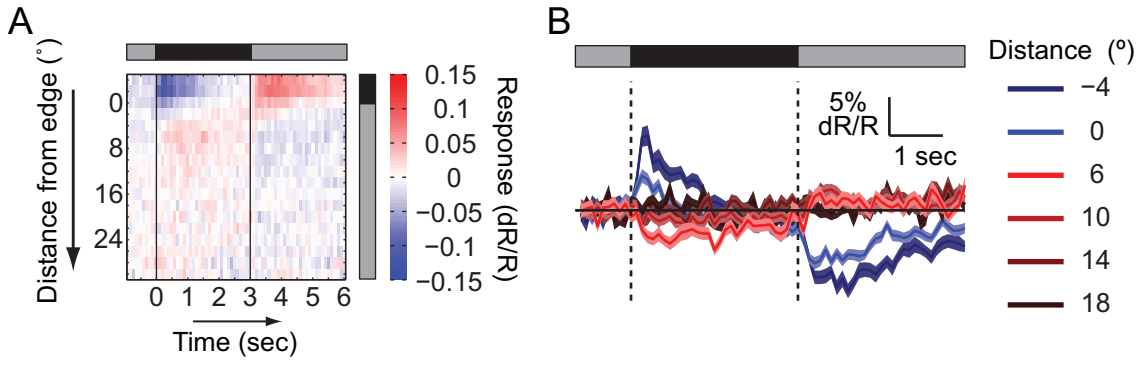

Figure 4.10: L2 cell responses following application of the $GABA_BR$ antagonist CGP54626, plotted as in Figure 4.2. Shading denotes ±1 SEM.

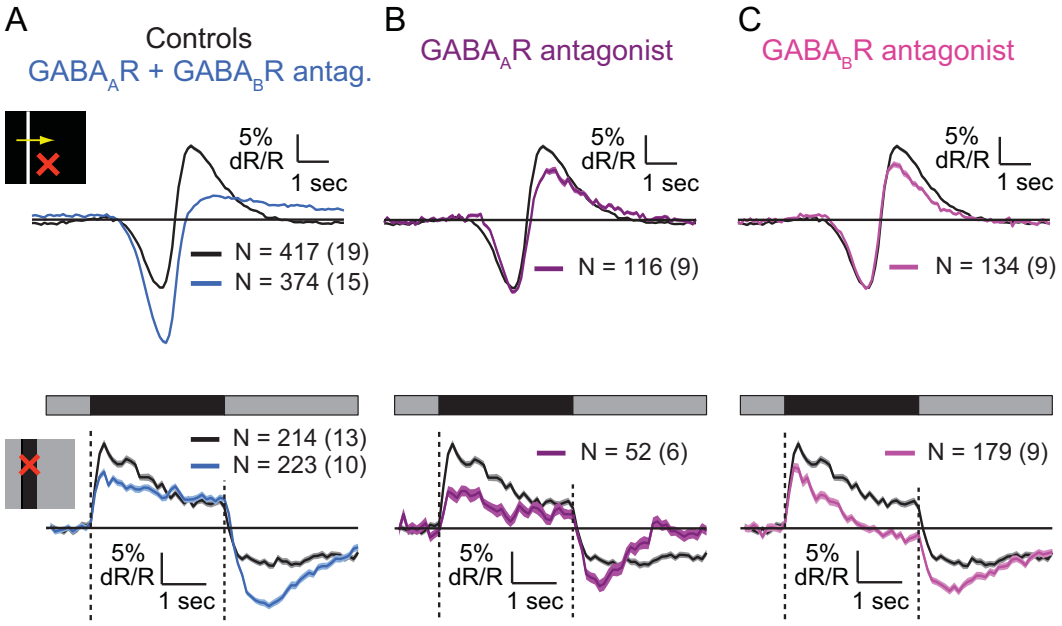

Figure 4.11: GABAR antagonists affect L2 response shapes and kinetics. **(A-C)** Mean response of controls and experimental cells to a moving bright bar on a dark background (top) and to a dark bar on an intermediate illumination level background (bottom), for cells with RF centers within the bar. Black - controls, TN-XXL expressed in L2 cells only. **(A)** Blue - application of GABAR antagonists. **(B)** Purple - application of the $GABA_AR$ antagonist picrotoxin. **(C)** Magenta - application of the $GABA_BR$ antagonist CGP54626.

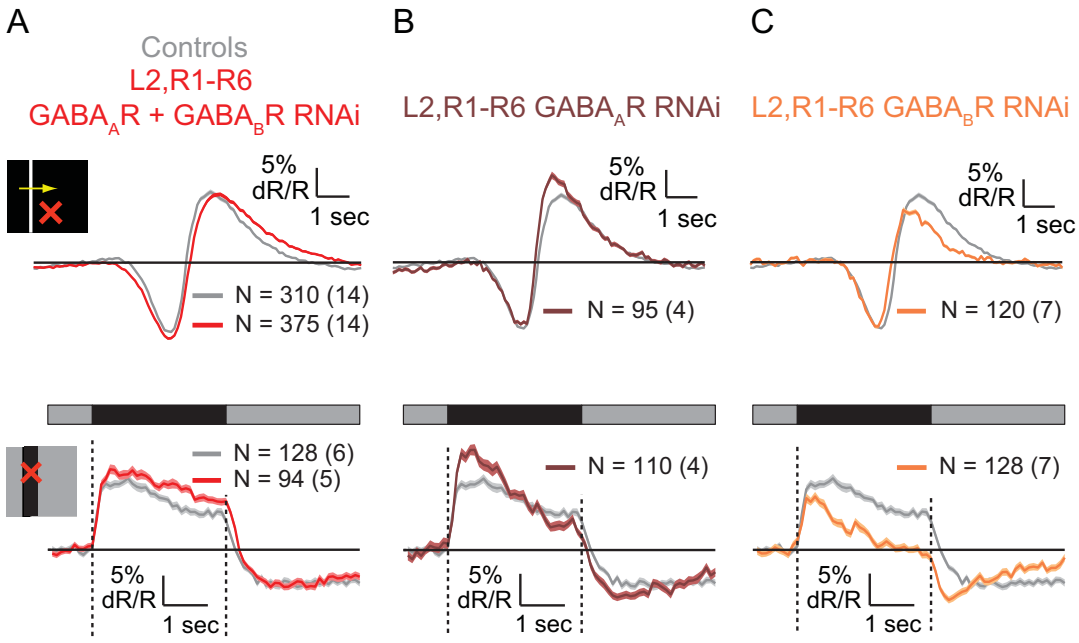

Figure 4.12: GABA$_B$R knockdown but not GABA$_A$R knockdown in L2 cells and R1-R6 photoreceptors has the same effect as antagonists application. **(A-C)** Mean response of controls and experimental cells to a moving bright bar on a dark background (top) and to a static dark bar on an intermediate illumination level background (bottom), for cells with RF centers within the bar. Gray - controls, TN-XXL expressed in L2 cells and R1-R6 photoreceptors. **(A)** Red - knockdown of both GABARs. **(B)** Brown - kncokdown of GABA$_A$Rs only. **(C)** Orange - knockdown of GABA$_B$R antagonist CGP54626.

4.3.3 GABAergic circuits linearize responses to contrast changes

The above described results implied that GABAergic inputs might enable L2 cells to balance responses to contrast increments and decrements. To test this hypothesis, we examined whether the linearity of L2 responses to sinusoidal contrast changes was affected by the application of GABAR antagonists. Indeed, this manipulation significantly altered the responses of L2 to sinusoids, as the responses to the brightening and darkening phases of this stimulus were no longer similar in amplitude (Figure 4.13). In particular, as with responses to other stimuli, the hyperpolarizing response to light increments became larger, while the depolarizing response to light decrements failed to track the darkening input and displayed saturation (Figure 4.13A). We quantified this deviation from linearity by computing the differences between measured responses and sine functions with matched amplitudes. Larger deviations between measured and predicted responses were found following addition of GABAR antagonists (Figures 4.13B and 4.13C). The same effect on linearity was observed in response to stimuli moving around either the pitch or yaw axes (Figure 4.14).

Interestingly, knockdown of GABARs in L2 and photoreceptors increased the linearity of responses to sinusoidal gratings (Figure 4.15). Nevertheless, both application of GABAR antagonists and knockdown of GABARs in L2 cells and photoreceptors suppressed the differences between the amplitudes of responses to gratings moving around the pitch and yaw axes (Figure 4.15). Thus, as the knockdown of GABARs mediates surround effects but does not affect contrast polarity sensitivity, these observations suggest that, under these stimulus conditions, surround effects cause a decrease in linearity of L2 responses to contrast. When GABARs are broadly blocked by antagonists, the small, positive effect of blocking GABARs in L2 and photoreceptors on linearity is overwhelmed by the much larger negative effect induced by the change in contrast polarity sensitivity mediated by a different circuit component. Thus, the role of GABAergic circuits in regulating contrast polarity sensitivity, not surround responses, is critical for linearizing responses to contrast in L2.

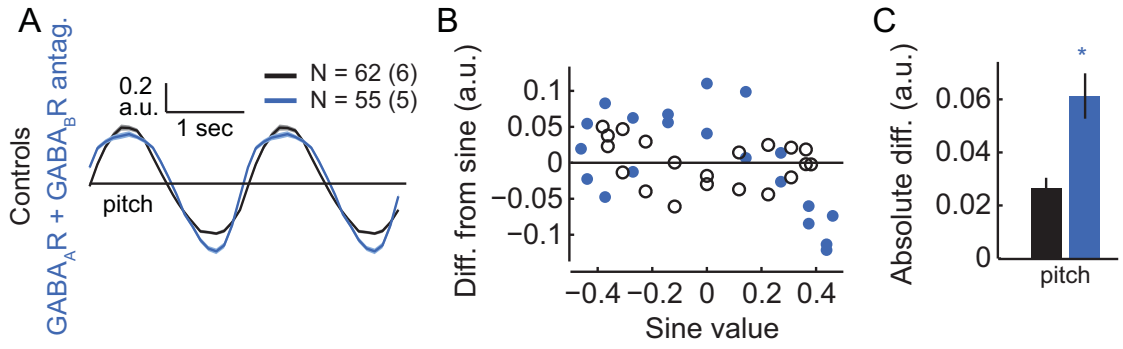

Figure 4.13: GABARs are required for L2 cells to respond linearly to contrast changes. **(A)** Mean responses to sinusoidal gratings with a spatial period of 40° moving around the pitch axis. **(B)** The difference between the measured mean response and a reference sinusoidal response with the same maximal amplitude, as a function of the reference response value. **(C)** The mean absolute difference across all response values presented in (B). $^*p < 0.05$ in a two-tailed student's t-test with unequal variances. Error bars denote ±1 SEM.

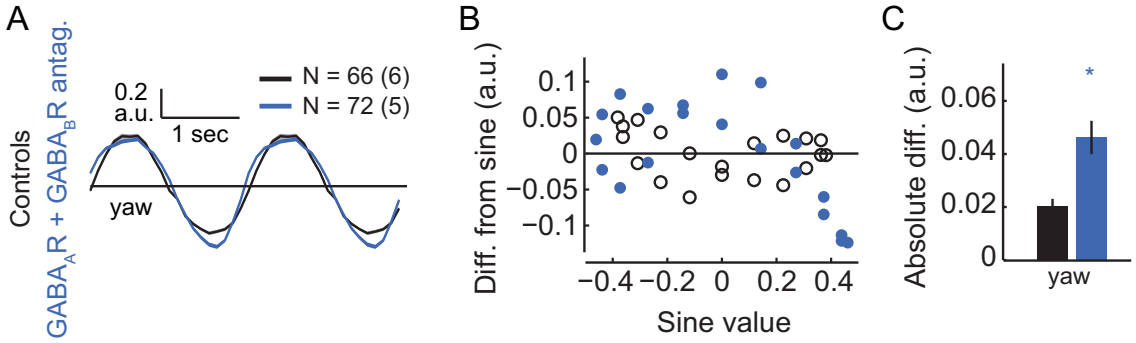

Figure 4.14: GABARs similarly affect L2 cell responses to sinusoidal moving gratings in the pitch and yaw orientations. Same as Figure 4.13 for responses to sinusoidal gratings moving around the yaw axis, showing the same effect on response shapes.

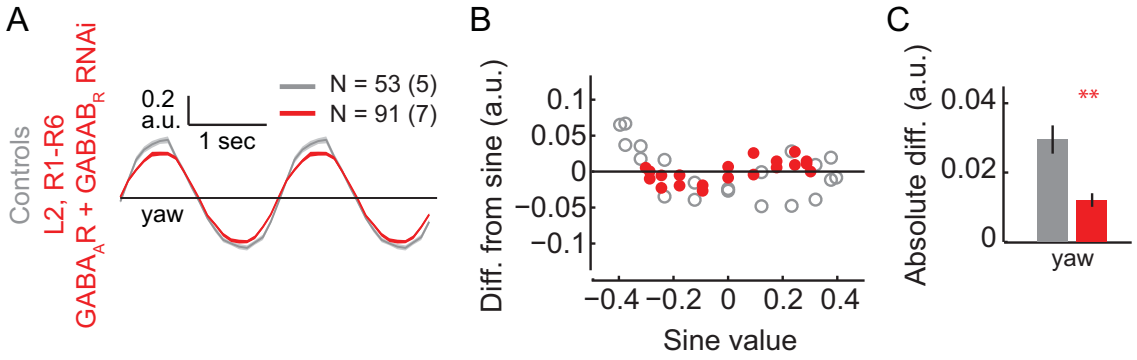

Figure 4.15: Knockdown of GABARs in L2 cells and R1-R6 photoreceptors does not decrease L2 cell response linearity. Same as Figure 4.14 for responses to sinusoidal gratings moving around the yaw axis, following knockdown of GABARs in both L2 cells and photoreceptors R1-R6, showing an increase rather than a decrease in response linearity.

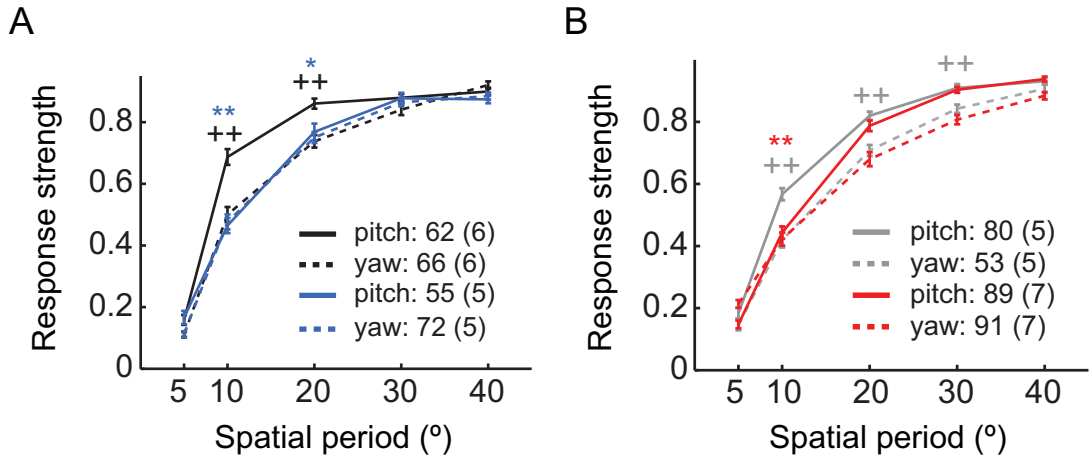

Figure 4.16: Both application of GABAR antagonists and knockdown of GABARs in L2 cells and R1-R6 photoreceptors reduces the acuity difference around the pitch and yaw axes. Same as Figure 3.24. **(A)** Black - controls, L2 cells expressing TN-XXL. Blue - following application of GABAR antagonists. **(B)** Gray - controls, L2 cells and R1-R6 photoreceptors expressing TN-XXL. Red - Following knockdown of GABARs in both L2 cells and R1-R6 photoreceptors.

4.4 Discussion

Using pharmacological and genetic manipulations, we have revealed that GABAergic circuitry, including pre-synaptic inhibition via GABARs on photoreceptors, mediates lateral antagonistic effects on L2. Moreover, these circuits are required for L2 to respond strongly to decrements, a critical component of dark moving object cues. Thus, these lateral and feedback circuits, rather than purely feed-forward signals from photoreceptors, enable the downstream circuits to become specialized to detect moving dark edges. Remarkably, our detailed characterization of L2 reveals that many visual processing properties are shared with first order interneurons in the vertebrate retina. These strikingly similar computational properties arise via distinct molecular mechanisms, arguing strongly for evolutionary convergence.

4.4.1 Lateral GABAergic circuits give rise to the center-surround organization of the L2 RF

Both ultrastructural and immunocytochemical studies describe a dense network of lateral and feedback connections in the lamina [138, 170, 204]. Here we show how some of these circuits, particularly GABAergic circuits, shape the functional properties of an LMC. Our results demonstrate that appropriately oriented pre-synaptic and other GABAergic inputs give rise to the anisotropic center-surround RF structure of L2. Photoreceptors receive direct GABAergic input that depends on both $GABA_A$Rs and $GABA_B$Rs and shapes the RF surround in L2 (and presumably other LMCs). Synapses elsewhere in the circuit that are dependent on $GABA_A$Rs are required to relay surround inputs into photoreceptors. Five cell-types are pre-synaptic to photoreceptors in the lamina by ultrastructural criteria. These are L2, the LMC L4, a type of lamina wide-field neuron, amacrine cells, and a centrifugal cell type, C3 [204]. Of these, only C3 is known to be GABAergic, making this cell type a possible surround input source [34, 138]. Furthermore, since our genetic manipulation of GABARs affected both L2 cells as well as photoreceptors, we cannot exclude the possibility that receptors on both cells are redundantly required. In particular, both GABAergic centrifugal cells, C2 and C3, are presynaptic to L2 and could provide such

inputs. Additional $GABA_A$Rs have been identified in L4 and another wide-field tangential cell [70, 138] and could mediate the distal effects of manipulating $GABA_A$Rs. Determining which cell type provides each of these inputs awaits the development of new cell-specific genetic tools.

Through multiple mechanisms, modulation of GABAergic signaling in L2 expands the RF center and increases spatial pooling. Such a change in RF shape increases signal to noise ratios and occurs under low light level conditions [63, 64]. Thus, we speculate that one physiological role of GABAergic inputs may be to allow dynamic modulation of spatial pooling as a function of the ambient light level. Interestingly, since presynaptic inhibition was also observed in early olfactory processing in flies [186, 206], in early visual processing in vertebrates [18, 73, 128, 240, 244] and in many other sensory systems [21, 37, 130], this mechanism appears general.

4.4.2 Lateral and feedback GABAergic circuitry tunes the L2 pathway for processing dark object motion cues

In addition to mediating surround responses, GABAergic inputs also shape center responses in L2. Blockade of $GABA_A$Rs distal in the circuit increases the amplitude of hyperpolarizing responses to light increments and makes them more transient, while decreasing the amplitude of depolarizing responses to decrements and making these more sustained. Since picrotoxin was used to block $GABA_A$Rs, it is possible that other picrotoxin-sensitive receptors such as ionotropic glutamate receptors [48] could mediate some of these effects. However, we note that while picrotoxin acts on other chloride channels [86, 101], it is unlikely that these effects are mediated by blocking the histamine gated chloride channels that respond to neurotransmitter release from photoreceptors. In particular, the effects of picrotoxin on L2 were to enhance, rather than suppress, light-mediated hyperpolarization. Furthermore, $GABA_B$Rs on photoreceptors or L2 cells have a partially overlapping role with $GABA_A$Rs. These receptors mediate depolarizing responses to decrements and shape the late stages of hyperpolarizing responses to increments. These roles of GABA are consistent with previous electrophysiological studies, which showed that LMC depolarizations

could be evoked by ionophoretic application of GABA [100], and that receptors distinct from histamine-binding Cl^- channels contribute to mediating OFF responses in LMCs [153, 254].

Previous work demonstrated that calcium signals in L2 cells follow both the depolarizing and hyperpolarizing changes in membrane potential evoked by light [47, 63, 113, 122, 145]. Here we show that GABAergic signaling is critical to achieving this response property, as blockade of GABAergic circuits disrupted the near linearity observed in the responses of L2 cells to sinusoidally changing contrast modulations. Thus, linearity requires regulatory inputs that counteract the otherwise non-linear responses of L2 that would intrinsically favor hyperpolarizing responses to light ON, reflecting direct photoreceptor inputs, over depolarizing responses to light OFF. L2 axon terminals were previously described as half-wave rectified [199]. However, the variability in response shapes we describe as emerging from differential filling of center and surround regions of different cells may account for much of the discrepancy in the literature [47, 199]. Importantly, in the absence of GABAergic circuit inputs, depolarizing responses to decrements are nearly eliminated. Thus, these circuits are required for decrement information to be transmitted to the downstream circuitry and enable its specialization for the detection of moving dark objects. Furthermore, we expect the supra-linear relation between intracellular Ca^{2+} concentration and synaptic transmitter to amplify the effect of GABAergic inputs on responses to decrements, contributing to the transformation of these intrinsically weak responses to into strong and robust signals. In addition, GABAergic circuits make responses of L2 cells to light decrements transient in the presence of surround inputs, enabling transmission of information about contrast and terminating signals evoked by constant intensity inputs. Thus, rather than being defined solely by the functional properties of the receptors for the photoreceptor neurotransmitter histamine, lateral and feedback circuit effects mediated through GABA receptors establish critical aspects of L2 responses.

4.4.3 Distinct molecular mechanisms give rise to a similar early visual processing strategy in flies and vertebrates

Early visual processing circuits in flies and vertebrates consist of analogue processing pathways embedded within a similar structure [39, 211]. In this parallel, LMCs like L2 are analogous to bipolar cells, first order interneurons in the vertebrate retina. Previous work demonstrated that both cell types have antagonistic center-surround RFs [54, 247, 113, 126, 148, 153, 172, 173, 214, 243, 260, 270]. However, our detailed characterization of L2 reveals that the functional parallel between these cells is much more significant. First, in both cell types, spatiotemporal coupling arises from delayed surround effects (Sections 3.3.3 and 3.3.4; [10, 63, 73, 148, 153, 243, 259, 260]). Second, in both cell types, GABAergic circuitry shapes responses via multiple pathways, and affects both response amplitudes and kinetics (This chapter; [62, 72, 158, 159, 189, 220, 250, 273]). Interestingly, a differential distribution of GABAergic circuit inputs and receptor types in bipolar cells contributes to heterogeneous responses [73, 240, 271].

Based on these observations, we hypothesize that different weightings of the same circuit elements that shape L2 responses also differentially shape other LMC responses to tune their function toward distinct downstream processing pathways. For example, L1 cells provide inputs to a pathway that is specialized for detecting moving light edges [47, 116]. We hypothesize that the GABAergic circuit inputs that enhance L2 depolarizing responses to light decrements act differently in L1, allowing this cell's response to be biased toward the hyperpolarizing responses evoked by contrast increments, while possibly preserving the advantages of responding to large and small objects differently.

In spite of these deep similarities, many of the molecular mechanisms that shape both center and surround responses in first order interneurons are different between flies and vertebrates. In OFF bipolar cells, an OFF response arises through a sign conserving synapse with photoreceptors, mediated by an ionotropic glutamate receptor, while a metabotropic receptor mediates sign-inverting responses of ON bipolar cells [60, 167, 179, 208]. However, in L2 cells, the OFF response is not mediated only

by the histamine binding Cl^- channel that transmits photoreceptor outputs, but is also driven by distinct GABAergic circuit mechanisms. Thus, lateral or feedback interactions are critical to establishing L2's signature response to contrast decrements.

Moreover, several mechanisms have been suggested to give rise to surround responses in bipolar cells, including pre-synaptic inhibition acting on photoreceptors [18, 73, 128, 223, 242, 244, 267]. Other suggested mechanisms include an ephaptic effect as well as proton modulation of the Ca^{2+} current and neurotransmitter release in cone photoreceptors [38, 52, 124, 134, 139, 249]. In LMCs, two different models, one based on presynaptic inhibition and one based on local, extracellular changes in electrical potential, have been proposed to mediate spatial and temporal inhibition as well as adaptation [100, 152, 147, 219, 218, 256]. In L2 cells, we found that presynaptic inhibition acting on photoreceptors contributes to surround responses, and $GABA_A$Rs further away from the photoreceptor-LMC synapse are also required (Sections 4.3.1 and 4.3.3). However, even strong blockade of all GABAergic receptor activity did not completely eliminate the surround. While it is possible that the block was incomplete, this suggests that additional mechanisms, such as ephaptic effects, are also involved in shaping the spatial properties of the L2 RF. Furthermore, synaptic mechanisms may interact with ephaptic effects, as activity of GABAergic receptors may give rise to significant changes in currents flowing through lamina cartridges.

Overall, the striking similarities between the functional properties of early visual processing circuits across taxa highlight the importance of these properties for efficient processing of visual information. Since these functional properties arise from different molecular mechanisms in flies and vertebrates, these similarities are unlikely to result from a common ancestral source. Rather, we propose that these parallels reflect convergence on a common processing strategy driven by similar biological constraints and natural input statistics. We speculate that analogous parallels will be found in many aspects of visual processing.

4.5 Future directions

4.5.1 Dissecting the microcircuits that shape L2 responses

Having observed many effects of GABAergic circuits on both the spatial as well as the temporal and contrast sensitivity properties of L2 responses, we next wanted to assess whether other circuit components may play additional roles in shaping L2 responses. In particular, via L4, L2 neurons receive input from nearby dorsal and ventral posterior columns. L2 neurons, in turn, are thought to be the main inputs to L4 cells from all three columns. Both L2 and L4 are likely cholinergic as they express Cha, the choline acetyltransferase and both cells express several nicotinic acetyl choline receptor (nAChR) subunits, suggesting a fast, excitatory interaction between these cells [234].

To test the potential functional roles of this cholinergic network (or additional cholinergic circuit components), we applied nAChR antagonists and monitored L2 responses to the same stimuli presented above. Responses of L2 cells to static dark bars revealed that these receptors play significant roles. In the presence of antagonists, L2 responses to both center and surround stimulation were significantly enhanced (Figure 4.17). In addition, both the center and the surround components of the spatial RF expanded, which could, at least in part, account for the response enhancement (Figure 4.18). In particular, we hypothesize that increased spatial pooling in both the center as well as the surround regions of the RF mediates response enhancement and increases SNR via averaging over more inputs.

Similarly, the hyperpolarization response to a moving bar passing through the cell RF was expanded in time, consistently with an expansion of the RF center (Figure 4.19). Furthermore, the depolarization response to the light decrement which occurs when the bar moves away from the RF was enhanced. Since the depolarization response to the moving bar is consistent with both a light decrement which occurs in the RF center as well as with stimulation of the surround region of the RF by the bright bar, additional experiments will be required to establish whether this enhancement is due to stronger center responses to decrements, a larger surround region, or both.

Interestingly, preliminary experiments performed by Helen Yang indicate that the

effects of cholinergic circuits on the shape of L2 responses are mediated at least in part via nAChRs expressed by L2 cells themselves. In these experiments, RNAi constructs were used to knockdown the Dα7 subunits of these receptors and similar effects to application of nAChR antagonists were found (data not shown). Further exploration of the exact manner in which receptors expressed by different cells give rise to the different effects observed following nAChR antagonist application is required to inform what micro-circuits are involved in this response shaping.

In order to fully understand how L2 responses are shaped, and unravel the structural characteristics of the microcircuits mediating these effects, additional experiments are required. In particular, while two types of circuits, GABAergic and Cholinergic, were found to shape L2 responses, we do not yet know how these circuits interact and to what extent they overlap. To define these interactions both circuits must be manipulated simultaneously. In addition, the cells that provide these inputs to L2 cells and photoreceptors must be identified. Input sources can be identified by silencing candidate cells such as L4 (in the case of potential cholinergic inputs) and C2 and C3 (in the case of potential GABAergic inputs). In addition, other circuits, such as glutamatergic circuits, may still pay additional roles in shaping L2 cells which can be identified by manipulating these circuit components as well. In particular, as the RF shape of L2 cells in the absence of signaling through nAChRs reflects spatial pooling of inputs from more than the set of receptors sampling a single point in space (the acceptance angle of the L2 RF following this manipulation is larger than that measured in photoreceptors), there must be an additional mechanisms mediating spatial pooling.

Finally, it will be beneficial combine manipulations of synaptic inputs with models capturing the effects of these manipulations on the extracellular polarization which may also play a role in shaping L2 responses [256].

The set of experiments described in this and the previous chapter provide a tool-set with which the effects of manipulations on L2 function can be probed. Using this tool-set to unravel the details of the microcircuits shaping L2 responses may be beneficial in two ways: first, it may enable identifying circuit motifs and in particular feedback circuit structures that are useful for endowing particular filtering properties

to cells and may be utilized in other circuits as well. Second, it may enable linking filtering properties incorporated into early stages of visual processing to downstream motion computation, as it is possible to measure both the effect of the manipulation at the early processing stage as well as its effect on motion detection via subsequent behavioral experiments (see below).

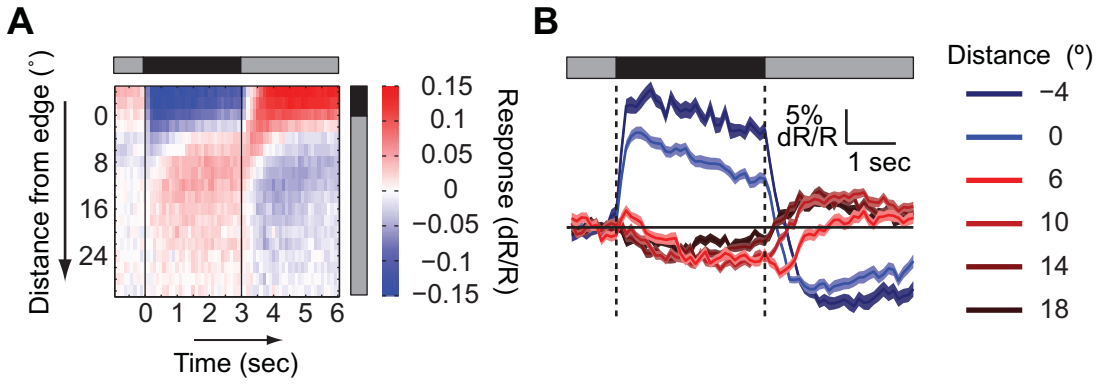

Figure 4.17: L2 cell responses following application of nAChR antagonists, plotted as in Figure 4.2. Shading denotes ±1 SEM.

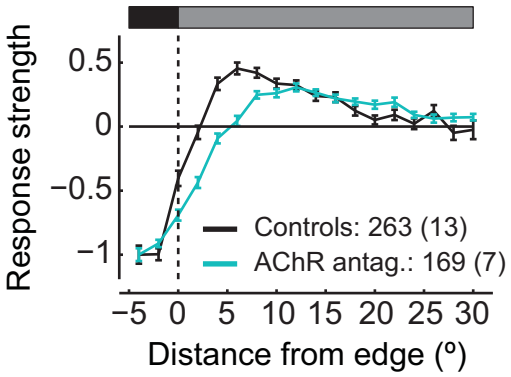

Figure 4.18: Application of nAChR antagonists expands the spatial RF. As in Figure 4.3, the normalized mean strength of the response as a function of the distance from the bar's edge. Error bars denote ±1 SEM. Cyan - Following application of nAChR antagonists. Black - controls, TN-XXL expressed in both L2 cells.

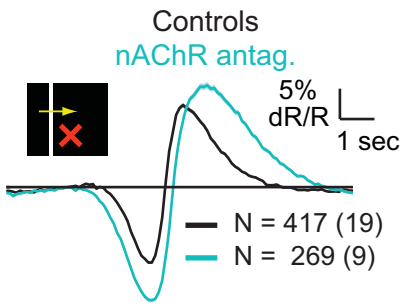

Figure 4.19: Application of nAChR antagonists expands the response to a moving bar in time. Mean response of controls and experimental cells to a moving bright bar on a dark background. Black -controls, TN-XXL expressed in L2 cells only. Cyan - Following application of nAChR antagonists

4.5.2 GABAergic and Cholinergic circuit components provide L2 cells with two alternate ways to adapt to light

Both GABAergic and cholinergic circuits affect the spatial RF shape of L2. By modulating the strength of surround inputs, GABAergic circuits may enable L2 cells to adapt to different light levels. In particular, in dark adapted conditions suppression of GABAergic surround inputs makes the RF center effectively larger. As a result, RF center signals reflect increased spatial pooling that makes these signals more robust against the deleterious effects of photon shot noise. However, this benefit comes at the expense of losing the ability to use predictive coding for efficient encoding of intensity inputs, which is enabled by a center-surround antagonistic RF structure [247, 227, 228]. Interestingly, Cholinergic inputs provide L2 with an alternate way to adapt to low light levels. Specifically, suppression of cholinergic inputs expands both the RF center as well as the RF surround. Thus, the robustness of both center and surround responses is increased by spatial pooling, but the ability to use predictive coding to efficiently represent light inputs is not lost. The qualitative effects of these two circuits on the shape of L2 RFs are captured by a schematic (Figure 4.20). Further experiments will be required to assess under what input conditions each of these mechanisms is used, and to what extent these mechanisms promote contrast sensitivity or encoding of information under low light levels.

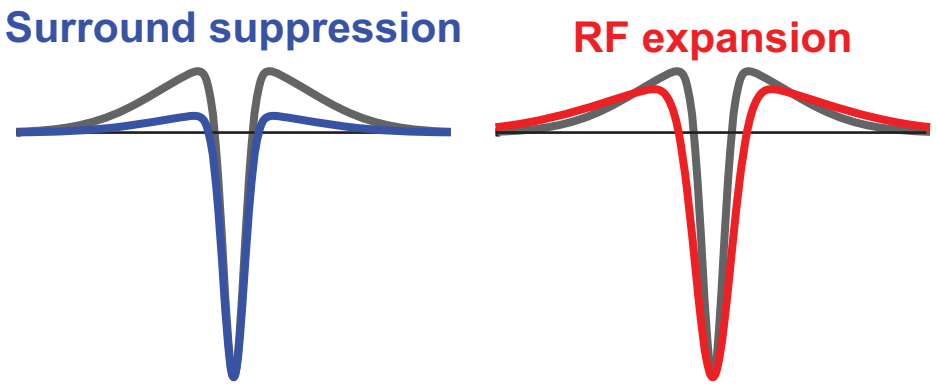

Figure 4.20: Mechanisms of light adaptation. Left - suppression of surround responses gives rise to an effectively wider center RF region, increasing spatial pooling. Right - expanding both components of the RF, the center and the surround, increases spatial pooling and the robustness of signaling for all input types and allows to combine these effects with the benefits of predictive coding.

4.5.3 Linking early visual processing characteristics with downstream motion detection computation

One of the important findings presented above is that the kinetics of L2 responses to dark and bright inputs of different sizes are different. Since filtering of visual inputs in L2 cells is hypothesized to represent the filtering stages performed within the arms of elementary motion detectors, a clearly useful next step for interpreting our results is to incorporate our findings in such models. As a first step, it would be useful to simulate responses of a single detector that has input units with center-surround antagonistic and spatiotemporally coupled RFs, where surround responses are delayed with respect to center responses, in both its arms. In particular, it would be of interest to probe the responses of this type of detector to bar pairs presented not only directly on the detector arm input centers but also nearby in the surround regions. This type of simulation may facilitate interpreting the results of behavioral experiments where some detectors are inactive (e.g., due to genetically induced silencing as described in Section 1.3.3), and an unusual response of a detector to surround inputs may compensate for the effects of the manipulation. More specifically, this type of simulation can determine whether a depolarizing response to a bright surround input can mediate responses to bright motion inputs given a rectification step that eliminates hyperpolarizing signals downstream of L2 cells, when L1 cells are silenced and hence the bright moving edge detection pathway is eliminated. Due to the delayed nature of surround responses the kinetics of this response are expected to be different from the kinetics of the response to center stimulation. Since behavioral responses in these two contexts also differ in kinetics [47], it would be interesting to figure out in what conditions these responses are likely to arise and whether the simulated kinetics differences match and thus explain the observed behavioral ones.

In addition, it would be informative to probe how spatiotemporal coupling, giving rise to different response kinetics for different moving object sizes, and differential responses to bright and dark objects, affects motion detector outputs in these different contexts. These predictions can then be compared with measured behaviors and may explain discrepancies currently existing in the literature which reflect different

response properties to different minimalistic motion cues [47, 67, 116]. For this purpose, it would be useful to further assess what novel response properties arise when an array of such receptors acts together to respond to motion inputs, as occurs in a behaving animal.

While the above described modeling efforts will shed light on the relation between input filtering and motion detector responses, it is also of interest to understand the role of each circuit involved in giving rise to these filtering properties in the context of motion detection. To understand the functional role of response shaping in the context of motion detection it would be beneficial to conduct behavioral experiments while eliminating activity in circuit components with known effects on the early stages of processing. Elimination of surround effects or expansion of both center and surround regions of the RF should change the spatial frequency tuning properties of behavioral responses to moving gratings as it does for L2 cells, in particular for long spatial periods. These effects can be tested both by modeling and by behavioral experiments. Furthermore, both knockdown of nAChRs in L2 cells and knockdown of $GABA_BRs$ in L2 cells and R1-R6 photoreceptors affect the strength and kinetics of depolarizing responses to light decrements. Thus, it would be useful to figure out, via both modeling as well as behavioral experiments, if these inputs indeed play a role in balancing the strength of responses to light and dark moving edges (as can be assessed by presenting opposing edges or individually moving edges of different contrasts, as in [47]). Furthermore, the speed tuning of responses to moving dark edges may be modified, and this can be similarly assessed by presenting, and simulating, responses to dark edges moving at different speeds.

If an effect for knocking down some of these receptors is found, it would be further interesting to probe the sensitivity of this modulation to contrast and illumination conditions. We hypothesize that suppression of surround responses mediated via GABARs, or expansion of the RF via blocking of nAChRs, are useful under dark adapted conditions. This hypothesis can be tested by applying the knockdowns in both light adapted and dark adapted conditions and assessing whether indeed, the knockdowns are only effective under high levels of illumination, suggesting that under dark adapted conditions these inputs are indeed suppressed in WT flies as well.

Chapter 5

Conclusion

In this dissertation I have presented studies characterizing the functional properties of early visual processing neurons in the fruit fly, *Drosophila*. To enable this characterization, we designed stimuli and analysis code for using two-photon Ca^{2+} imaging data to characterize responses to visual inputs in detail. In particular, our stimuli enabled the rapid characterization of spatial RF shapes via Ca^{2+} imaging. These methods can be applied to many different cell types following different manipulations and thus may facilitate future studies of early visual processing cells via imaging in different animal models.

The presented studies focused on the characteristics of L1 and L2 neurons in the *Drosophila* optic lobe, which receive direct photoreceptor inputs and relay their outputs to motion detecting circuits. Interestingly, while the pathways downstream of these neurons are specialized for the detection of bright and dark moving edges, respectively, both these neurons relay information about both light increments and light decrements (Chapter 2). Responses of these neurons differed only in their detailed kinetics and adaptation properties, albeit some asymmetry in the amplitude of responses to light and dark stimuli was also noted, with L2 cells responding more strongly to decrements and L1 cells responding equally to both inputs. Nevertheless, an in depth characterization of the sensitivities of L2 neurons to spatiotemporal distributions of light inputs revealed that responses of these cells to dark and bright inputs do differ, and thus the function of these cells represents a tradeoff between

transmitting all light input information and facilitating the computation conducted in a downstream circuit specialized for detecting moving dark edges (Chapter 3). We expect this tradeoff, between efficient encoding of all information and specialization to extract specific features, to be reflected in the function of many similar first-order interneurons in many systems.

Our detailed studies of the functional characteristics of L2 cells revealed that these cells have an antagonistic, anisotropic and spatiotemporally coupled receptive field structure. Furthermore, L2 cell responses reflected non-linear integration of light inputs over space. Nevertheless, the functional properties of L2 cells were captured by a simple computational model which posits that L2 cell responses arise from a weighted combination of center inputs with delayed antagonistic inputs. In L2 cells, and likely in many similar visual processing cells, linear systems analysis fails to capture the critical RF properties that are required for the function of the downstream visual pathway. Nevertheless, as in the case of L2 cells, it is still possible to derive the functional properties of such cells using a limited set of inputs, albeit via a different approach for functional characterization. In particular, knowledge of the downstream pathway specialization from behavioral experiments and of the functional properties of inputs into the cells to be characterized, can be used to give rise to hypotheses for computational functional models which may apply to these cells. Using these models, appropriate inputs can be displayed to refute or prove the fit of the hypothesized models to the cell function. We hope that this approach will enable the characterization of many visual processing cells in different systems in the future as it enabled the characterization of L2.

An attractive future direction for these studies of early visual processing cells in *Drosophila* is to integrate L2 functional properties, or similarly characterized functional properties of other lamina cells, with motion detection models to infer the exact contribution of mechanisms shaping the inputs to motion detecting circuits to the motion computation itself. Hypotheses derived from such modeling studies can then be experimentally tested if the detailed mechanisms shaping L2 (or other lamina cell) responses are also inferred and thus can be genetically manipulated while behavioral responses to motion are monitored. Such studies may shed light on controversies

that currently exist in the literature regarding how the specialization of the L1 and L2 pathways for dark and bright moving edges arises [47, 69, 116, 117]. For example, since L2 responses to bright and dark objects of different sizes differ, speed tuning and differential polarity sensitivity of the downstream pathway may arise from speed tuning and differential polarity sensitivity at the input stage. Furthermore, these studies may facilitate identifying which of many different suggested models of motion computation is in fact implemented by the brain [1, 104].

Using pharmacological and genetic manipulations of specific types of receptors, our studies further revealed that responses of L2 cells to dark objects are enhanced by lateral and feedback GABAergic circuits modulating the direct effects of photoreceptors inputs on these cells (Chapter 4). Accordingly, these circuits play a critical role in enabling the downstream circuit to be specialized for the detection of moving dark edges. In particular, we have found that surround responses in L2 are mediated at least in part presynaptically by GABA receptors on photoreceptors. Additional GABAergic circuits acting more indirectly enhance the center response of L2 cells to dark objects. Furthermore, other, cholinergic circuits, also play a role in shaping L2 cell responses. These circuits control the size of the entire RF, consisting of both its center and surround regions. As a result, the extent of spatial pooling used in giving rise to center and surround responses is controlled by these circuits. Thus, these studies associate functional roles with the dense connectivity of the lamina, the first visual neuropil of the fly, which has been previously characterized in anatomical studies [170, 204]. Importantly, we suggest that similar circuits to the ones acting on L2 cells may act to shape responses of other lamina neurons providing inputs to other pathways. Even more broadly, similar circuits may shape responses of early visual processing neurons in many different systems.

In support of the expectation that studies of early visual processing in the fly will shed light on mechanisms of visual processing in other model animals and even humans, the detailed functional characterization of L2 cells revealed strikingly similar characteristics of these cells and first order interneurons in the vertebrate retina - the bipolar cells. Since these characteristics are arrived at using different molecular mechanisms in each system, this argues for evolutional convergence due to the

functional significance of these characteristics. i.e., these different visual processing systems have converged on the same strategy for processing visual cues. Furthermore, similarly to how L2 neurons have functional characteristics that facilitate a downstream, pathway specific, computation, and arrive at these characteristics via lateral and feedback circuits; it is likely that other early visual processing neurons providing inputs to specialized pathways in both flies and vertebrate retinas use similar circuit patterns to arrive at similar specializations. Thus, a clear future direction for these studies is to characterize additional early visual processing neurons in different systems and the microcircuits shaping their outputs to identify the set of tools used by the nervous system to shape early sensory processing. This endeavor will be of particular interest if theoretical explanations are found for how these tools give rise to efficient and robust visual processing and more specifically how early visual processing is transformed to downstream computational specialization. This, in turn, will enable answering questions such as to what extent computational specialization observed at the outputs of sensory processing systems such as the retina are arrived at gradually? To what extent do differentially specialized pathways interact and use modular computational units that can serve these different pathway computations? To what extent are such units similar across species in spite of different requirements posed to these circuits by different behaviors, environments and needs? Thus, while our studies were focused on specific cells in the visual processing circuits of the fruit fly, we hope that a deeper understanding of how the brain computes and in particular how sensory information is represented and processed will eventually emerge from this and similar endeavors.

Bibliography

[1] Adelson, E. H., and Bergen, J. R. Spatiotemporal energy models for the perception of motion. *J. Opt. Soc. Am. A*, 2(2), 284–299, 1985.

[2] Akerboom, J., Calderón, N. C., Tian, L., Wabnig, S., Prigge, M., Tolö, J., Gordus, A., Orger, M. B., Severi, K. E., Macklin, J. J., et al. Genetically encoded calcium indicators for multi-color neural activity imaging and combination with optogenetics. *Frontiers in molecular neuroscience*, 6, 2013.

[3] Akerboom, J., Chen, T.-W., Wardill, T. J., Tian, L., Marvin, J. S., Mutlu, S., Calderón, N. C., Esposti, F., Borghuis, B. G., Sun, X. R., et al. Optimization of a GCaMP calcium indicator for neural activity imaging. *The Journal of Neuroscience*, 32(40), 13819–13840, 2012.

[4] Aptekar, J. W., Shoemaker, P. A., and Frye, M. A. Figure tracking by flies is supported by parallel visual streams. *Current biology*, 22(6), 482–487, 2012.

[5] Arnett, D. W. Spatial and temporal integration properties of units in the first optic ganglion of dipterans. *Journal of Neurophysiology*, 35(4), 429–444, 1972.

[6] Ataka, K., and Pieribone, V. A. A genetically targetable fluorescent probe of channel gating with rapid kinetics. *Biophysical journal*, 82(1), 509–516, 2002.

[7] Atick, J. J. Could information theory provide an ecological theory of sensory processing? *Network: Computation in Neural Systems*, 3(2), 213–251, 1992.

[8] Autrum, H., and Hoffmann, C. Diphasic and monophasic responses in the compound eye of Calliphora. *Journal of Insect Physiology*, 4(2), 122–127, 1960.

[9] Babiloni, C., Pizzella, V., Gratta, C. D., Ferretti, A., and Romani, G. L. Fundamentals of electroencefalography, magnetoencefalography, and functional magnetic resonance imaging. *International review of neurobiology*, 86, 67–80, 2009.

[10] Baccus, S. A., lveczky, B. P., Manu, M., and Meister, M. A retinal circuit that computes object motion. *The Journal of Neuroscience*, 28(27), 6807–6817, 2008.

[11] Baccus, S. A., and Meister, M. Fast and slow contrast adaptation in retinal circuitry. *Neuron*, 36(5), 909–919, 2002.

[12] Baines, R. A., Uhler, J. P., Thompson, A., Sweeney, S. T., and Bate, M. Altered electrical properties in drosophilaneurons developing without synaptic transmission. *The Journal of Neuroscience*, 21(5), 1523–1531, 2001.

[13] Barlow, H., and Levick, W. R. The mechanism of directionally selective units in rabbit's retina. *The Journal of physiology*, 178(3), 477, 1965.

[14] Barlow, H. B. Possible principles underlying the transformation of sensory messages. *Sensory communication*, 217–234, 1961.

[15] Barlow, R. B. Inhibitory fields in the limulus lateral eye. *The Journal of General Physiology*, 54(3), 383–396, 1969.

[16] Barnett, L., Platisa, J., Popovic, M., Pieribone, V. A., and Hughes, T. A fluorescent, genetically-encoded voltage probe capable of resolving action potentials. *PloS one*, 7(9), e43454, 2012.

[17] Bausenwein, B., Dittrich, A., and Fischbach, K.-F. The optic lobe of Drosophila melanogaster. *Cell and tissue research*, 267(1), 17–28, 1992.

[18] Baylor, D. A., Fuortes, M. G. F., and O'Bryan, P. M. Receptive fields of cones in the retina of the turtle. *The Journal of Physiology*, 214(2), 265–294, 1971.

[19] Bellen, H. J., Tong, C., and Tsuda, H. 100 years of Drosophila research and its impact on vertebrate neuroscience: a history lesson for the future. *Nature Reviews Neuroscience*, 11(7), 514–522, 2010.

[20] Benzer, S. Behavioral mutants of Drosophila isolated by counter-current distribution. *Proceedings of the National Academy of Sciences of the United States of America*, 58(3), 1112, 1967.

[21] Blagburn, J. M., and Sattelle, D. B. Presynaptic depolarization mediates presynaptic inhibition at a synapse between an identified mechanosensory neurone and giant interneurone 3 in the first instar cockroach, periplaneta americana. *Journal of Experimental Biology*, 127(1), 135–157, 1987.

[22] Blondeau, J., and Heisenberg, M. The three-dimensional optomotor torque system of Drosophila melanogaster. *Journal of comparative physiology*, 145(3), 321–329, 1982.

[23] Borst, A. Drosophila's view on insect vision. *Current Biology*, 19(1), R36–R47, 2009.

[24] Borst, A., and Egelhaaf, M. Principles of visual motion detection. *Trends in neurosciences*, 12(8), 297–306, 1989.

[25] Borst, A., and Euler, T. Seeing things in motion: models, circuits, and mechanisms. *Neuron*, 71(6), 974–994, 2011.

[26] Borst, A., and Haag, J. Neural networks in the cockpit of the fly. *Journal of Comparative Physiology A*, 188(6), 419–437, 2002.

[27] Borst, A., Haag, J., and Reiff, D. F. Fly motion vision. *Annual review of neuroscience*, 33, 49–70, 2010.

[28] Borst, A., Reisenman, C., and Haag, J. Adaptation of response transients in fly motion vision. II: model studies. *Vision Research*, 43(11), 1311–1324, 2003.

[29] Bours, R. J., Kroes, M. C., and Lankheet, M. J. Sensitivity for reverse-phi motion. *Vision research*, 49(1), 1–9, 2009.

[30] Braitenberg, V. Patterns of projection in the visual system of the fly. i. retina-lamina projections. *Experimental Brain Research*, 3(3), 271–298, 1967.

[31] Brand, A. H., and Perrimon, N. Targeted gene expression as a means of altering cell fates and generating dominant phenotypes. *Development*, 118(2), 401–415, 1993.

[32] Brent, R., and Ptashne, M. A eukaryotic transcriptional activator bearing the DNA specificity of a prokaryotic repressor. *Cell*, 43(3), 729–736, 1985.

[33] Brumberg, J. C., Pinto, D. J., and Simons, D. J. Spatial gradients and inhibitory summation in the rat whisker barrel system. *Journal of neurophysiology*, 76(1), 130–140, 1996.

[34] Buchner, D. E., Bader, R., Buchner, S., Cox, J., Emson, P. C., Flory, E., Heizmann, C. W., Hemm, S., Hofbauer, A., and Oertel, W. H. Cell-specific immuno-probes for the brain of normal and mutant Drosophila melanogaster. *Cell and Tissue Research*, 253(2), 357–370, 1988.

[35] Buchner, E. Elementary movement detectors in an insect visual system. *Biological Cybernetics*, 24(2), 85–101, 1976.

[36] Buchner, E., Buchner, S., and Bülthoff, I. Deoxyglucose mapping of nervous activity induced in Drosophila brain by visual movement. *Journal of Comparative Physiology A*, 155(4), 471–483, 1984.

[37] Burrows, M., and Matheson, T. A presynaptic gain control mechanism among sensory neurons of a locust leg proprioceptor. *The Journal of Neuroscience*, 14(1), 272–282, 1994.

[38] Cadetti, L., and Thoreson, W. B. Feedback effects of horizontal cell membrane potential on cone calcium currents studied with simultaneous recordings. *Journal of Neurophysiology*, 95(3), 1992–1995, 2006.

[39] Cajal, S., and Sanchez, D. Contribucion al conocimiento de los centros nerviosos de los insectos. *Trab. Lab. Invest. Biol. Univ. Madrid.*, 13, 1–167, 1915.

[40] Card, G., and Dickinson, M. H. Visually mediated motor planning in the escape response of Drosophila. *Current Biology*, 18(17), 1300–1307, 2008.

[41] Chiappe, M. E., and Jayaraman, V. Performing electrophysiology and two-photon calcium imaging in the adult Drosophila central brain during walking behavior. In *Genetically Encoded Functional Indicators*. Springer, 2012, pp. 83–101.

[42] Chiappe, M. E., Seelig, J. D., Reiser, M. B., and Jayaraman, V. Walking modulates speed sensitivity in Drosophila motion vision. *Current Biology*, 20(16), 1470–1475, 2010.

[43] Chichilnisky, E. A simple white noise analysis of neuronal light responses. *Network: Computation in Neural Systems*, 12(2), 199–213, 2001.

[44] Choe, K.-M., and Clandinin, T. R. Thinking about visual behavior; learning about photoreceptor function. *Current topics in developmental biology*, 69, 187–213, 2005.

[45] Chou, W.-H., Huber, A., Bentrop, J., Schulz, S., Schwab, K., Chadwell, L. V., Paulsen, R., and Britt, S. G. Patterning of the R7 and R8 photoreceptor cells of Drosophila: evidence for induced and default cell-fate specification. *Development*, 126(4), 607–616, 1999.

[46] Clandinin, T. R., Lee, C.-H., Herman, T., Lee, R. C., Yang, A. Y., Ovasapyan, S., and Zipursky, S. L. Drosophila LAR regulates R1-R6 and R7 target specificity in the visual system. *Neuron*, 32(2), 237–248, 2001.

[47] Clark, D. A., Bursztyn, L., Horowitz, M. A., Schnitzer, M. J., and Clandinin, T. R. Defining the computational structure of the motion detector in Drosophila. *Neuron*, 70(6), 1165–1177, 2011.

[48] Cleland, T. A. Inhibitory glutamate receptor channels. *Molecular Neurobiology*, 13(2), 97–136, 1996.

[49] Clifford, C., Ibbotson, M., et al. Fundamental mechanisms of visual motion detection: models, cells and functions. *Progress in neurobiology*, 68(6), 409, 2002.

[50] Clyne, P., Grant, A., O'Connell, R., and Carlson, J. R. Odorant response of individual sensilla on the Drosophila antenna. *Invertebrate Neuroscience*, 3(2-3), 127–135, 1997.

[51] Cosens, D., and Spatz, H. C. Flicker fusion studies in the lamina and receptor region of the Drosophila eye. *Journal of Insect Physiology*, 24(8), 587–594, 1978.

[52] Crook, J. D., Manookin, M. B., Packer, O. S., and Dacey, D. M. Horizontal cell feedback without cone type-selective inhibition mediates redgreen color opponency in midget ganglion cells of the primate retina. *The Journal of Neuroscience*, 31(5), 1762–1772, 2011.

[53] Dacey, D., Packer, O. S., Diller, L., Brainard, D., Peterson, B., and Lee, B. Center surround receptive field structure of cone bipolar cells in primate retina. *Vision research*, 40(14), 1801–1811, 2000.

[54] Davis, G. W., and Naka, K. Spatial organization of catfish retinal neurons. i. single- and random-bar stimulation. *Journal of Neurophysiology*, 43(3), 807–831, 1980.

[55] de Vries, S., Clandinin, T., et al. Optogenetic stimulation of escape behavior in Drosophila melanogaster. *Journal of visualized experiments: JoVE*(71), 2012.

[56] de Vries, S. E., and Clandinin, T. R. Loom-sensitive neurons link computation to action in the Drosophila visual system. *Current Biology*, 22(5), 353–362, 2012.

[57] Deisseroth, K. Optogenetics. *Nature methods*, 8(1), 26–29, 2010.

[58] Denk, W., Strickler, J. H., and Webb, W. W. Two-photon laser scanning fluorescence microscopy. *Science*, 248(4951), 73–76, 1990.

[59] Denk, W., and Svoboda, K. Photon upmanship: Techreview why multiphoton imaging is more than a gimmick. *Neuron*, 18, 351–357, 1997.

[60] DeVries, S. H. Bipolar cells use kainate and AMPA receptors to filter visual information into separate channels. *Neuron*, 28(3), 847–856, 2000.

[61] Dimitrov, D., He, Y., Mutoh, H., Baker, B. J., Cohen, L., Akemann, W., and Knöpfel, T. Engineering and characterization of an enhanced fluorescent protein voltage sensor. *PLoS One*, 2(5), e440, 2007.

[62] Dong, C.-J., and Werblin, F. S. Temporal contrast enhancement via GABAC feedback at bipolar terminals in the tiger salamander retina. *Journal of Neurophysiology*, 79(4), 2171–2180, 1998.

[63] Dubs, A. The spatial integration of signals in the retina and lamina of the fly compound eye under different conditions of luminance. *Journal of Comparative Physiology A: Neuroethology, Sensory, Neural, and Behavioral Physiology*, 146(3), 321–343, 1982.

[64] Dubs, A., Laughlin, S. B., and Srinivasan, M. V. Single photon signals in fly photoreceptors and first order interneurones at behavioral threshold. *The Journal of Physiology*, 317(1), 317–334, 1981.

[65] Duistermars, B. J., Chow, D. M., Condro, M., and Frye, M. A. The spatial, temporal and contrast properties of expansion and rotation flight optomotor responses in Drosophila. *Journal of Experimental Biology*, 210(18), 3218–3227, 2007.

[66] Egelhaaf, M. Fly vision: Neural mechanisms of motion computation. *Current Biology*, 18(8), R339–R341, 2008.

[67] Egelhaaf, M., and Borst, A. Are there separate ON and OFF channels in fly motion vision? *Visual neuroscience*, 8(02), 151–164, 1992.

[68] Eggers, E. D., and Lukasiewicz, P. D. Multiple pathways of inhibition shape bipolar cell responses in the retina. *Visual neuroscience*, 28(01), 95–108, 2011.

[69] Eichner, H., Joesch, M., Schnell, B., Reiff, D. F., and Borst, A. Internal structure of the fly elementary motion detector. *Neuron*, 70(6), 1155–1164, 2011.

[70] Enell, L., Hamasaka, Y., Kolodziejczyk, A., and Nssel, D. R. gamma-aminobutyric acid (GABA) signaling components in Drosophila: Immunocytochemical localization of GABAB receptors in relation to the GABAA receptor subunit RDL and a vesicular GABA transporter. *The Journal of Comparative Neurology*, 505(1), 1831, 2007.

[71] Enroth-Cugell, C., and Freeman, A. W. The receptive-field spatial structure of cat retinal Y cells. *The Journal of Physiology*, 384(1), 49–79, 1987.

[72] Euler, T., and Masland, R. H. Light-evoked responses of bipolar cells in a mammalian retina. *Journal of Neurophysiology*, 83(4), 1817–1829, 2000.

[73] Fahey, P. K., and Burkhardt, D. A. Center-surround organization in bipolar cells: symmetry for opposing contrasts. *Visual Neuroscience*, 20(01), 1–10, 2003.

[74] Fischbach, K.-F., and Dittrich, A. The optic lobe of Drosophila melanogaster. I. a golgi analysis of wild-type structure. *Cell and tissue research*, 258(3), 441–475, 1989.

[75] Fleet, D. J., Hallett, P. E., and Jepson, A. D. Spatiotemporal inseparability in early visual processing. *Biological Cybernetics*, 52(3), 153–164, 1985.

[76] Fleet, D. J., and Jepson, A. D. Spatiotemporal inseparability in early vision: centre-surround models and velocity selectivity. *Computational Intelligence*, 1(1), 89102, 1985.

[77] Fortini, M., and Rubin, G. Analysis of cis-acting requirements of the Rh3 and Rh4 genes reveals a bipartite organization to rhodopsin promoters in Drosophila melanogaster. *Genes & development*, 4(3), 444–463, 1990.

[78] Freifeld, L., Clark, D. A., Schnitzer, M. J., Horowitz, M. A., and Clandinin, T. R. GABAergic lateral interactions tune the early stages of visual processing in Drosophila. *Neuron*, 78(6), 1075–1089, 2013.

[79] French, A. Practical nonlinear system analysis by wiener kernel estimation in the frequency domain. *Biological Cybernetics*, 24(2), 111–119, 1976.

[80] French, A., and Järvilehto, M. The transmission of information by first and second order neurons in the fly visual system. *Journal of Comparative Physiology A: Neuroethology, Sensory, Neural, and Behavioral Physiology*, 126(1), 87–96, 1978.

[81] Frye, M. A. Multisensory systems integration for high-performance motor control in flies. *Current opinion in neurobiology*, 20(3), 347–352, 2010.

[82] Frye, M. A., Dickinson, M. H., et al. Fly flight: a model for the neural control of complex behavior. *Neuron*, 32(3), 385–388, 2001.

[83] Frye, M. A., Dickinson, M. H., et al. Closing the loop between neurobiology and flight behavior in Drosophila. *Current opinion in neurobiology*, 14(6), 729–736, 2004.

[84] Gao, S., Takemura, S.-y., Ting, C.-Y., Huang, S., Lu, Z., Luan, H., Rister, J., Thum, A. S., Yang, M., Hong, S.-T., et al. The neural substrate of spectral preference in Drosophila. *Neuron*, 60(2), 328, 2008.

[85] Garaschuk, O., and Griesbeck, O. Monitoring calcium levels with genetically encoded indicators. In *Calcium Measurement Methods*. Springer, 2010, pp. 101–117.

[86] Gisselmann, G., Plonka, J., Pusch, H., and Hatt, H. Unusual functional properties of homo- and heteromultimeric histamine-gated chloride channels of Drosophila melanogaster: spontaneous currents and dual gating by GABA and histamine. *Neuroscience Letters*, 372(12), 151–156, 2004.

[87] Glantz, R. M., and Bartels, A. The spatiotemporal transfer function of crayfish lamina monopolar neurons. *Journal of Neurophysiology*, 71(6), 2168–2182, 1994.

[88] Göbel, W., and Helmchen, F. In vivo calcium imaging of neural network function. *Physiology*, 22(6), 358–365, 2007.

[89] Gohl, D. M., Silies, M. A., and Clandinin, T. R. Drosophila as a genetic model to investigate motion vision. In *The Making and Un-Making of Neuronal Circuits in Drosophila*. Springer, 2012, pp. 201–221.

[90] Gohl, D. M., Silies, M. A., Gao, X. J., Bhalerao, S., Luongo, F. J., Lin, C.-C., Potter, C. J., and Clandinin, T. R. A versatile in vivo system for directed dissection of gene expression patterns. *Nature methods*, 8(3), 231–237, 2011.

[91] Gollisch, T., and Meister, M. Eye smarter than scientists believed: neural computations in circuits of the retina. *Neuron*, 65(2), 150–164, 2010.

[92] Götz, K. G. Flight control in Drosophila by visual perception of motion. *Kybernetik*, 4(6), 199–208, 1968.

[93] Götz, K. G. Fractionation of Drosophila populations according to optomotor traits. *Journal of Experimental Biology*, 52(2), 419–436, 1970.

[94] Götz, K. G., and Wenking, H. Visual control of locomotion in the walking fruit fly Drosophila. *Journal of comparative physiology*, 85(3), 235–266, 1973.

[95] Greenspan, R. J. Fly pushing: the theory and practice of Drosophila genetics.

[96] Grewe, B. F., Helmchen, F., et al. Optical probing of neuronal ensemble activity. *Current opinion in neurobiology*, 19(5), 520–529, 2009.

[97] Grienberger, C., and Konnerth, A. Imaging calcium in neurons. *Neuron*, 73(5), 862–885, 2012.

[98] Hardie, R. A histamine-activated chloride channel involved in neurotransmission at a photoreceptor synapse. *Nature*, 339(6227), 704–706, 1989.

[99] Hardie, R. C. The photoreceptor array of the dipteran retina. *Trends in Neurosciences*, 9, 419–423, 1986.

[100] Hardie, R. C. Is histamine a neurotransmitter in insect photoreceptors? *Journal of Comparative Physiology A*, 161(2), 201–213, 1987.

[101] Hardie, R. C. Effects of antagonists on putative histamine receptors in the first visual neuropile of the housefly (musca domestica). *Journal of Experimental Biology*, 138(1), 221–241, 1988.

[102] Hardie, R. C., and Raghu, P. Visual transduction in Drosophila. *Nature*, 413(6852), 186–193, 2001.

[103] Hartline, H. K., and Ratliff, F. Spatial summation of inhibitory influences in the eye of limulus, and the mutual interaction of receptor units. *The Journal of general physiology*, 41(5), 1049–1066, 1958.

[104] Hassenstein, B., and Reichardt, W. Systemtheoretische analyse der zeit-, reihenfolgen-und vorzeichenauswertung bei der bewegungsperzeption des rüsselkäfers chlorophanus. *Z. Naturforsch*, 11, 513–524, 1956.

[105] Heisenberg, M., and Buchner, E. The role of retinula cell types in visual behavior of Drosophila melanogaster. *Journal of comparative physiology*, 117(2), 127–162, 1977.

[106] Helmchen, F., and Denk, W. Deep tissue two-photon microscopy. *Nature methods*, 2(12), 932–940, 2005.

[107] Holmes, T. C., Sheeba, V., Mizrak, D., Rubovszky, B., and Dahdal, D. 2 circuit-breaking and behavioral analysis by molecular genetic manipulation of neural activity in Drosophila. *Cold Spring Harbor Monograph Archive*, 49(0), 19–52, Jan. 2007.

[108] Homma, R., Baker, B. J., Jin, L., Garaschuk, O., Konnerth, A., Cohen, L. B., Bleau, C. X., Canepari, M., Djurisic, M., and Zecevic, D. Wide-field and two-photon imaging of brain activity with voltage and calcium-sensitive dyes. In *Dynamic Brain Imaging*. Springer, 2009, pp. 43–79.

[109] Hosie, A. M., and Sattelle, D. B. Allosteric modulation of an expressed homo-oligomeric GABA-gated chloride channel of Drosophila melanogaster. *British Journal of Pharmacology*, 117(6), 1229–1237, 1996.

[110] Howard, J., Dubs, A., and Payne, R. The dynamics of phototransduction in insects. *Journal of Comparative Physiology A*, 154(5), 707–718, 1984.

[111] Jacob, K., Willmund, R., Folkers, E., Fischbach, K., and Spatz, H. C. T-maze phototaxis of Drosophila melanogaster and several mutants in the visual systems. *Journal of comparative physiology*, 116(2), 209–225, 1977.

[112] James, A. C., and Osorio, D. Characterisation of columnar neurons and visual signal processing in the medulla of the locust optic lobe by system identification techniques. *Journal of Comparative Physiology A: Neuroethology, Sensory, Neural, and Behavioral Physiology*, 178(2), 183–199, 1996.

[113] Järvilehto, M., and Zettler, F. Electrophysiological-histological studies on some functional properties of visual cells and second order neurons of an insect retina. *Cell and Tissue Research*, 136(2), 291–306, 1973.

[114] Jenett, A., Rubin, G. M., Ngo, T.-T., Shepherd, D., Murphy, C., Dionne, H., Pfeiffer, B. D., Cavallaro, A., Hall, D., Jeter, J., et al. A Gal4-driver line resource for Drosophila neurobiology. *Cell reports*, 2012.

[115] Joesch, M., Plett, J., Borst, A., and Reiff, D. F. Response properties of motion-sensitive visual interneurons in the lobula plate of Drosophila melanogaster. *Current Biology*, 18(5), 368–374, 2008.

[116] Joesch, M., Schnell, B., Raghu, S. V., Reiff, D. F., and Borst, A. ON and OFF pathways in Drosophila motion vision. *Nature*, 468(7321), 300–304, 2010.

[117] Joesch, M., Weber, F., Eichner, H., and Borst, A. Functional specialization of parallel motion detection circuits in the fly. *The Journal of Neuroscience*, 33(3), 902–905, 2013.

[118] Johns, D. C., Marx, R., Mains, R. E., ORourke, B., and Marbán, E. Inducible genetic suppression of neuronal excitability. *The Journal of neuroscience*, 19(5), 1691–1697, 1999.

[119] Johnston, D., and Wachtel, H. Electrophysiological basis for the spatial dependence of the inhibitory coupling in the limulus retina. *The Journal of General Physiology*, 67(1), 1–25, 1976.

[120] Juusola, M., and French, A. S. Visual acuity for moving objects in first- and second-order neurons of the fly compound eye. *Journal of Neurophysiology*, 77(3), 1487–1495, 1997.

[121] Juusola, M., French, A. S., Uusitalo, R. O., and Weckström, M. Information processing by graded-potential transmission through tonically active synapses. *Trends in neurosciences*, 19(7), 292–297, 1996.

[122] Juusola, M., Uusitalo, R., and Weckström, M. Transfer of graded potentials at the photoreceptor-interneuron synapse. *The Journal of general physiology*, 105(1), 117–148, 1995.

[123] Kalmus, H. Animals as mathematicians. *Nature*, 202, 1156, 1964.

[124] Kamermans, M., Fahrenfort, I., Schultz, K., Janssen-Bienhold, U., Sjoerdsma, T., and Weiler, R. Hemichannel-mediated inhibition in the outer retina. *Science*, 292(5519), 1178–1180, 2001.

[125] Kandel, E. R., Schwartz, J. H., Jessell, T. M., et al. *Principles of neural science*, vol. 4. McGraw-Hill New York, 2000.

[126] Kaneko, A. Physiological and morphological identification of horizontal, bipolar and amacrine cells in goldfish retina. *The Journal of Physiology*, 207(3), 623–633, 1970.

[127] Kaneko, A. Receptive field organization of bipolar and amacrine cells in the goldfish retina. *The Journal of physiology*, 235(1), 133–153, 1973.

[128] Kaneko, A., and Tachibana, M. Effects of gamma-aminobutyric acid on isolated cone photoreceptors of the turtle retina. *The Journal of Physiology*, 373(1), 443–461, 1986.

[129] Katsov, A. Y., and Clandinin, T. R. Motion processing streams in Drosophila are behaviorally specialized. *Neuron*, 59(2), 322, 2008.

[130] Kennedy, D., Calabrese, R. L., and Wine, J. J. Presynaptic inhibition: primary afferent depolarization in crayfish neurons. *Science*, 186, 451–454, 1974.

[131] Kerr, J. N., and Denk, W. Imaging in vivo: watching the brain in action. *Nature Reviews Neuroscience*, 9(3), 195–205, 2008.

[132] Kirschfeld, K. Die projektion der optischen umwelt auf das raster der rhabdomere im komplexauge von musca. *Experimental Brain Research*, 3(3), 248–270, 1967.

[133] Kitamoto, T. Conditional modification of behavior in Drosophila by targeted expression of a temperature-sensitive shibire allele in defined neurons. *Journal of neurobiology*, 47(2), 81–92, 2001.

[134] Klaassen, L. J., Sun, Z., Steijaert, M. N., Bolte, P., Fahrenfort, I., Sjoerdsma, T., Klooster, J., Claassen, Y., Shields, C. R., Ten Eikelder, H. M. M., Janssen-Bienhold, U., Zoidl, G., McMahon, D. G., and Kamermans, M. Synaptic transmission from horizontal cells to cones is impaired by loss of connexin hemichannels. *PLoS Biol*, 9(7), e1001107, 2011.

[135] Knöpfel, T. Genetically encoded optical indicators for the analysis of neuronal circuits. *Nature Reviews Neuroscience*, 2012.

[136] Knöpfel, T., Díez-García, J., and Akemann, W. Optical probing of neuronal circuit dynamics: genetically encoded versus classical fluorescent sensors. *Trends in neurosciences*, 29(3), 160–166, 2006.

[137] Knudsen, E. I., and Konishi, M. Center-surround organization of auditory receptive fields in the owl. *Science*, 202(4369), 778–780, 1978.

[138] Kolodziejczyk, A., Sun, X., Meinertzhagen, I. A., and Nssel, D. R. Glutamate, GABA and acetylcholine signaling components in the lamina of the Drosophila visual system. *PLoS ONE*, 3, e2110, 2008.

[139] Kraaij, D. A., Spekreijse, H., and Kamermans, M. The nature of surround-induced depolarizing responses in goldfish cones. *The Journal of General Physiology*, 115(1), 3–15, 2000.

[140] Krapp, H. G., Hengstenberg, B., and Hengstenberg, R. Dendritic structure and receptive-field organization of optic flow processing interneurons in the fly. *Journal of Neurophysiology*, 79(4), 1902–1917, 1998.

[141] Krapp, H. G., Hengstenberg, R., and Egelhaaf, M. Binocular contributions to optic flow processing in the fly visual system. *Journal of Neurophysiology*, 85(2), 724–734, 2001.

[142] Krekelberg, B., and Albright, T. D. Motion mechanisms in macaque MT. *Journal of Neurophysiology*, 93(5), 2908–2921, 2005.

[143] Kurtz, R., Kalb, J., Spalthoff, C., et al. Examination of fly motion vision by functional fluorescence techniques. *Frontiers in bioscience: a journal and virtual library*, 13, 3009, 2008.

[144] Land, M. F. Visual acuity in insects. *Annual review of entomology*, 42(1), 147–177, 1997.

[145] Laughlin, S., Howard, J., and Blakeslee, B. Synaptic limitations to contrast coding in the retina of the blowfly Calliphora. *Proceedings of the Royal society of London. Series B. Biological sciences*, 231(1265), 437–467, 1987.

[146] Laughlin, S. B. Neural integration in the first optic neuropile of dragonflies (i.) signal amplification in dark-adapted second-order neurons. *Journal of Comparative Physiology A: Neuroethology, Sensory, Neural, and Behavioral Physiology*, 84(4), 335–355, 1973.

[147] Laughlin, S. B. Neural integration in the first optic neuropile of dragonflies (ii.) receptor signal interactions in the lamina. *Journal of Comparative Physiology A: Neuroethology, Sensory, Neural, and Behavioral Physiology*, 92(4), 357–375, 1974.

[148] Laughlin, S. B. Neural integration in the first optic neuropile of dragonflies (iii.) the transfer of angular information. *Journal of Comparative Physiology A: Neuroethology, Sensory, Neural, and Behavioral Physiology*, 92(4), 377–396, 1974.

[149] Laughlin, S. B. Form and function in retinal processing. *Trends in Neurosciences*, 10(11), 478–483, 1987.

[150] Laughlin, S. B. Matching coding, circuits, cells, and molecules to signals: general principles of retinal design in the fly's eye. *Progress in retinal and eye research*, 13(1), 165–196, 1994.

[151] Laughlin, S. B., et al. A simple coding procedure enhances a neurons information capacity. *Z. Naturforsch*, 36(51), 910–912, 1981.

[152] Laughlin, S. B., and Hardie, R. C. Common strategies for light adaptation in the peripheral visual systems of fly and dragonfly. *Journal of Comparative Physiology A: Neuroethology, Sensory, Neural, and Behavioral Physiology*, 128(4), 319–340, 1978.

[153] Laughlin, S. B., and Osorio, D. Mechanisms for neural signal enhancement in the blowfly compound eye. *Journal of experimental biology*, 144(1), 113–146, 1989.

[154] Lichtman, J. W., and Conchello, J.-A. Fluorescence microscopy. *Nature Methods*, 2(12), 910–919, 2005.

[155] Liu, X., Krause, W. C., and Davis, R. L. GABA(A) receptor RDL inhibits Drosophila olfactory associative learning. *Neuron*, 56(6), 1090–1102, 2007.

[156] Looger, L. L., and Griesbeck, O. Genetically encoded neural activity indicators. *Current opinion in neurobiology*, 22(1), 18–23, 2012.

[157] Luan, H., and White, B. H. Combinatorial methods for refined neuronal gene targeting. *Current opinion in neurobiology*, 17(5), 572–580, 2007.

[158] Lukasiewicz, P. D., Eggers, E. D., Sagdullaev, B. T., and McCall, M. A. GABAC receptor-mediated inhibition in the retina. *Vision Research*, 44(28), 3289–3296, 2004.

[159] Lukasiewicz, P. D., and Shields, C. R. Different combinations of GABAA and GABAC receptors confer distinct temporal properties to retinal synaptic responses. *Journal of Neurophysiology*, 79(6), 3157–3167, 1998.

[160] Lütcke, H., and Helmchen, F. Two-photon imaging and analysis of neural network dynamics. *Reports on Progress in Physics*, 74(8), 086602, 2011.

[161] Maimon, G., Straw, A. D., and Dickinson, M. H. A simple vision-based algorithm for decision making in flying Drosophila. *Current Biology*, 18(6), 464–470, 2008.

[162] Maimon, G., Straw, A. D., and Dickinson, M. H. Active flight increases the gain of visual motion processing in Drosophila. *Nature neuroscience*, 13(3), 393–399, 2010.

[163] Mank, M., Reiff, D., Heim, N., Friedrich, M., Borst, A., and Griesbeck, O. A FRET-based calcium biosensor with fast signal kinetics and high fluorescence change. *Biophysical journal*, 90(5), 1790, 2006.

[164] Mank, M., Santos, A. F., Direnberger, S., Mrsic-Flogel, T. D., Hofer, S. B., Stein, V., Hendel, T., Reiff, D. F., Levelt, C., Borst, A., et al. A genetically encoded calcium indicator for chronic in vivo two-photon imaging. *Nature methods*, 5(9), 805–811, 2008.

[165] Marr, D. Vision: A computational investigation into the human representation and processing of visual information, henry holt and co. *Inc., New York, NY*, 1982.

[166] Masland, R. H., et al. The fundamental plan of the retina. *Nature neuroscience*, 4(9), 877–886, 2001.

[167] Masu, M., Iwakabe, H., Tagawa, Y., Miyoshi, T., Yamashita, M., Fukuda, Y., Sasaki, H., Hiroi, K., Nakamura, Y., Shigemoto, R., Takada, M., Nakamura, K., Nakao, K., Katsuki, M., and Nakanishi, S. Specific deficit of the ON response in visual transmission by targeted disruption of the mGIuR6 gene. *Cell*, 80(5), 757–765, 1995.

[168] Meinertzhagen, I., and Sorra, K. Synaptic organization in the fly's optic lamina: few cells, many synapses and divergent microcircuits. *Progress in brain research*, 131, 53–69, 2001.

[169] Meinertzhagen, I. A., Lee, C.-H., et al. The genetic analysis of functional connectomics in Drosophila. *Advances in genetics*, 80, 99–151, 2011.

[170] Meinertzhagen, I. A., and O'Neil, S. D. Synaptic organization of columnar elements in the lamina of the wild type in Drosophila melanogaster. *The Journal of Comparative Neurology*, 305(2), 232263, 1991.

[171] Meister, M., and Berry II, M. J. The neural code of the retina. *Neuron*, 22(3), 435–450, 1999.

[172] Mimura, K. Some spatial properties in the first optic ganglion of the fly. *Journal of Comparative Physiology A: Neuroethology, Sensory, Neural, and Behavioral Physiology*, 105(1), 65–82, 1976.

[173] Molnar, A., and Werblin, F. Inhibitory feedback shapes bipolar cell responses in the rabbit retina. *Journal of Neurophysiology*, 98(6), 3423–3435, 2007.

[174] Montell, C. Visual transduction in Drosophila. *Annual review of cell and developmental biology*, 15(1), 231–268, 1999.

[175] Mronz, M., and Lehmann, F.-O. The free-flight response of Drosophila to motion of the visual environment. *Journal of Experimental Biology*, 211(13), 2026–2045, 2008.

[176] Murthy, M., and Turner, G. Whole-cell in vivo patch-clamp recordings in the Drosophila brain. *Cold Spring Harbor Protocols*, 2013(2), pdb–prot071704, 2013.

[177] Mutoh, H., and Knöpfel, T. Probing neuronal activities with genetically encoded optical indicators: from a historical to a forward-looking perspective. *Pflügers Archiv-European Journal of Physiology*, 465(3), 361–371, 2013.

[178] Naka, K.-l. Functional organization of catfish retina. *Journal of neurophysiology*, 40(1), 26–43, 1977.

[179] Nakanishi, S., Nakajima, Y., Masu, M., Ueda, Y., Nakahara, K., Watanabe, D., Yamaguchi, S., Kawabata, S., and Okada, M. Glutamate receptors: brain function and signal transduction. *Brain Research Reviews*, 26(23), 230–235, 1998.

[180] Nicol, D., and Meinertzhagen, I. A. An analysis of the number and composition of the synaptic populations formed by photoreceptors of the fly. *The Journal of Comparative Neurology*, 207(1), 29–44, 1982.

[181] Niven, J. E., Anderson, J. C., and Laughlin, S. B. Fly photoreceptors demonstrate energy-information trade-offs in neural coding. *PLoS biology*, 5(4), e116, 2007.

[182] Novina, C. D., and Sharp, P. A. The RNAi revolution. *Nature*, 430(6996), 161–164, 2004.

[183] Oheim, M., Beaurepaire, E., Chaigneau, E., Mertz, J., and Charpak, S. Two-photon microscopy in brain tissue: parameters influencing the imaging depth. *Journal of neuroscience methods*, 111(1), 29–37, 2001.

[184] Oheim, M., Michael, D. J., Geisbauer, M., Madsen, D., and Chow, R. H. Principles of two-photon excitation fluorescence microscopy and other nonlinear imaging approaches. *Advanced drug delivery reviews*, 58(7), 788–808, 2006.

[185] Olsen, S. R., and Wilson, R. I. Cracking neural circuits in a tiny brain: new approaches for understanding the neural circuitry of Drosophila. *Trends in neurosciences*, 31(10), 512–520, 2008.

[186] Olsen, S. R., and Wilson, R. I. Lateral presynaptic inhibition mediates gain control in an olfactory circuit. *Nature*, 452(7190), 956–960, 2008.

[187] Olshausen, B. A., and Field, D. J. Natural image statistics and efficient coding. *Network: Computation in Neural Systems*, 7(2), 333–339, 1996.

[188] Orger, M. B., Kampff, A. R., Severi, K. E., Bollmann, J. H., and Engert, F. Control of visually guided behavior by distinct populations of spinal projection neurons. *Nature neuroscience*, 11(3), 327–333, 2008.

[189] Owen, W. G., and Hare, W. A. Signal transfer from photoreceptors to bipolar cells in the retina of the tiger salamander. *Neuroscience Research Supplements*, 10, S77–S87, 1989.

[190] Papatsenko, D., Sheng, G., and Desplan, C. A new rhodopsin in R8 photoreceptors of Drosophila: evidence for coordinate expression with Rh3 in R7 cells. *Development*, 124(9), 1665–1673, 1997.

[191] Paradis, S., Sweeney, S. T., and Davis, G. W. Homeostatic control of presynaptic release is triggered by postsynaptic membrane depolarization. *Neuron*, 30(3), 737–749, 2001.

[192] Paulk, A., Millard, S. S., and van Swinderen, B. Vision in Drosophila: Seeing the world through a model's eyes. *Annual Review of Entomology*, 58, 313–332, 2013.

[193] Peterka, D. S., Takahashi, H., and Yuste, R. Imaging voltage in neurons. *Neuron*, 69(1), 9, 2011.

[194] Pitkow, X., and Meister, M. Decorrelation and efficient coding by retinal ganglion cells. *Nature Neuroscience*, 15(4), 628–635, 2012.

[195] Pollok, B. A., and Heim, R. Using GFP in FRET-based applications. *Trends in cell biology*, 9(2), 57–60, 1999.

[196] Potter, C. J., Tasic, B., Russler, E. V., Liang, L., and Luo, L. The Q system: a repressible binary system for transgene expression, lineage tracing, and mosaic analysis. *Cell*, 141(3), 536–548, 2010.

[197] Pulver, S. R., Pashkovski, S. L., Hornstein, N. J., Garrity, P. A., and Griffith, L. C. Temporal dynamics of neuronal activation by Channelrhodopsin-2 and TRPA1 determine behavioral output in Drosophila larvae. *Journal of neurophysiology*, 101(6), 3075–3088, 2009.

[198] Ratliff, F., Hartline, H. K., and Miller, W. H. Spatial and temporal aspects of retinal inhibitory interaction. *Journal of the Optical Society of America*, 53(1), 110–120, 1963.

[199] Reiff, D. F., Plett, J., Mank, M., Griesbeck, O., and Borst, A. Visualizing retinotopic half-wave rectified input to the motion detection circuitry of Drosophila. *Nature neuroscience*, 13(8), 973–978, 2010.

[200] Reiser, M. B., and Dickinson, M. H. Visual motion speed determines a behavioral switch from forward flight to expansion avoidance in Drosophila. *The Journal of experimental biology*, 216(4), 719–732, 2013.

[201] Richter, J., and Ullman, S. A model for the temporal organization of X- and Y-type receptive fields in the primate retina. *Biological Cybernetics*, 43(2), 127–145, 1982.

[202] Riemensperger, T., Pech, U., Dipt, S., and Fiala, A. Optical calcium imaging in the nervous system of Drosophila melanogaster. *Biochimica et Biophysica Acta (BBA)-General Subjects*, 2012.

[203] Rister, J., Pauls, D., Schnell, B., Ting, C.-Y., Lee, C.-H., Sinakevitch, I., Morante, J., Strausfeld, N. J., Ito, K., and Heisenberg, M. Dissection of the

peripheral motion channel in the visual system of Drosophila melanogaster. *Neuron*, 56(1), 155–170, 2007.

[204] Rivera-Alba, M., Vitaladevuni, S. N., Mischenko, Y., Lu, Z., Takemura, S.-y., Scheffer, L., Meinertzhagen, I. A., Chklovskii, D. B., and de Polavieja, G. G. Wiring economy and volume exclusion determine neuronal placement. *Current Biology*, 21(23), 1–6, 2011.

[205] Rodieck, R. Quantitative analysis of cat retinal ganglion cell response to visual stimuli. *Vision Research*, 5(12), 583–601, 1965.

[206] Root, C. M., Masuyama, K., Green, D. S., Enell, L. E., Nssel, D. R., Lee, C.-H., and Wang, J. W. A presynaptic gain control mechanism fine-tunes olfactory behavior. *Neuron*, 59(2), 311–321, 2008.

[207] Ruck, P. Photoreceptor cell response and flicker fusion frequency in the compound eye of the fly, lucilia sericata (meigen). *The Biological Bulletin*, 120(3), 375–383, 1961.

[208] Saito, T., Kondo, H., and Toyoda, J. I. Ionic mechanisms of two types of on-center bipolar cells in the carp retina. i. the responses to central illumination. *The Journal of General Physiology*, 73(1), 73–90, 1979.

[209] Sakai, H. M., Naka, K., Korenberg, M. J., et al. White-noise analysis in visual neuroscience. *Vis Neurosci*, 1(03), 287–296, 1988.

[210] Salcedo, E., Huber, A., Henrich, S., Chadwell, L. V., Chou, W.-H., Paulsen, R., and Britt, S. G. Blue-and green-absorbing visual pigments of Drosophila: Ectopic expression and physiological characterization of the R8 photoreceptor cell-specific Rh5 and Rh6 rhodopsins. *The Journal of Neuroscience*, 19(24), 10716–10726, 1999.

[211] Sanes, J. R., and Zipursky, S. L. Design principles of insect and vertebrate visual systems. *Neuron*, 66(1), 15, 2010.

[212] Schnell, B., Joesch, M., Forstner, F., Raghu, S. V., Otsuna, H., Ito, K., Borst, A., and Reiff, D. F. Processing of horizontal optic flow in three visual interneurons of the Drosophila brain. *Journal of neurophysiology*, 103(3), 1646–1657, 2010.

[213] Schnell, B., Raghu, S. V., Nern, A., and Borst, A. Columnar cells necessary for motion responses of wide-field visual interneurons in Drosophila. *Journal of Comparative Physiology A*, 198(5), 389–395, 2012.

[214] Schwartz, E. Responses of bipolar cells in the retina of the turtle. *The Journal of physiology*, 236(1), 211–224, 1974.

[215] Schwartz, G., and Rieke, F. Nonlinear spatial encoding by retinal ganglion cells: when $1+1 \neq 2$. *The Journal of general physiology*, 138(3), 283–290, 2011.

[216] Scott, E. K., Raabe, T., and Luo, L. Structure of the vertical and horizontal system neurons of the lobula plate in Drosophila. *Journal of Comparative Neurology*, 454(4), 470–481, 2002.

[217] Shapley, R., and Lennie, P. Spatial frequency analysis in the visual system. *Annual Review of Neuroscience*, 8(1), 547–581, 1985.

[218] Shaw, S. Retinal resistance barriers and electrical lateral inhibition. *Nature*, 255(5508), 480–483, 1975.

[219] Shaw, S. Early visual processing in insects. *Journal of Experimental Biology*, 112(1), 225 –251, 1984.

[220] Shields, C. R., Tran, M. N., Wong, R. O., and Lukasiewicz, P. D. Distinct ionotropic GABA receptors mediate presynaptic and postsynaptic inhibition in retinal bipolar cells. *The Journal of Neuroscience*, 20(7), 2673–2682, 2000.

[221] Siegel, M. S., and Isacoff, E. Y. A genetically encoded optical probe of membrane voltage. *Neuron*, 19(4), 735–741, 1997.

[222] Simpson, J. H. Mapping and manipulating neural circuits in the fly brain. *Advances in genetics*, 65, 79–143, 2009.

[223] Skrzypek, J., and Werblin, F. Lateral interactions in absence of feedback to cones. *Journal of Neurophysiology*, 49(4), 1007–1016, 1983.

[224] Song, Z., Postma, M., Billings, S. A., Coca, D., Hardie, R. C., and Juusola, M. Stochastic, adaptive sampling of information by microvilli in fly photoreceptors. *Current Biology*, 2012.

[225] Srinivasan, M. Generalized gradient schemes for the measurement of two-dimensional image motion. *Biological Cybernetics*, 63(6), 421–431, 1990.

[226] Srinivasan, M., and Dvorak, D. Spatial processing of visual information in the movement-detecting pathway of the fly. *Journal of Comparative Physiology A: Neuroethology, Sensory, Neural, and Behavioral Physiology*, 140(1), 1–23, 1980.

[227] Srinivasan, M., Pinter, R., and Osorio, D. Matched filtering in the visual system of the fly: large monopolar cells of the lamina are optimized to detect moving edges and blobs. *Proceedings of the Royal Society of London. B. Biological Sciences*, 240(1298), 279–293, 1990.

[228] Srinivasan, M. V., Laughlin, S. B., and Dubs, A. Predictive coding: a fresh view of inhibition in the retina. *Proceedings of the Royal Society of London. Series B. Biological Sciences*, 216(1205), 427 –459, 1982.

[229] Stark, W. S., Ivanyshyn, A. M., and Greenberg, R. M. Sensitivity and photopigments of R1-6, a two-peaked photoreceptor, in Drosophila, Calliphora and Musca. *Journal of comparative physiology*, 121(3), 289–305, 1977.

[230] Stavenga, D. Angular and spectral sensitivity of fly photoreceptors. II. dependence on facet lens F-number and rhabdomere type in Drosophila. *Journal of Comparative Physiology A: Neuroethology, Sensory, Neural, and Behavioral Physiology*, 189(3), 189–202, 2003.

[231] Straw, A. D., Lee, S., and Dickinson, M. H. Visual control of altitude in flying Drosophila. *Current Biology*, 20(17), 1550–1556, 2010.

[232] Su, H., and O'Dowd, D. K. Fast synaptic currents in Drosophila mushroom body kenyon cells are mediated by alpha-bungarotoxin-sensitive nicotinic acetylcholine receptors and picrotoxin-sensitive GABA receptors. *The Journal of Neuroscience*, 23(27), 9246–9253, 2003.

[233] Svoboda, K., Yasuda, R., et al. Principles of two-photon excitation microscopy and its applications to neuroscience. *Neuron*, 50(6), 823, 2006.

[234] Takemura, S.-y., Karuppudurai, T., Ting, C.-Y., Lu, Z., Lee, C.-H., and Meinertzhagen, I. A. Cholinergic circuits integrate neighboring visual signals in a Drosophila motion detection pathway. *Current Biology*, 2011.

[235] Takemura, S.-Y., Lu, Z., and Meinertzhagen, I. A. Synaptic circuits of the Drosophila optic lobe: the input terminals to the medulla. *Journal of Comparative Neurology*, 509(5), 493–513, 2008.

[236] Tammero, L. F., Frye, M. A., and Dickinson, M. H. Spatial organization of visuomotor reflexes in Drosophila. *Journal of experimental biology*, 207(1), 113–122, 2004.

[237] Taylor, G. K., and Krapp, H. G. Sensory systems and flight stability: what do insects measure and why? *Advances in insect physiology*, 34, 231–316, 2007.

[238] Theobald, J. C., Ringach, D. L., and Frye, M. A. Dynamics of optomotor responses in Drosophila to perturbations in optic flow. *The Journal of experimental biology*, 213(8), 1366–1375, 2010.

[239] Thevenaz, P., Ruttimann, U., and Unser, M. A pyramid approach to subpixel registration based on intensity. *IEEE Transactions on Image Processing*, 7(1), 27–41, 1998.

[240] Thoreson, W. B., and Mangel, S. C. Lateral interactions in the outer retina. *Progress in Retinal and Eye Research*, 31(5), 407–441, 2012.

[241] Tian, L., Hires, S. A., and Looger, L. L. Imaging neuronal activity with genetically encoded calcium indicators. *Cold Spring Harbor Protocols*, 2012(6), pdb–top069609, 2012.

[242] Toyoda, J., and Kujiraoka, T. Analyses of bipolar cell responses elicited by polarization of horizontal cells. *The Journal of General Physiology*, 79(1), 131–145, 1982.

[243] Toyoda, J.-I. Membrane resistance changes underlying the bipolar cell response in the carp retina. *Vision Research*, 13(2), 283–294, 1973.

[244] Toyoda, J.-I., and Fujimoto, M. Analyses of neural mechanisms mediating the effect of horizontal cell polarization. *Vision Research*, 23(10), 1143–1150, 1983.

[245] Tuthill, J. C., Chiappe, M. E., and Reiser, M. B. Neural correlates of illusory motion perception in Drosophila. *Proceedings of the National Academy of Sciences*, 108(23), 9685–9690, 2011.

[246] van Breugel, F., and Dickinson, M. H. The visual control of landing and obstacle avoidance in the fruit fly Drosophila melanogaster. *The Journal of Experimental Biology*, 215(11), 1783–1798, 2012.

[247] Van Hateren, J. H. Theoretical predictions of spatiotemporal receptive fields of fly LMCs, and experimental validation. *Journal of Comparative Physiology A: Neuroethology, Sensory, Neural, and Behavioral Physiology*, 171(2), 157–170, 1992.

[248] Venken, K. J., Simpson, J. H., and Bellen, H. J. Genetic manipulation of genes and cells in the nervous system of the fruit fly. *Neuron*, 72(2), 202–230, 2011.

[249] Verweij, J., Hornstein, E. P., and Schnapf, J. L. Surround antagonism in macaque cone photoreceptors. *The Journal of Neuroscience*, 23(32), 10249–10257, 2003.

[250] Vigh, J., Vickers, E., and Von Gersdorff, H. Light-evoked lateral GABAergic inhibition at single bipolar cell synaptic terminals is driven by distinct retinal microcircuits. *The Journal of Neuroscience*, 31(44), 15884–15893, 2011.

[251] Vigier, P. Mécanisme de la synthese des impressions lumineuses recueilles par les yeux composés des dipteres. *CR Acad Sci*, 148, 1221–1223, 1909.

[252] Wardill, T. J., List, O., Li, X., Dongre, S., McCulloch, M., Ting, C.-Y., O'Kane, C. J., Tang, S., Lee, C.-H., Hardie, R. C., et al. Multiple spectral inputs improve motion discrimination in the Drosophila visual system. *Science Signaling*, 336(6083), 925, 2012.

[253] Weber, F., Machens, C. K., and Borst, A. Spatiotemporal response properties of optic-flow processing neurons. *Neuron*, 67(4), 629–642, 2010.

[254] Weckstrm, M., Kouvalainen, E., Djupsund, K., and Jrvilehto, M. More than one type of conductance is activated during responses of blowfly monopolar neurones. *Journal of Experimental Biology*, 144(1), 147–154, 1989.

[255] Weckstrm, M., Kouvalainen, E., and Jrvilehto, M. Nonlinearities in response properties of insect visual cells: An analysis in time and frequency domain. *Acta Physiologica Scandinavica*, 132(1), 103–113, 1988.

[256] Weckstrm, M., and Laughlin, S. Extracellular potentials modify the transfer of information at photoreceptor output synapses in the blowfly compound eye. *The Journal of Neuroscience*, 30(28), 9557 –9566, 2010.

[257] Weir, P. T., and Dickinson, M. H. Flying Drosophila orient to sky polarization. *Current Biology*, 22(1), 21–27, 2012.

[258] Welch, P. The use of fast fourier transform for the estimation of power spectra: a method based on time averaging over short, modified periodograms. *Audio and Electroacoustics, IEEE Transactions on*, 15(2), 70–73, 1967.

[259] Werblin, F. S. Control of retinal sensitivity II. lateral interactions at the outer plexiform layer. *The Journal of General Physiology*, 63(1), 62–87, 1974.

[260] Werblin, F. S., and Dowling, J. E. Organization of the retina of the mudpuppy, necturus maculosus. ii. intracellular recording. *Journal of neurophysiology*, 32(3), 339–355, 1969.

[261] Wernet, M. F., Velez, M. M., Clark, D. A., Baumann-Klausener, F., Brown, J. R., Klovstad, M., Labhart, T., and Clandinin, T. R. Genetic dissection reveals two separate retinal substrates for polarization vision in Drosophila. *Current Biology*, 22(1), 12–20, 2012.

[262] Wilson, R. I., and Laurent, G. Role of GABAergic inhibition in shaping odor-evoked spatiotemporal patterns in the Drosophila antennal lobe. *The Journal of neuroscience*, 25(40), 9069–9079, 2005.

[263] Wilson, R. I., Turner, G. C., and Laurent, G. Transformation of olfactory representations in the Drosophila antennal lobe. *Science Signaling*, 303(5656), 366, 2004.

[264] Wilt, B. A., Burns, L. D., Ho, E. T. W., Ghosh, K. K., Mukamel, E. A., and Schnitzer, M. J. Advances in light microscopy for neuroscience. *Annu. Rev. Neurosci*, 32, 435–506, 2009.

[265] Yamaguchi, S., Desplan, C., and Heisenberg, M. Contribution of photoreceptor subtypes to spectral wavelength preference in Drosophila. *Proceedings of the National Academy of Sciences*, 107(12), 5634–5639, 2010.

[266] Yamaguchi, S., Wolf, R., Desplan, C., and Heisenberg, M. Motion vision is independent of color in Drosophila. *Proceedings of the National Academy of Sciences*, 105(12), 4910–4915, 2008.

[267] Yang, X. L., and Wu, S. M. Feedforward lateral inhibition in retinal bipolar cells: input-output relation of the horizontal cell-depolarizing bipolar cell synapse. *Proceedings of the National Academy of Sciences*, 88(8), 3310–3313, 1991.

[268] Yizhar, O., Fenno, L. E., Davidson, T. J., Mogri, M., and Deisseroth, K. Optogenetics in neural systems. *Neuron*, 71(1), 9–34, 2011.

[269] Zanker, J. M., Srinivasan, M. V., and Egelhaaf, M. Speed tuning in elementary motion detectors of the correlation type. *Biological Cybernetics*, 80(2), 109–116, 1999.

[270] Zettler, F., and Jrvilehto, M. Lateral inhibition in an insect eye. *Zeitschrift fr Vergleichende Physiologie*, 76(3), 233–244, 1972.

[271] Zhang, A. J., and Wu, S. M. Receptive fields of retinal bipolar cells are mediated by heterogeneous synaptic circuitry. *The Journal of Neuroscience*, 29(3), 789–797, 2009.

[272] Zhang, H. G., Lee, H. J., Rocheleau, T., ffrench Constant, R. H., and Jackson, M. B. Subunit composition determines picrotoxin and bicuculline sensitivity of Drosophila gamma-aminobutyric acid receptors. *Molecular Pharmacology*, 48(5), 835–840, 1995.

[273] Zhang, J., Chang-Sub, J., and Slaughter, M. M. Serial inhibitory synapses in retina. *Visual Neuroscience*, 14(03), 553–563, 1997.

[274] Zhao, Y., Araki, S., Wu, J., Teramoto, T., Chang, Y.-F., Nakano, M., Abdelfattah, A. S., Fujiwara, M., Ishihara, T., Nagai, T., et al. An expanded palette of genetically encoded Ca2+ indicators. *Science Signaling*, 333(6051), 1888, 2011.

[275] Zheng, L., De Polavieja, G. G., Wolfram, V., Asyali, M. H., Hardie, R. C., and Juusola, M. Feedback network controls photoreceptor output at the layer of first visual synapses in Drosophila. *The Journal of general physiology*, 127(5), 495–510, 2006.

[276] Zheng, W., and Knudsen, E. I. Functional selection of adaptive auditory space map by GABAA-mediated inhibition. *Science*, 284(5416), 962–965, 1999.

[277] Zhu, Y., Nern, A., Zipursky, S. L., and Frye, M. A. Peripheral visual circuits functionally segregate motion and phototaxis behaviors in the fly. *Current biology: CB*, 19(7), 613, 2009.